Advances in fluorescent and colorimetric sensors for anionic species

Daniel A. McNaughton,[a] Mohamed Fares,[a] Giacomo Picci[b], Philip A. Gale[a,*] and Claudia Caltagirone[b,*]

a School of Chemistry, University of Sydney, NSW 2006, Australia. E-mail: philip.gale@sydney.edu.au

b Università degli Studi di Cagliari, Department of Chemical and Geological Science, S.S.554 Bivio per Sestu, 09042 Monserrato (CA), Italy E-mail: ccaltagirone@unica.it

Abstract

In this review we cover recent developments in fluorescent and colorimetric anion sensors. These systems employ a range of different non-covalent interactions including hydrogen- and halogen-bonding, Lewis acidic boron-based sensors, metal-based sensors, charged systems, compounds that use anion-pi interactions to stabilise complexes, photoswitchable systems, the use of excimers and molecular logic gates in sensing. Recent developments in anion-selective chemodosimeters are also surveyed.

1. Introduction

Anions play many essential roles in industrial processes, in the environment and in biological systems. There is therefore a continuing need for the development of sensors for anionic guests. In this review, we provide an update on advances in this area since our previous review in 2018.[1] We have seen continuous development of sensors that function in cells in addition to systems that function under real-world conditions – for example as test strips. The review is structured according to the type. of non-covalent interaction used to bind the anionic analyte. In addition, we cover the development of molecular logic gates, systems that use excimer formation or break-up in sensing, arrays and chemodosimeters

2. Hydrogen bond-based chemosensors

Although the formation of hydrogen bonds is still one of the main strategies used for the development of anion optical sensors, the detectable changes of many systems are triggered by the deprotonation of sensors by basic anions such as fluoride or cyanide [2-19]. Ureas, thioureas, amides and sulfonamides are still the most commonly used binding motifs based on hydrogen bonds. For example, a urea functionalised 4-amino-1,8-naphthalimide based fluorescent anion sensor **1** has been reported by Lenehan and co-workers [20]. The properties of ureas and thioureas appended with this fluorophore have been extensively investigated in the past by Gunnlaugsson's group [21-27], however the Lenehan and co-workers showed that sensor **1** is able to interact with acetate, dihydrogen phosphate and bromide in hydrated DMSO with an on-off fluorescence response (Fig. 1). Interestingly, analysis of the binding mode of **1** via ^{1}H-NMR titrations highlighted that, in the presence of a significant excess of **1,** the urea moieties of two adjacent molecules of the sensor could self-assemble to interact with acetate such that the initial formation of a 1:1 adduct (log K_{11} = 3.17 ± 0.02) could evolve to the formation of both 1:2 (log K_{12} = 0.51 ± 0.04) and 2:1 (log K_{11} = 2.38 ± 0.009) (**1**:acetate) adducts.

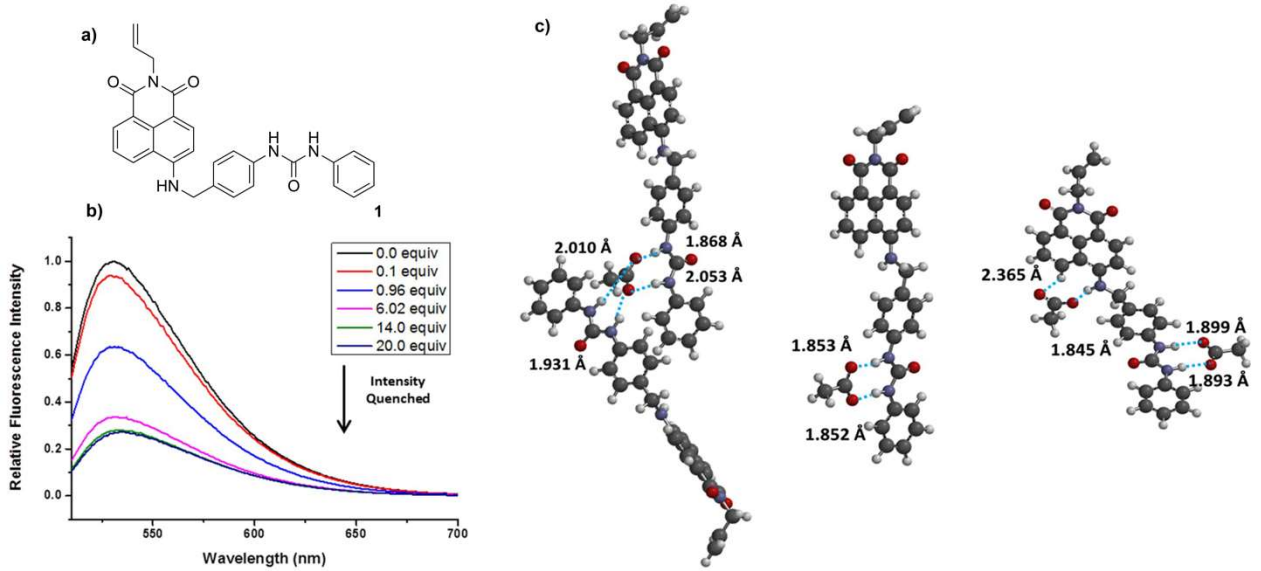

Fig. 1. a) The structure of chemosensor **1**; b) fluorescence response of sensor **1** in the presence of increasing amounts of tetrabutylammonium acetate in DMSO containing 0.5% water λ_{ex} = 503.93nm; c) calculated 2:1, 1:1, and 1:2 adducts of **1** with acetate (Hartree Fock 6-31G*). Reproduced with permission from Ref. [20].

Two new pyrene-ferrocene dyads (**2**-**3**) have been described by Huang, Cao, and co-workers [28]. The presence of ferrocene as an electrochemically active unit enabled the use of cyclic voltammetry (CV) and differential pulse voltammetry (DPV) analysis to monitor the changes in the electrochemical properties of the dyads upon addition of various anions. CV and DPV potentials showed a large cathodic shift in the presence of F^-, AcO^-, and $H_2PO_4^-$ in acetonitrile solution, suggesting anion complexation was taking place. Subsequent analysis of the fluorescent properties of the dyads indicated that the typical monomer pyrene emission band present for **2** and **3** was quenched only in the presence of F^- in acetonitrile (see Fig. 2b in the case of sensor **3**). The fluorescence quenching confirmed the presence that a strong NH···F^- hydrogen bond interaction which may increase the photoinduced electron transfer (PET) process from the sulfur atom of the thiourea subunit, and/or nitrogen atom of the amide group, to the excited pyrene fluorophore.

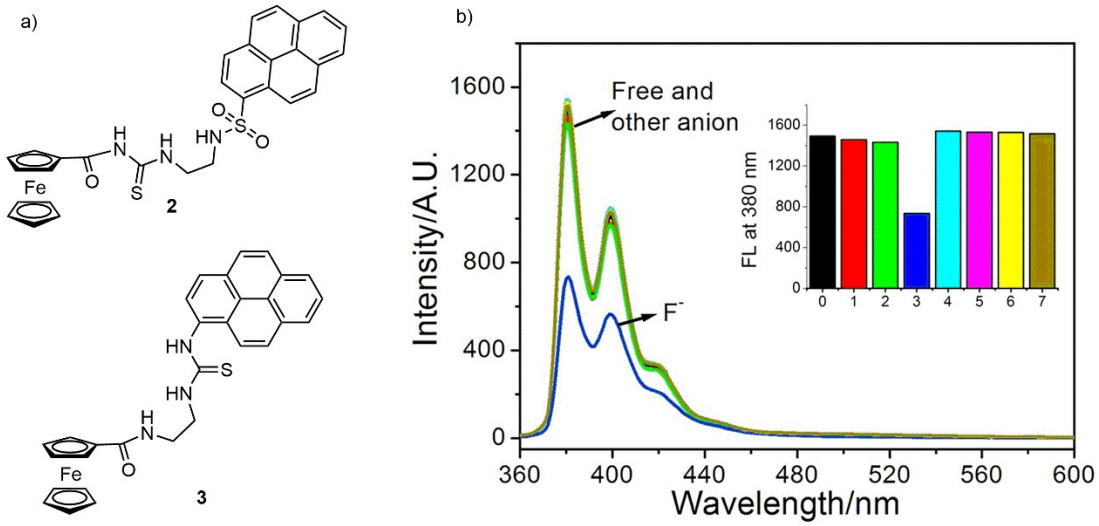

Fig. 2. a) The structures of chemosensors **2** and **3**; b) changes in the fluorescence emission of sensor **3** upon addition of 20 equiv. of anions in acetonitrile. The histogram shows the emission at 380 nm for 0-free **3**, 1- **3** + 20 equiv. of $H_2PO_4^-$, 2-**3** + 20 equiv. of AcO^-, 3-**3** + 20 equiv. of F^-, 4-**3** + 20 equiv. of HSO_4^-, 5-**3** + 20 equiv. of Cl^-, 6-**3** + 20 equiv. of Br^-, 7-**3** + 20 equiv. of I^-. Adapted with permission from Ref. [28].

Bisurea compound **4,** based on 2,2'-bianthracene, was recently reported by Kondo and collaborators [29]. Sensor **4** (Fig. 3) exhibits a green-yellow fluorescence at around 510 nm when excited at 365 nm in THF. Upon addition of tetrabutylammonium acetate, a decrease in the fluorescence emission was observed due to the formation of a 1:1 adduct (K_{11} = 1.61 (± 0.04) × 10^6), which was more significant compared to the other anions tested.

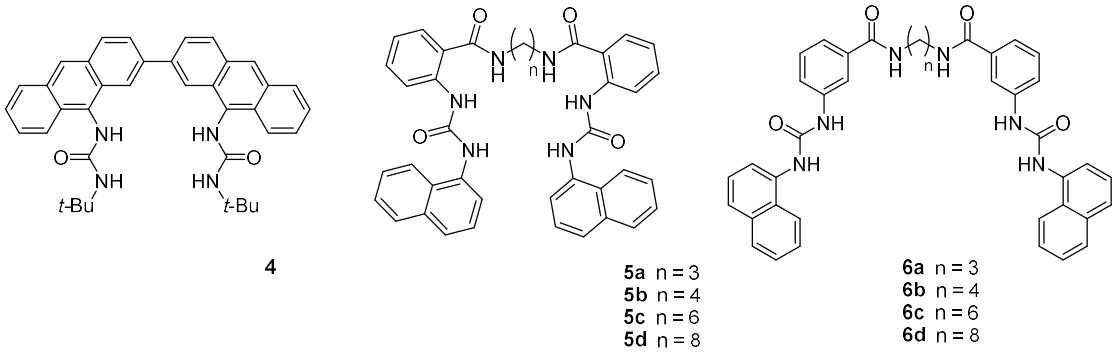

Fig. 3. The structures of chemosensor **4** and chemosensor families **5** and **6**.

A family of fluorescent bis(naphthylureylbenzamide)-based sensors (**5a-d** and **6a-d**) were described by Ochoa-Lara and Ochoa-Téran [30]. The position of the urea and amide groups (in *ortho* or *meta* position for **5a-d** and **6a-d**, respectively) as well as the length of the alkyl chain, influenced the fluorescence behaviour of the sensors with a ON-OFF-ON response observed for the *meta*- family and an OFF-ON response for the *ortho*- family. The most significant changes were observed in the presence of hydrogen phosphate and hydrogen pyrophosphate in acetonitrile. The formation of both 1:1 and 2:1 adducts was observed in the experimental conditions. The ON-OFF-ON behaviour observed for sensors **6a-d** was attributed to the roles of more than one electronic process involved in anion recognition. The quenching of the fluorescence band of the free sensors at around 368 nm was postulated to be due to an electron-transfer (eT) process from the carbonyl oxygen of the urea, which assumes a partial negative charge in the interaction with the anion, facing the excited naphthyl group. This quenching occurred upon addition of 0.5 equiv. of anion guest and was associated with the formation of the 2:1 adduct. Electron density is transferred to the oxygen from the coordinated anion through H-bonds at this stage. Subsequently, a new band at 375 nm appeared and exhibited an increase of fluorescence intensity upon addition of more than 0.5 equiv. of anion guest. The increase of the new fluorescence band intensity was attributed to a charge transfer (cT) process as a consequence of a partial deprotonation of the urea moieties and was confirmed by ^{1}H-NMR titrations.

Gupta and co-workers demonstrated that pyridine-2,6-dicarboxamide-based scaffolds with different appendages can act as chemosensors for the selective detection of the S^{2-} ion, as well as gaseous H_2S, in aqueous media [31]. In particular, sensor **7** (Fig. 4a), bearing a benzothiazole ring as the active unit of the system, demonstrated considerable sensing ability of both S^{2-} and H_2S. In a solution of 1 % HEPES in DMF, at pH = 7.2, a quenching of the emission band of the free sensor at 480 nm was selectively observed upon addition of Na_2S (Fig. 4b). A detailed ^{1}H-NMR analysis and pH study revealed that quenching occurred due to the deprotonation of the sensor by S^{2-} to form HS^-, which is then able to bind to the pseudo-cavity of the receptor. This process was demonstrated to be reversible, as upon addition of acetic acid as a proton source the original fluorescence of free **7** could be restored several times (Fig. 4c). Sensor **7** was also applied for use in cell imaging. Murine cells L929 incubated with **7** showed a strong fluorescence (green channel, (Fig. 4d, b20× and b100×), which was quenched after being treated with S^{2-} (Fig. 4d, c20× and c100×).

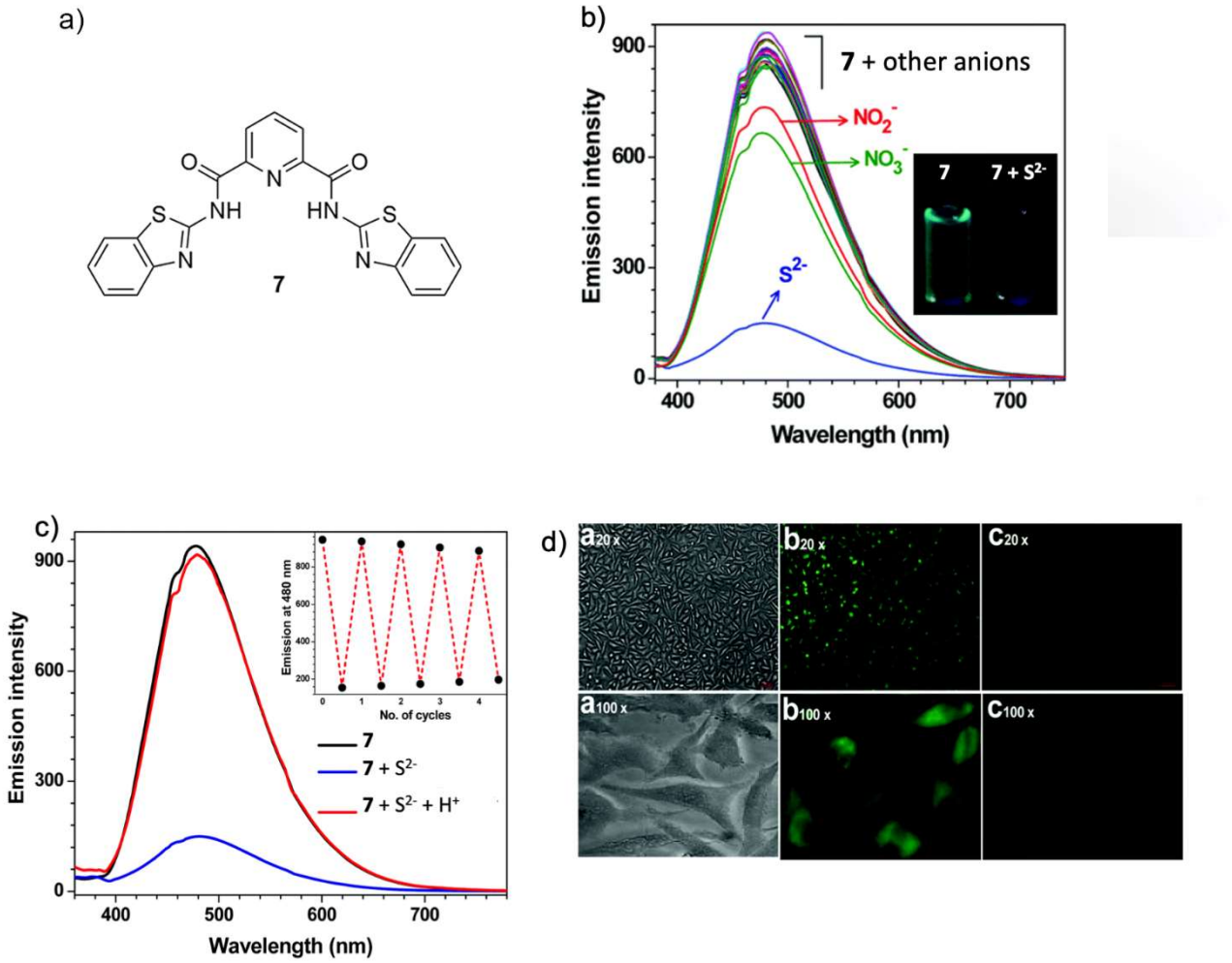

Fig. 4. a) The structure of chemosensor **7**; b) change in the emission intensity of **7** (10 µM) in the presence of different anions (1 mM) in HEPES buffer; c) change in the emission intensity of **7** (10 µM) in the presence of Na_2S (1 mM) and its reversibility in the presence of CH_3COOH (1 mM) in HEPES buffer (1% DMF, 10 mM, pH = 7.2), inset: reversibility cycles for **7** (10 µM) at 480 nm upon the addition of Na_2S and subsequent addition of CH_3COOH; d) fluorescence microscopic images of L929 cells: (a and b) brightfield and green channel images of cells treated with **7** (10 µm), respectively; (c) green channel images of cells treated with **7** (10 µM) and S^{2-} ion (1 mM). Adapted with permission from Ref. [31].

The pyridine-2,6-dicarboxamide scaffold was also used by Kataev to develop the sulfate chemosensor **8**, in which the active unit is a pH-sensitive naphthalimide fluorophore [32]. At acidic pH, the piperazine moieties are protonated, thus offering a perfect binding pocket for sulfate. As shown in Fig. 5b, an increase in the fluorescence emission of the chemosensor at 515 nm was observed upon addition of sulfate with respect to the other anions tested in 1:1 water/THF containing 50 mM acetate buffer (pH = 4.1) and a log K =3.30 for the 1:1 adduct with sulfate was determined.

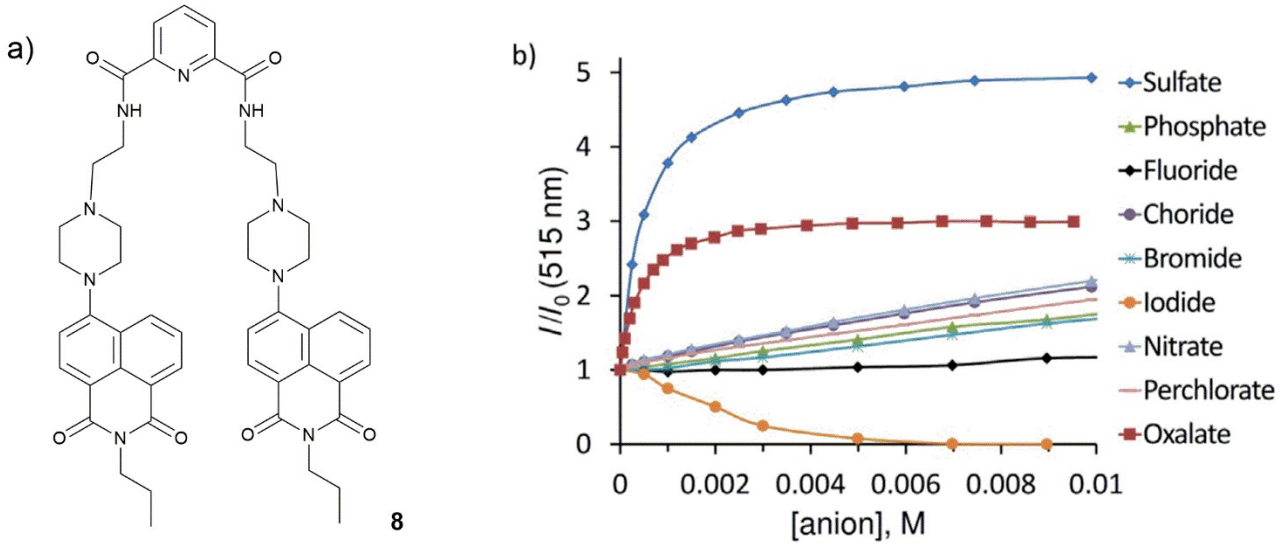

Fig. 5. a) The structure of chemosensor **8**; b) binding isotherms obtained by fluorescence titrations of **8** in a 1:1 buffer-THF (pH 4.1) with anions as their sodium salts. Reproduced with permission from Ref. [32].

A novel approach for fluoride sensing was proposed by Lin, Liu, Wei and co-workers [33]. A supramolecular polymerisation was demonstrated to occur between the tripodal naphthalene imide chemosensor **9** (Fig. 6a) and F^-, leading to strong aggregation induced enhanced emission (AIEE). In DMSO/H_2O (7.4:2.6 v/v), **9** exhibits a weak emission band at 430 nm. However, upon addition of fluoride a very strong blue emission was observed, while negligible changes were observed in the presence of the other tested anions (Fig. 6b). A remarkable limit of detection (LOD) of 8.67 x 10^{-9} M was measured. The increase in fluorescence intensity was attributed to the polymerization of **9** upon fluoride complexation and SEM analysis confirmed this hypothesis. Chemosensor **9** exists in an irregular powder structure (Fig. 6c), while analysis upon the addition of 1 equiv. of F^- revealed the formation of regular fibres (Fig. 6d). The fluoride anion is sandwiched between two receptors and experiences an anion- π interaction with the central phenyl core as well as multiple H-bonding interactions with imide protons directed above and below their corresponding sensor unit. Additional π- π stacking interactions between the naphthalene groups on neighbouring molecules provide an additional driving force for polymerisation. Interestingly, upon addition of Fe^{3+} the polymer was destroyed due to the formation of $[FeF_x]^{n-}$ and the AIEE fluorescence was quenched. The authors also demonstrated that the chemosensor **9** could be used for removing fluoride from water, with an absorption rate of 85%.

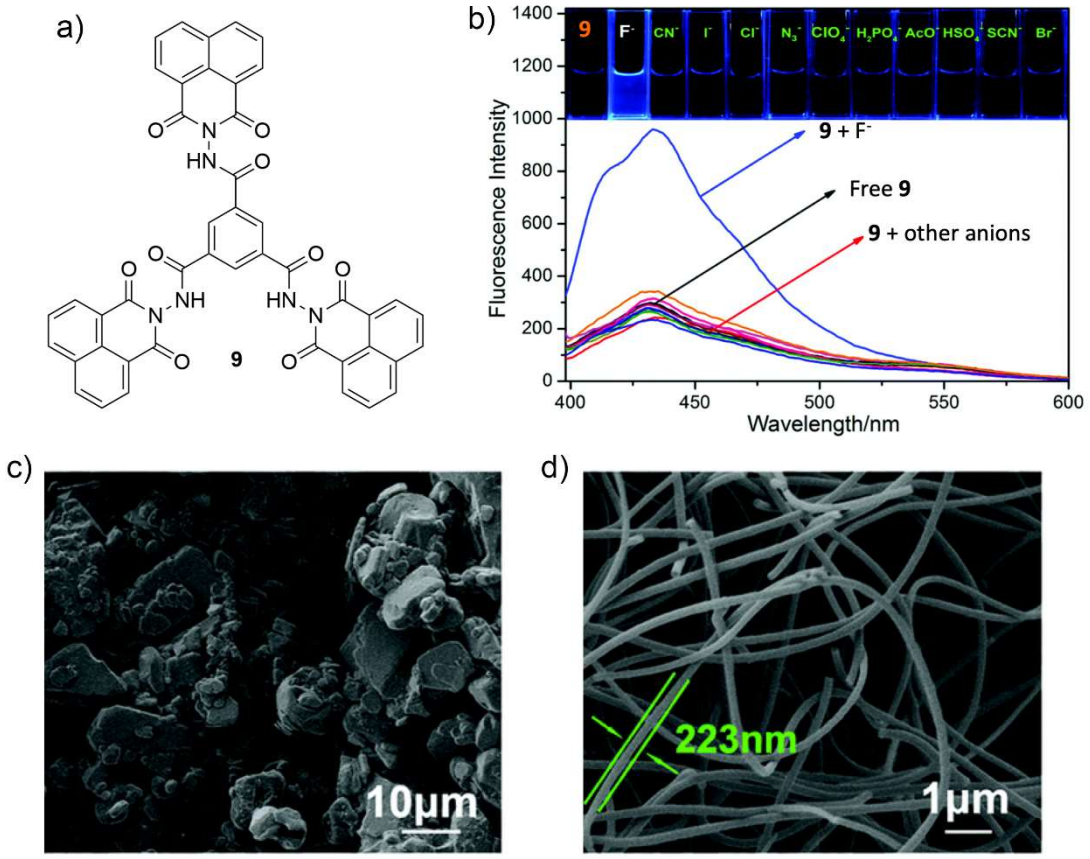

Fig, 6. a) The structure of compound **9**; b) fluorescence emission spectra of **9** (1 x 10^{-4} M) in DMSO/H_2O (7.4:2.6, v/v) solution in the presence of F^- and other anions (2.0 equiv.), (λ_{ex} = 380 nm); c) SEM images of **9** and d) **9** + 1 equiv. F^-. Adapted with permission from Ref. [33].

A series of bisamide derivatives of 1,8-diaminocarbazole and 1,8-diamino-3,6-dichlorocarbazole were described by Chmielewski and co-workers [34]. In particular, chemosensor **10** was found to have good affinity for oxoanions in DMSO/0.5 % H_2O (K_{11} = 1.02 x 10^4 M^{-1} and K_{11} = 4.65 x 10^3 M^{-1} for $H_2PO_4^-$ and AcO^-, respectively). Upon excitation at 335 nm, the fluorescence emission intensity of **10** at 400 nm increased by more than 15 times upon addition of $H_2PO_4^-$ (Fig. 7) and AcO^-.

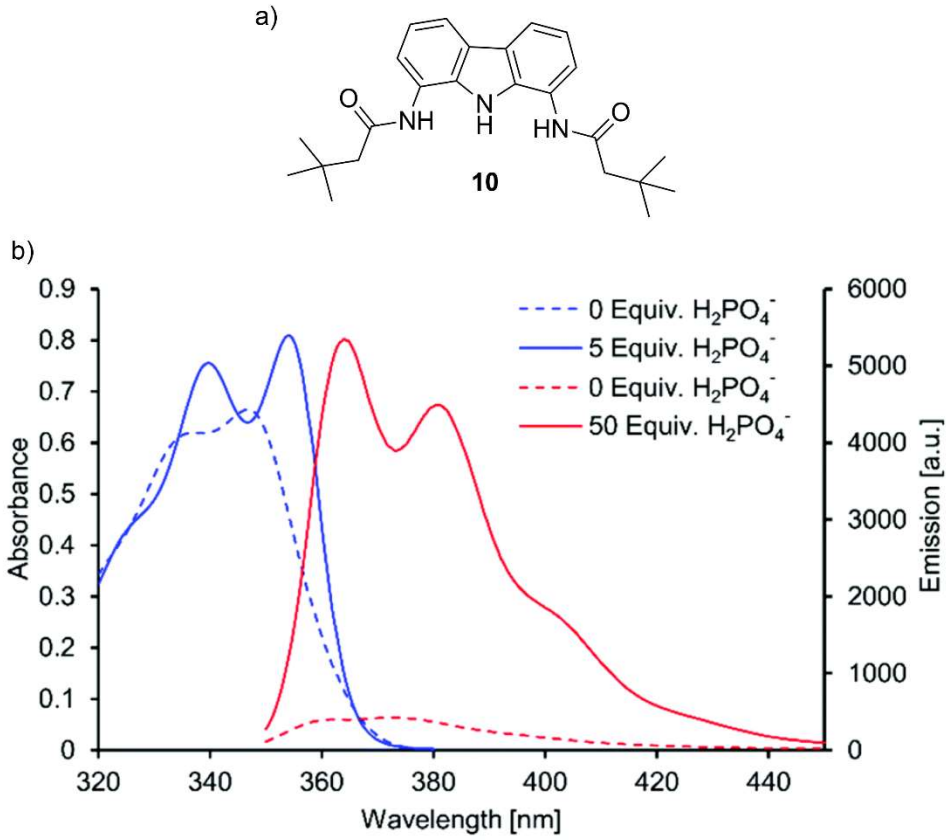

Fig. 7. UV-Vis absorption (blue lines) and emission (red lines, excitation at 335 nm) spectra of **10** upon addition of $H_2PO_4^-$ in DMSO/0.5% H_2O. Reproduced with permission from Ref. [34].

A useful hydrogen bond donor group for the design of optical anion chemosensors is hydrazine. Azo-hydrazone tautomerism (akin to that of azo-dyes) is a well-known mechanism in which labile protons can be intramolecularly exchanged, leading to tautomers with different optical properties [35]. Chemosensor **11** was reported by Trivedi and co-workers (Fig 8a) [36], and UV-Vis studies indicated that in DMSO solution the absorption band of **11** at 402 nm, was red-shifted after the addition of F^-, AcO^-, and to a lesser extent $H_2PO_4^-$. This was attributed to an intramolecular charge transfer process between the oxygen of the hydroxyl group on the quinoline ring and the electron withdrawing phenyl ring, due to the formation of a H-bond complex between the hydroxyl groups of **11** and the anionic species. The change in fluorescence of compound **11** in DMSO upon addition of aliquots of acetate is shown in Figure 8b. In DMSO/HEPES buffer solution (9:1, v/v, pH 7.4) the system became selective for AcO^- (Fig. 8c).

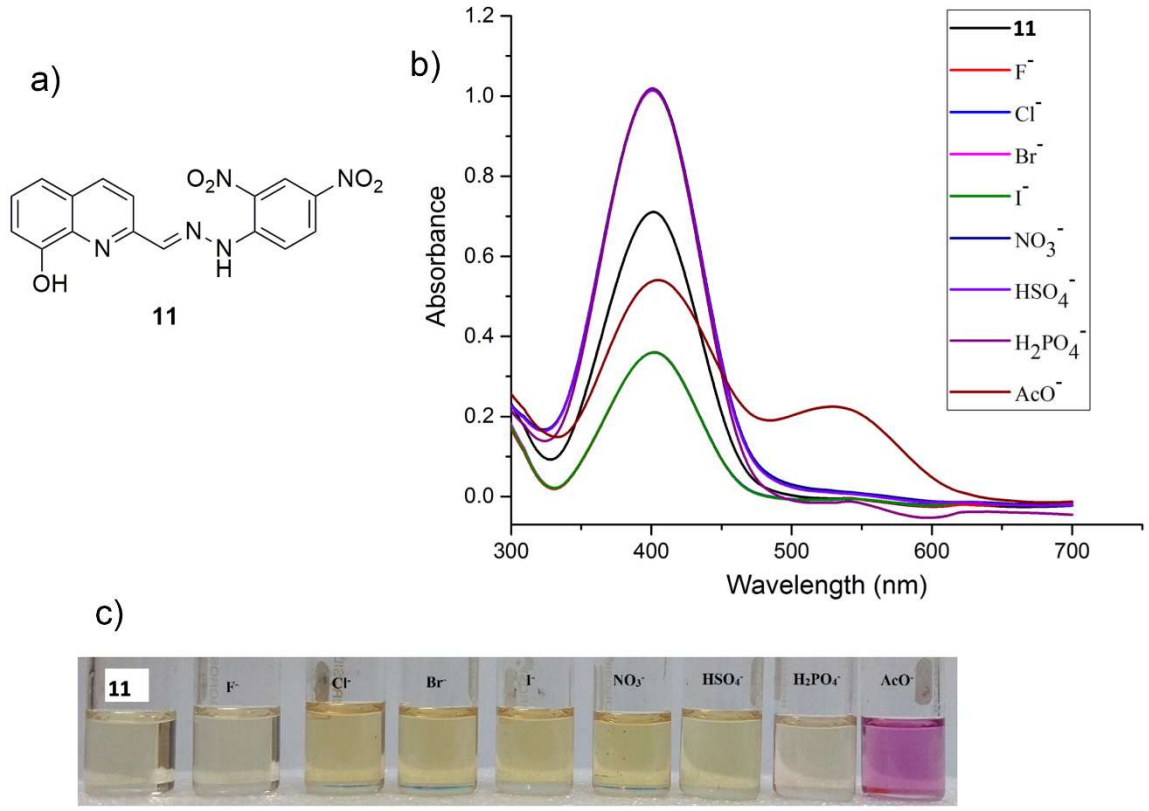

Fig. 8. a) The structure of chemosensor **11**; b) fluorescence titration spectra of **11** upon incremental addition of acetate in DMSO c) colour change of **11** in the presence of 1 equiv. of different anions as their tetrabutylammonium salts in DMSO:HEPES buffer (9:1, v/v). Adapted with permission from Ref. [36].

Chemosensor **12** was able to recognize $H_2PO_4^-$ in DMSO *via* the formation of a 1:1 complex [37]. In this case, the colour of the solution faded upon addition of the anion. This behaviour is presumably due to the disruption of the intramolecular H-bond between the phenanthroline nitrogens and the internal urea protons of the free receptor, triggered by the formation of the adduct.

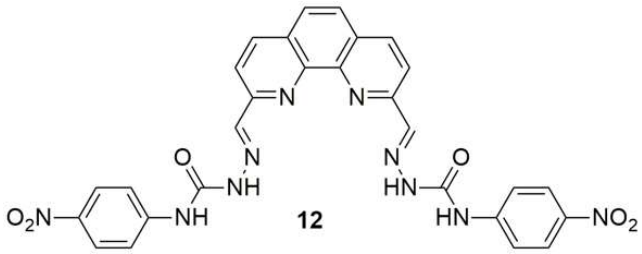

Fig. 9. The structure of chemosensor **12.**

An interesting example of a bis-(salamo)-based fluorescent chemosensor for $B_4O_7^{2-}$ recognition was developed by Pu, Dong and co-workers [38]. In tris-HCl buffer solution (DMF/H_2O 9:1, v/v) at pH = 7 the fluorescence of the free receptor **13** was weak, likely due an intramolecular photoinduced electron transfer (PET) induced by the lone pairs of the nitrogen atoms. In the presence of $B_4O_7^{2-}$ a Chelation Enhanced Fluorescence (CHEF) effect was observed with a formation of an emission band at 423 nm (Fig. 10a). Job plot analysis was performed to attribute this to the formation of a 1:1 adduct (K_{11} = 4.72 x 10^3 M^{-1}). Selectivity for $B_4O_7^{2-}$ was observed in the presence of other anions as well as homocysteine (Hcy) and H_2O_2 species, and a

LOD for $B_4O_7^{2-}$ as low as 8.61 x 10^{-7} M was determined. Fluorescent imaging on BHK-21 cells indicated that **13** has an excellent permeability in living cells and that it is able to monitor intracellular $B_4O_7^{2-}$ (Fig. 10b).

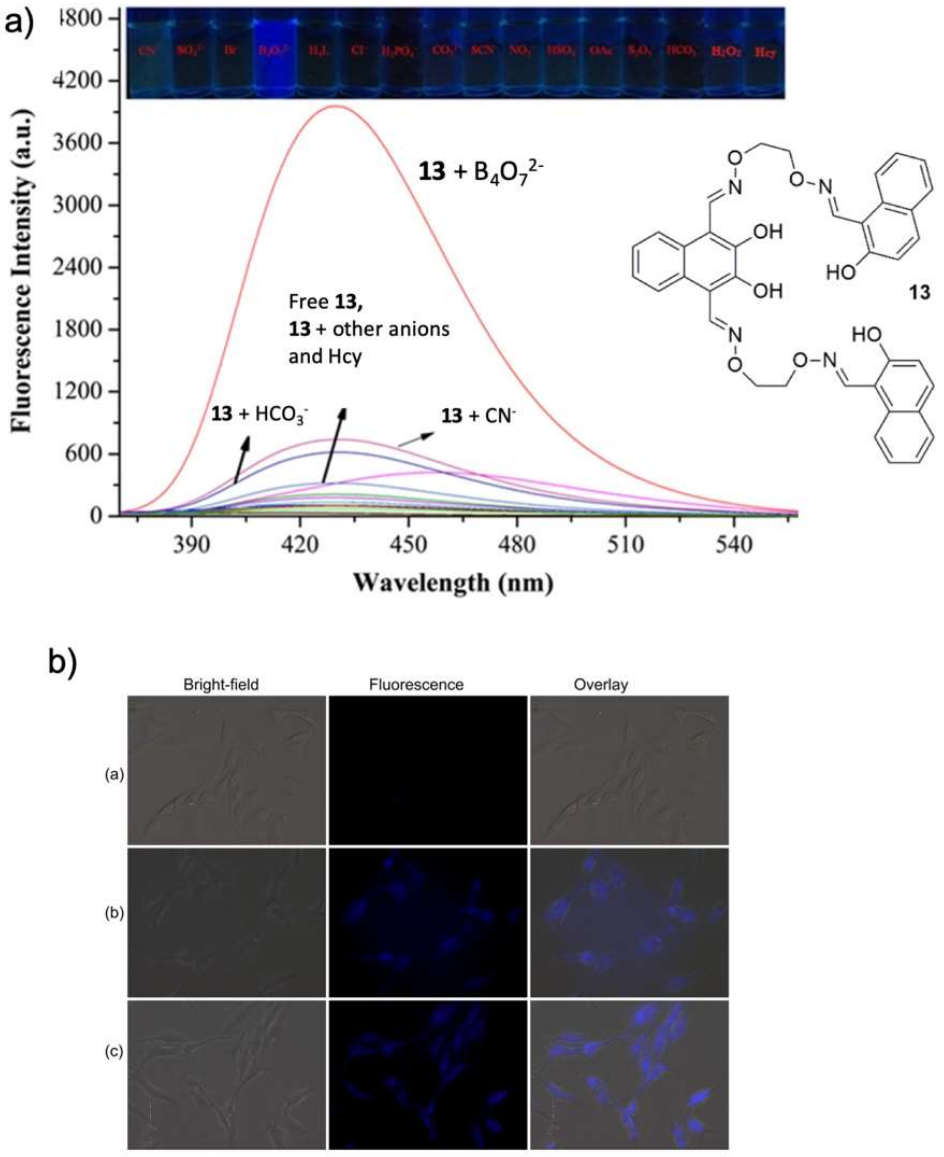

Fig. 10. a) Fluorescence spectra of **13** (0.01 mM) in the presence of various guests (40.0 equiv. of $B_4O_7^{2-}$, Br^-, Cl^-, CN^-, CO_3^{2-}, HCO_3^-, $H_2PO_4^-$, HSO_4^-, NO_3^-, AcO^-, $S_2O_3^-$, SCN^-, SO_4^{2-}, Hcy and H_2O_2) in Tris-HCl buffer (DMF/H_2O= 9:1, *v*/*v*, pH= 7), inset: chemical structure of **13**; b) confocal luminescence images of BHK-21 cells. (a) BHK-21 cells were incubated with sensor **13** (30μM) for 30 min at 37 °C and (b) then further incubated with $B_4O_7^{2-}$ (100 μM) for 30 min; (c) further incubated with $B_4O_7^{2-}$ (100 μM) for 3h. Adapted with permission from Ref. [38].

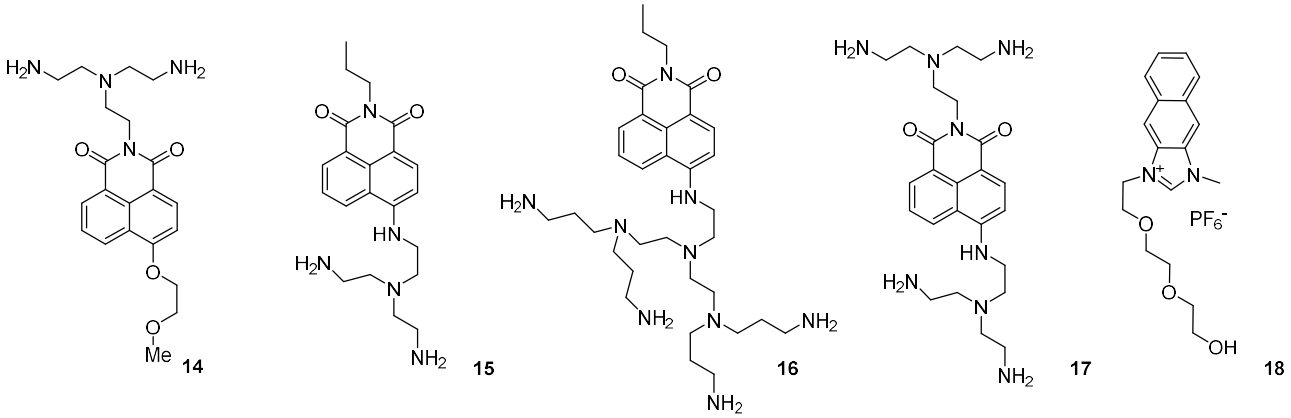

Fig.11. The structures of chemosensors **14**-**18**.

Polyammonium groups have proved to be a regularly reliable choice in the design of anion receptors [39]. Naphthalimide-based polyammonium chemosensors (**14**-**17**) have been proposed by Kataev and co-workers [40]. The four chemosensors, shown in Fig. 11, bind pyrophosphate in buffered aqueous solution at pH 8.6 for **14**, **15** and **17**, and at pH 5.6 for **16** with binding affinities of 10^3-10^5 M^{-1}. The compounds were shown to function as pH sensors in water with multiple protonation equilibria, and fluorescence-pH dependency studies were performed to determine which protonation event affected fluorescence. The presence of the anion also leads to protonation of the amino groups; therefore buffer solutions and pH values were chosen such that the addition of an anion resulted in a turn-on fluorescence response. Interestingly, in the case of **17** both a turn-on and a turn-off behaviour was observed depending on the pH of the solution. This was attributed to an initial protonation of the amino groups triggered by the anionic guest, which hindered the PET process. Consequently, the anion induced aggregation of the receptor caused a quenching of the fluorescent emission of the naphthalimide group.

Imidazolium moieties have also been extensively used for anion recognition [41] and recently were applied by Yoon and co-workers for anion sensing using naphthoimidazolium derivative **18** (Fig. 11) [42]. Upon addition of various anion guests in acetonitrile, the formation of an CH^+-anion H-bond caused an hypsochromic shift in the fluorescent maximum emission, from 465 nm to 375 nm, only in the case of fluoride and cyanide. Notably, the researchers discovered that when CO_2 was bubbled through a solution of **18** in the presence of CN^- the original fluorescent emission at 465 nm was restored. The naphthoimidazolium system was also proposed by Yoon, in collaboration with James and Park [43], as the active unit and the anion recognition site in chemosensor **19** (Fig 12a). In this receptor, the naphthoimidazolium is coupled with a cholesteryl moiety which acts as a chiral barrier and induces enantiomeric selectivity. This system was able to recognize chiral carboxylates (Boc-D-Phe, Fig. 12b) over other D-protected aminoacids, and over Boc-L-Phe, (Fig. 12c). Addition of Boc-D- Phe to a solution of **19** in acetonitrile/DMSO (95:5 v/v) caused a ratiometric response with a decrease in intensity of the emission band of the free receptor at 452 nm, and a concomitant formation of a blue-shifted emission band at 375 nm (Fig 12d).

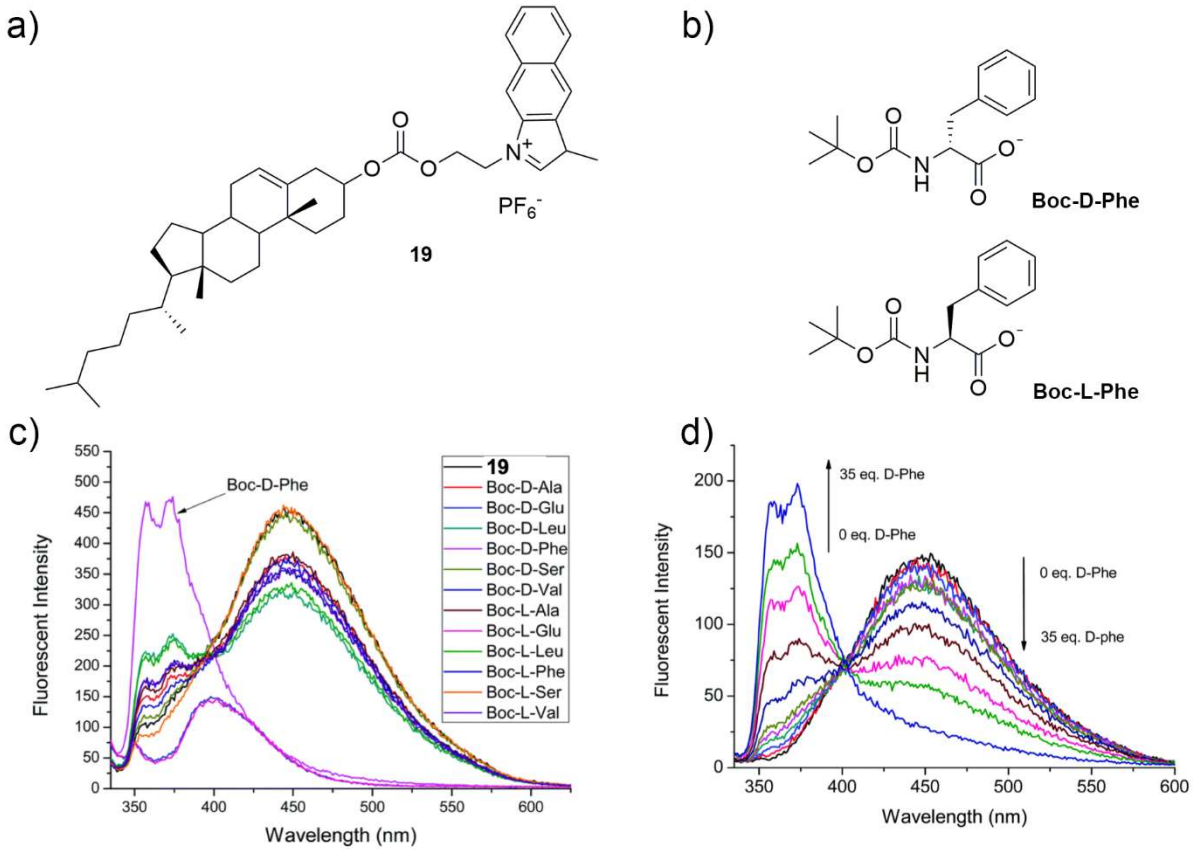

Fig. 12. a) Structure of **19**; b) structures of the enantiomeric anions of Boc-phenylalanine; c) fluorescence alterations of **19** in acetonitrile/DMSO (95: 5, v/v) with D and L isomers of Ala, Glu, Leu, Phe, Ser and Val; d) fluorescence titration of **19** in acetonitrile/DMSO (95: 5, v/v) with various equivalents of Boc-D-Phe. Reproduced with permission from Ref. [43].

Among recently reported pyrrole-containing chemosensors [44-46], an interesting example has been described by Sessler and co-workers [47]. The researchers designed pyrene-functionalized tetrakis-(1H-pyrrole-2-carbaldehyde) chemosensor **20**, which has an intense fluorescence in chloroform at 390 nm when excited with 365 nm wavelength light. Upon addition of $TBAH_2PO_4$ a dramatic decrease of the fluorescence emission was observed (Fig. 13b) due to a photoinduced electron transfer (PET) quenching mechanism, with a calculated LOD of 46 nM. An association constant for the formation of a 1:1 adduct of $(1.9 \pm 0.6) \times 10^6$ M^{-1} was determined. In the solid state **20** formed a sandwich-type adduct $[\mathbf{20}\cdot 3TBAH_2PO_4]_2$ in which two molecules of **20** bound an S-shaped dihydrogen phosphate hexamer (Fig. 13c) in a unique fashion.

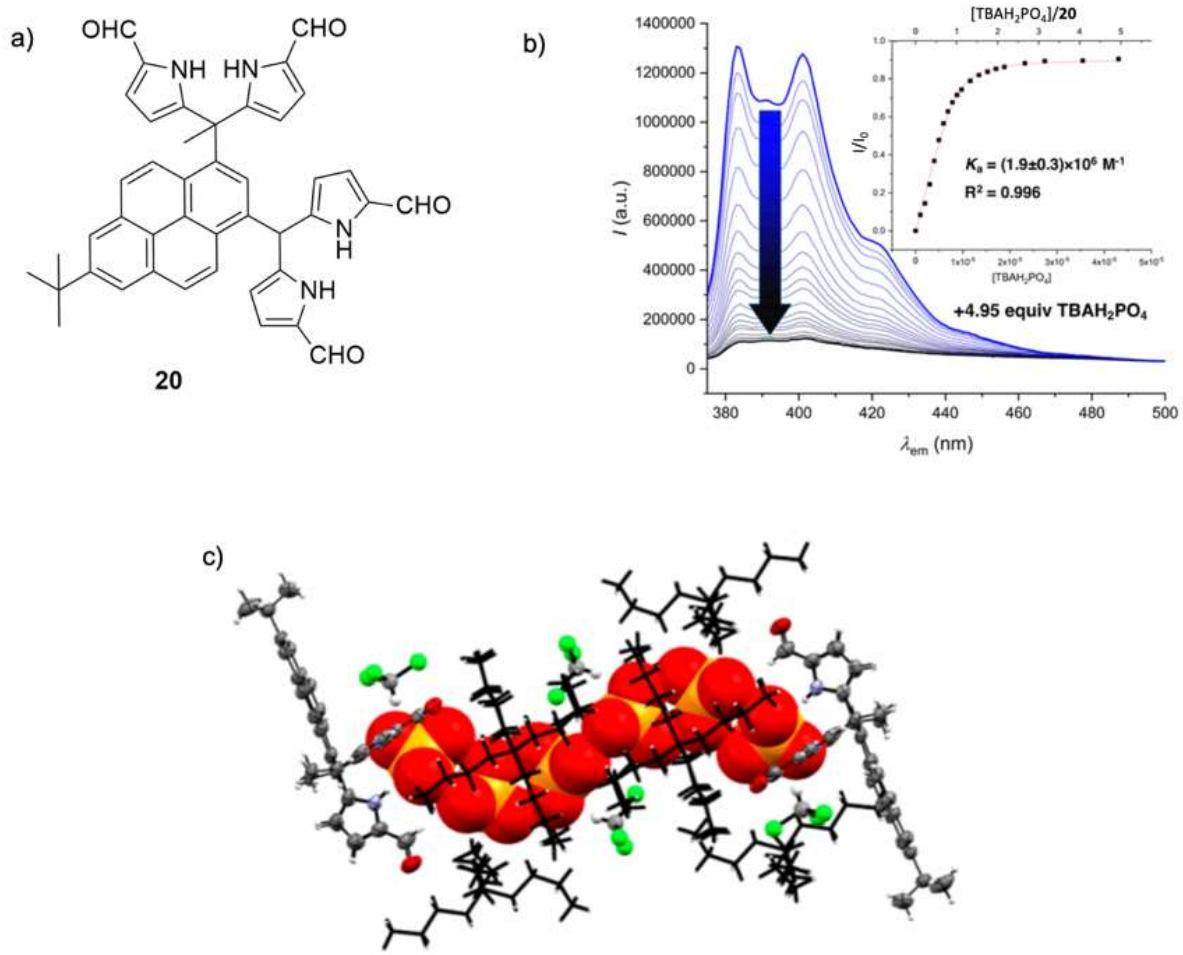

Fig. 13. a) The structure of chemosensor **20**; b) fluorescence titration of **20** with $TBAH_2PO_4$ in chloroform (λ_{ex} 365 nm, inset: nonlinear least-squares nonlinear fitting of the changes in emission intensity at 401 nm to a 1:1 binding profile; c) X-ray crystal structure of the receptor-phosphate adduct [**20**·3$TBAH_2PO_4$]$_2$ showing the dihydrogen phosphate hexamer sandwiched between two molecules of **20**. Adapted with permission from Ref. [47].

Various groups have been engaged in the development of chemosensors based around macrocyclic receptor scaffolds which include polyamines, calixarenes, calixpyrroles and porphyrins[48-56]. Kataev and co-workers proposed the bicyclic, anthracene-containing receptor **21** as an OFF-ON chemosensor for nitrate in buffered aqueous solution [57]. In 50 mM acetate buffer solution (5% DMSO, pH 3.6), an increase in fluorescence emission of the free chemosensor was observed upon addition of $NaNO_3$. The observed behaviour was rationalised by the authors by suggesting that nitrate, a chaotropic anion, disrupts the solvation shell inside and outside **21** leading to diminishing rates of nonradiative quenching processes induced by surrounding water. ITC titrations revealed that nitrate recognition (log K_{11} = 2.49 $\pm$ 0.2), has both an enthalpically and entropically favourable contribution, with the latter being attributed to the release of one or more water molecules from the cavity of the receptor upon binding. The same research group also reported macrocycle **22**, which is able to selectively bind cyclic guanosine monophosphate (cGMP) (Log K = 4.91 in 50 mM acetate buffer (2% DMSO, pH 3.6)) over other nucleoside mono-, di-, and triphosphates. The macrocyclic core of the receptor is responsible for the recognition of the phosphate residue, while the naphthalimide fragment is able to intercalate with nucleobases and with the aromatic rings of the receptor [58].

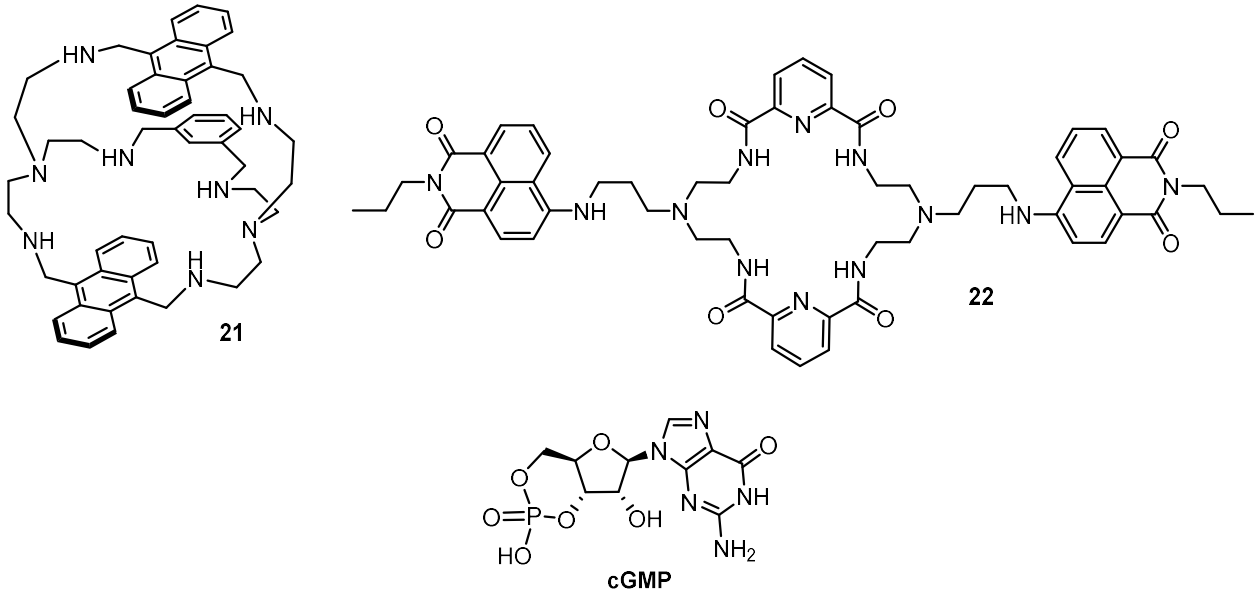

Fig. 14. The structures of macrocyclic chemosensors **21**, **22** and monophosphate anion cGMP.

A fluoride selective chemosensor based on *p-tert*-butyl-calix[4]arene (**23**), functionalised with a benzooxadiazole fluorescent signalling unit, was reported by Rao and co-workers [59]. Among the various anion guests tested, a selective quenching of the emission band at 520 nm was observed only upon addition of fluoride to a solution of **23** in THF (Fig. 15b). The group proved the recognition event is reversible upon addition of 0.5 equiv. Ca^{2+}, as the original emission of the free chemosensor was restored. The formation of a 1:1 adduct with fluoride in solution was confirmed by ESI-MS and ^{1}H-NMR spectroscopy and DFT calculations revealed the formation of six non-covalent interactions of the type X-H···F (where X = O, N, or C). Interestingly, **23** self-aggregated in THF forming a 3D sheet of aggregates, as revealed by SEM and TEM studies (Fig. 15c. a,c). However, after the addition of F^{-}, smaller spherical particles of approximately 20-30 nm size were formed (Fig. 15c. b,d). The F^{-} induced disaggregation of **23** was further proven by optical microscopy images, displayed in Fig. 15c. e,f, and fluorescence microscopy revealed the fluorescence quenching of **23** upon addition of the anion (Fig. 15c. g,h). Finally, confocal fluorescence microscopy on HeLa cells demonstrated that **23** is able to detect fluoride *in vitro* (Fig 15d).

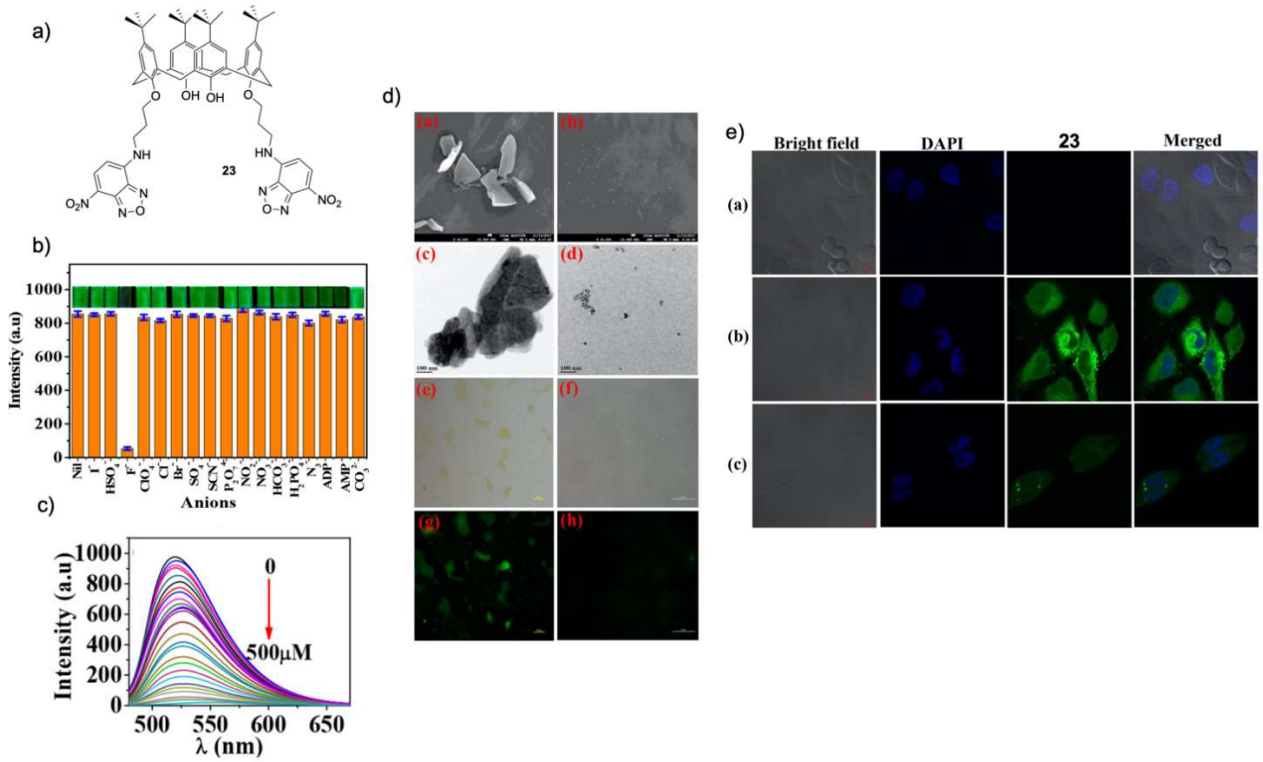

Fig. 15. a) The structure of calixarene **23**; b) plot of emission intensity of **23** at 520 nm vs different anions and photographs of the vials containing **23** + 5 equiv. anion in THF when illuminated under UV light; c) emission spectra of **23** upon addition of increasing amounts of fluoride in THF; d) Left column (a, c, e, g) **23** and right column (b, d, f, h) **23** + F^-. (a and b) SEM images. (c and d) TEM images. (e and f) Optical microscopy images. (g and h) Fluorescence microscopy images. Scale bar for micrographs: (a-d) 100 nm; (e, f) 100 µm; (g, h) 50 µm; e) Confocal microscopy images of HeLa cells: (a) cells without treatment; (b) cells treated with **23**; (c) cells incubated with fluoride after treatment of L. The blue colour represents nuclei stained with DAPI, green color represents **23**. The scale bar for all confocal microscopy images in a-c is 10 µm. Adapted with permission from Ref. [59].

The fluorescence sensing, in acetonitrile, of aromatic and aliphatic dicarboxylate anions of different shapes and lengths was reported by Sessler, Tian and co-workers using the bis-calix [4]pyrrole chemosensor **24** incorporating a vibration-induced emission (VIE) phenazine core [60]. VIE is a recently reported fluorescence phenomenon in which the reversible bent-to-planar motion of two aromatic moieties is used to produce multiple emissions from a single chromophore system, firstly discovered in Tian's laboratory [61]. In chemosensor **24** calix[4]pyrrole is the anion recognition site, while 9,14-diphenyl-9,14-dihydrodibenzo[a,c]phenazine (DPAC) is the VIE probe. As shown in Fig 16a, the shape and the geometry of the dicarboxylate analytes can induce a unique fluorescent signature allowing discrimination to be achieved by simple visualization using the naked eye. Addition of linear saturated dicarboxylate guests (C2—C12) to a solution of **24** in acetonitrile did not cause any significant change to the UV-Vis spectrum of the free chemosensor, suggesting that the ground-state properties of the systems are not affected by the presence of the anions. Conversely, emission spectra showed remarkable changes (Fig. 16b) with a unique point on the chromaticity coordinates (CIE) for each 1:1 adduct (Fig 16C). Chemosensor **24** was also able to discriminate between the three phthalate isomers. The differences and very specific responses observed in the presence of the various anionic guests were ascribed to the different degrees of DPCA planarization imposed by the recognition event.

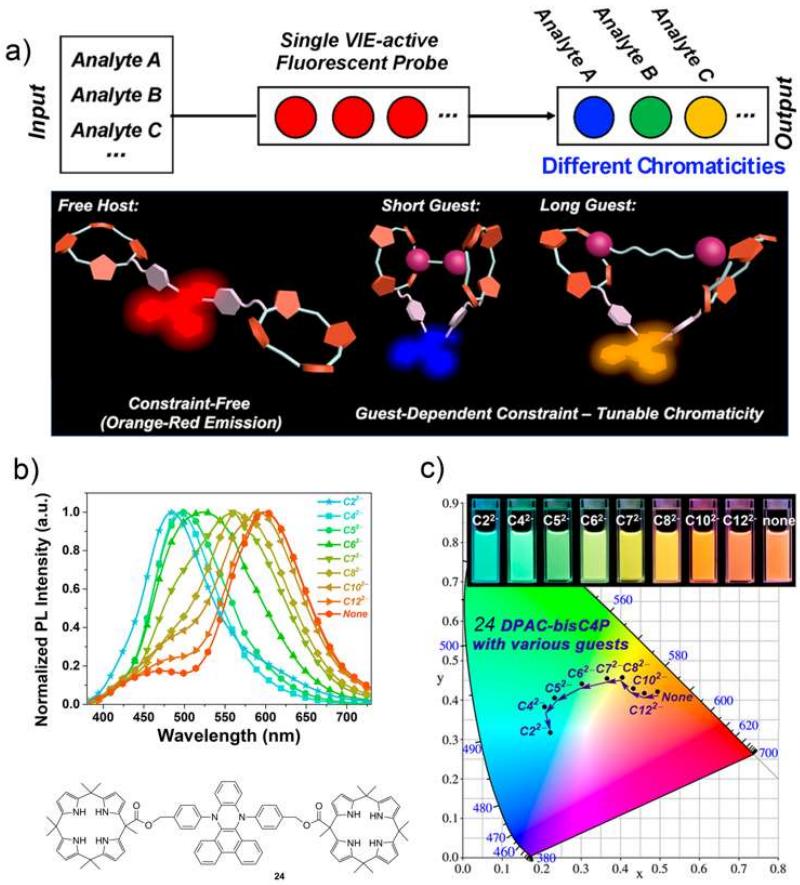

Fig. 16. a) Proposed mechanism for the fluorescence tuning and dicarboxylate anion sensing of **24**; b) fluorescence emission spectra of free **24** and in the presence of various linear saturated dicarboxylates at the end of titrations in acetonitrile; c) chromaticity coordinates (CIE) of free **24** and the host-guest adducts of **24** with dicarboxylate guests in acetonitrile, inset: fluorescence images of the adducts and free **24** recorded in acetonitrile upon irradiation with 365 nm UV light. Adapted with permission from Ref. [61].

3. Halogen bond chemosensors

The design of halogen-bond (XB) based receptors for anion recognition has been an active research field in recent years [62, 63]. Caballero, in collaboration with Molina, described the ability of the Zn^{2+} complex of chemosensor **25** (Fig. 17) to recognize HSO_4^- over a large set of anions in acetonitrile [64]. An increase in intensity and concomitant blue shift of the emission band of the complex [**25**·2Zn]$^{4+}$ was observed upon addition of one equivalent of HSO_4^-. DFT calculation demonstrated that upon chelating the metal ion with two imidazole nitrogen atoms, the receptor could adopt an ideal conformation for HSO_4^- through a combination of C(sp^2)–H···O and C(sp^3)–H···O hydrogen bonding, C^+(sp^2)–Br···O halogen bonding and C(sp^2)···O tetrel bonding.

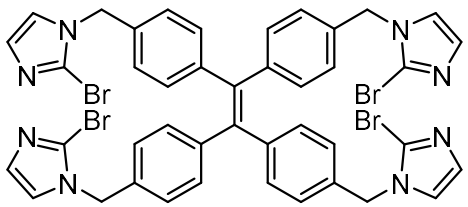

26

Fig. 17. The structure of chemosensor **25**.

Beer and co-workers described a family of novel chiral halogen (**26a**) and chalcogen (**26b**) bonding receptors which exhibit different levels of selectivity for stereo- and geometric dicarboxylate isomers (S and R tartates and glutamates, maleate, fumarate, phthalate and isophthalate), compared to a hydrogen bonding analogue (**26c**) (Fig. 18a) [65]. After a careful evaluation of the binding properties of the three receptors, both **26a** and **26b** displayed augmented discrimination for dicarboxylate geometric isomers compared to **26c**, dictated by more prominent directionality and better host–guest size and geometric complementarity as demonstrated through MD simulations. The authors described their properties as fluorescent chemosensors in acetone/H_2O (85:15 v/v). The addition of all anions resulted in an increase of the fluorescent emission band of **26a**, attributed to a modulation of the intramolecular heavy-atom effect due to the XB-donor iodine atoms interacting with the anion guest species, concomitant with notable bathochromic shifts of the emission band (Fig. 18b). With **26c**, all anions elicited significant fluorescence quenching with a hypsochromic shift of the maximum present in the case of isophthalate. In comparison, **26b** displayed unique fluorescence intensity responses with different fluorescent responses upon binding of different dicarboxylate anions (Fig. 18c). Compared with **26a**, the greater stability of **26b** to anions and more varied fluorescent responses renders this σ-hole receptor potentially more useful for optical guest discrimination.

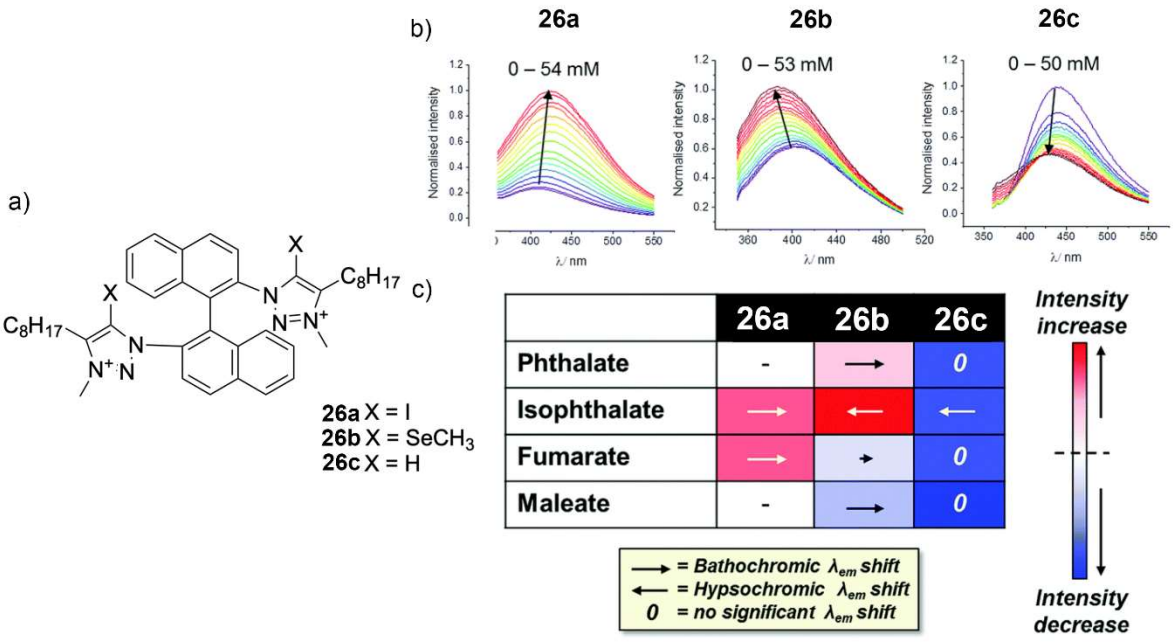

Fig. 18. a) The structure of chemosensors **26a**-**c**; b) fluorescence spectra of chemosensors **26a** (λ_{ex} = 325 nm), **26b** (λ_{ex} = 330 nm) and **26c** (λ_{ex} = 320 nm) in the presence of increasing quantities of isophthalate, with concentrations indicated; c) summary chart of the fluorescence intensity changes and λ_{em} shifts for each chemosensor with different dicarboxylate geometric isomers. The length of each arrow denotes the

magnitude of λ_{em} shift while the shade of red/ blue indicates the extent of fluorescence change from 0 to 20 mM of guest ([host] = 50 mM; acetone/H_2O (85 : 15 v/v), T = 293 K). Adapted with permission from Ref. [65].

The Beer group also reported the enantioselective binding of dicarboxylate anions with rotaxane **27**, containing two pyridinium bis-iodotriazole units promoting halogen-bonding, connected by a central (S)-BINOL motif as the fluorescent active unit [66]. The incorporation of two macrocycles onto the axle allowed for the recognition of dicarboxylates by the formation of 1:1 stoichiometric sandwich-type complexes. Rotaxane **27** was able to discriminate between dicarboxylate enantiomers ((S)Glu^{2-}> (R)-Glu^{2-},K_S/K_R= 5.7), and geometric isomers (Fum^{2-}>-Mal^{2-},K_{Fum}/K_{Mal}= 4.4), when analysed using fluorescence titration experiments in a $CHCl_3/CH_3OH/H_2O$ (60:39:1 v/v/v) solvent mixture. Complete quenching of rotaxane emission was observed, albeit in the presence of large excesses of analyte.

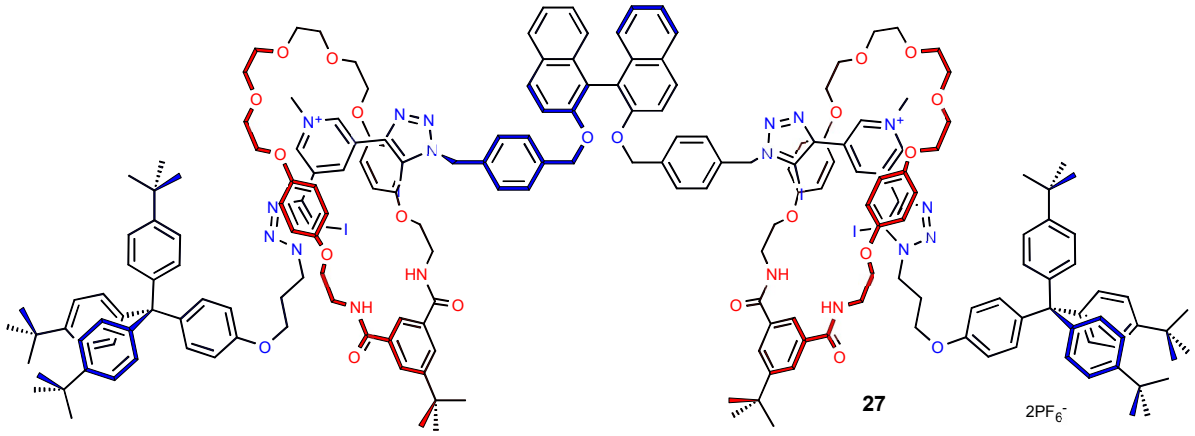

Fig. 19. The structure of rotaxane **27**.

[2]Rotaxane **28**, reported by the same group, contains a benzimidazole-iodotriazole XB station directly conjugated to a naphthalimide station [67]. In $CHCl_3$, the macrocycle shuttled between stations in response to the protonation state of the host and the nature of the counter anion. In its neutral state, the electron rich hydroquinone macrocycle was found to reside at the electron deficient aromatic naphthalimide station, and addition of Cl^- or protonation with HBF_4 did not induce shuttling. Only the addition of aqueous HCl, or Cl^- to the HBF_4 complex of **29**, resulted in translocation of the macrocycle to the XB donor station, with a corresponding naked-eye detect-able colour change of the solution and increase in fluorescence intensity (Fig. 20).

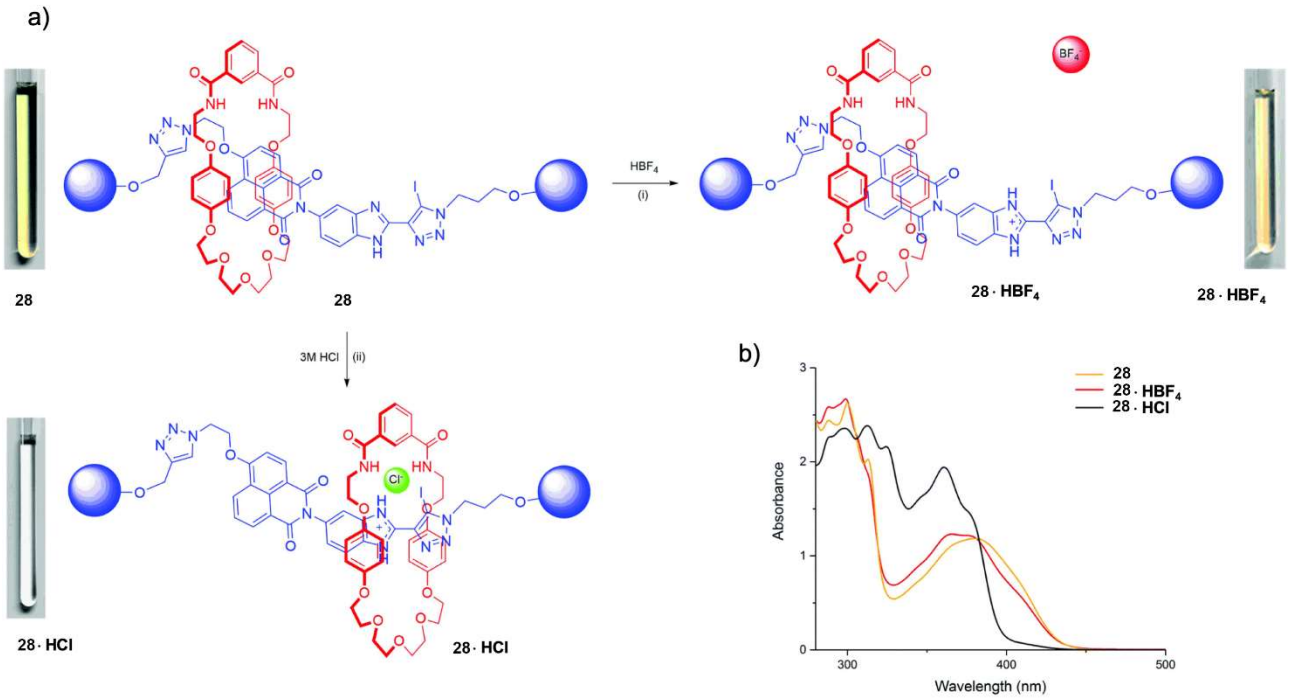

Fig. 20. a) Protonation of [2]rotaxane **28** with (i) HBF_4, causing no significant change in colour, and (ii) HCl, inducing loss of colour, indicative of macrocycle translocation; b) UV-vis spectra of each rotaxane in $CHCl_3$. Significant spectral change upon HCl addition compared to HBF_4 addition suggests observed colour changing behaviour. Adapted with permission from Ref. [67].

4. Boron-based chemosensors

Boron sensors relying on Lewis acidic boron centres or boron dipyrromethane (BDP) and dipyrrolyldiketone boron motifs have been used in a number of anion sensors recently. Xing, Zhang and co-workers have reported the synthesis of aza-boron dipyrromethene derivative (BDP) **29** for the continuous ratiometric recognition and imaging of superoxide anion ($O_2^{\cdot-}$) and glutathione (GSH) *in vivo* [68]. The *ortho*-phenolic hydroxyl groups on BDP can be reversibly and readily oxidized *in vitro* and *in vivo* by the superoxide anion with a concomitant absorbance drop at 680 nm and increase at 750 nm, leading to large photoacoustic (PA_{750}/PA_{680}) ratio (Fig. 21) [68]. GSH can reduce the 1,2-benzoquinone derivative **30** to **29** resulting in recovery of the photoacoustic ratio [68].

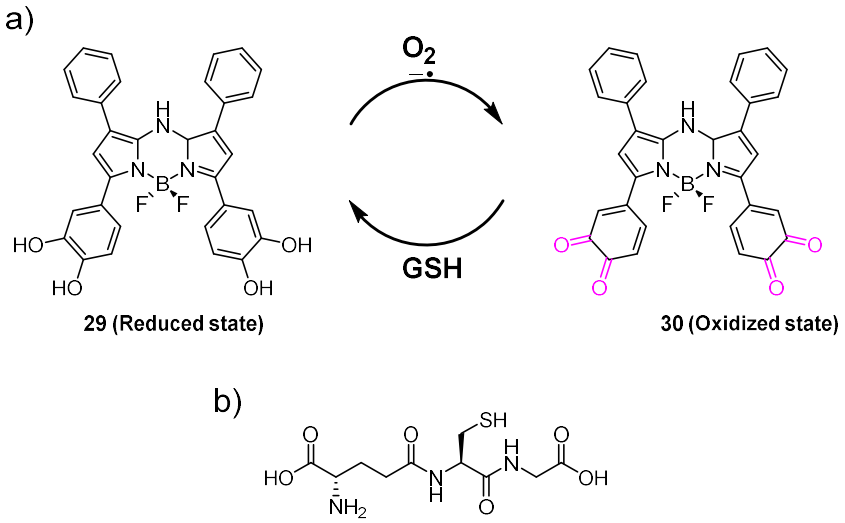

Fig. 21. a) Schematic representation of the reversible photoacoustic recognition of the superoxide anion and GSH by probe **29**; b) structure of the glutathione anion.

Photoacoustic tomography is a non-invasive technique based on light-induced ultrasound wave detection merging optical illumination and ultrasound (US) detection (Fig. 22a) [68]. Probe **29** showed selective sensing of the superoxide anion over the other species tested (hypochlorite, peroxynitrate, iron III, copper II, hydrogen peroxide and oxygen) in phosphate buffered saline (PBS) buffer at pH = 7.4 (Fig. 22b). Interestingly, compound **29** showed a ratiometric photoacoustic ratio (PA_{750}/PA_{680}) with superoxide anion and GSH (Fig. 22c and 22d) [68]. As shown in Fig. 22e, the superoxide anion-initiated increase in the photoacoustic ratio could be recuperated to the original value after glutathione addition [68], and this behaviour was could be repeated through three cycles of addition and at different concentrations of the superoxide anion and GSH. The switchable fluorescence ON-OFF-ON behaviour of probe **29** was studied in EMT6 cells and in mice (Fig. 22a) [68]. The results suggested the feasibility of probe **29** in visualizing the redox state in living systems and the ability of this system to identify redox state changes with high resolution [68].

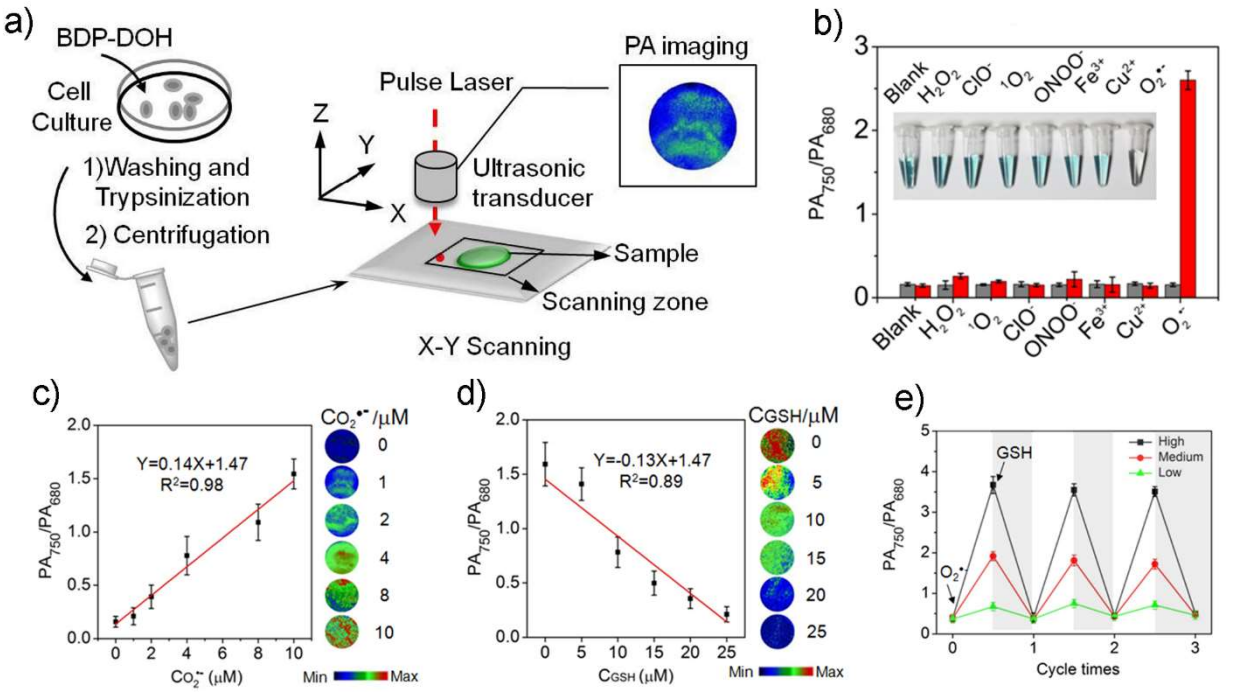

Fig. 22. a) Schematic presentation of photoacoustic (PA) imaging by X-Y scanning; b) photoacoustic ratio (PA_{750}/PA_{680}) intensity toward superoxide anion and other analytes; c) the PA_{750}/PA_{680} intensity of probe **29** with different concentrations of superoxide anion and d) subsequent addition of GSH; e) redox cycles of 10 µM of probe **29** by the addition of superoxide anion (20, 5, and 1 µM) followed by GSH (50, 10, and 5 µM) in PBS buffer solution (pH 7.4). Adapted with permission from Ref. [68].

Maeda in collaboration with Kobayashi and Yasuda recently described poly aryl-substituted dipyrrolyldiketone boron complexes **31** and **32** that demonstrated anion-responsive emissive properties (Fig. 23) [69]. Single-crystal X-ray analysis of **31** revealed the complex's twisted structure due to steric hindrance by the 3-phenyl rings (Fig. 24a). Interestingly, compound **31** adopted a sandwich-like [2:1] binding mode with chloride as illustrated in the X-ray crystal structure of $(\mathbf{31})_2Cl^-TBA^+$ (Fig. 24b). The complex is stabilized by hydrogen bonding of chloride with the pyrrole NHs, CHs from the bridge and from the adjacent phenyl rings. Conversely to the X-ray analysis data, ^1H NMR titrations of compound **31** in CD_2Cl_2 with chloride provided evidence in support of the formation of a [1:1]-type complex *via* hydrogen bonding of Cl^- with the pyrrole NHs and bridging CHs in solution.

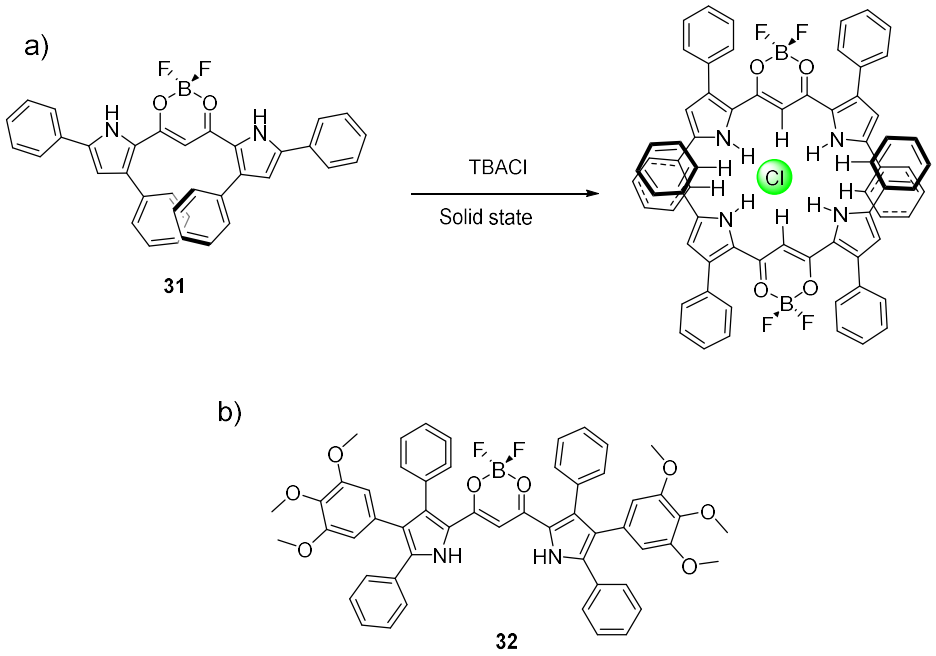

Fig. 23. a) Chloride binding behaviour of **32** as demonstrated from X-ray crystal structures of the probe **31** and for $(\mathbf{31})_2 \cdot Cl$ complex; b) chemical structure of compound **32**.

Upon addition of increasing amounts of chloride and bromide as tetrabutylammonium salts to compound **32** in dichloromethane, an increase of the intensity of the fluorescence emission was observed (Fig. 24c-e). Addition of acetate resulted in a quenching in the fluorescence intensity, which was attributed to photoinduced electron transfer (PET) from the anion binding site to the core unit.

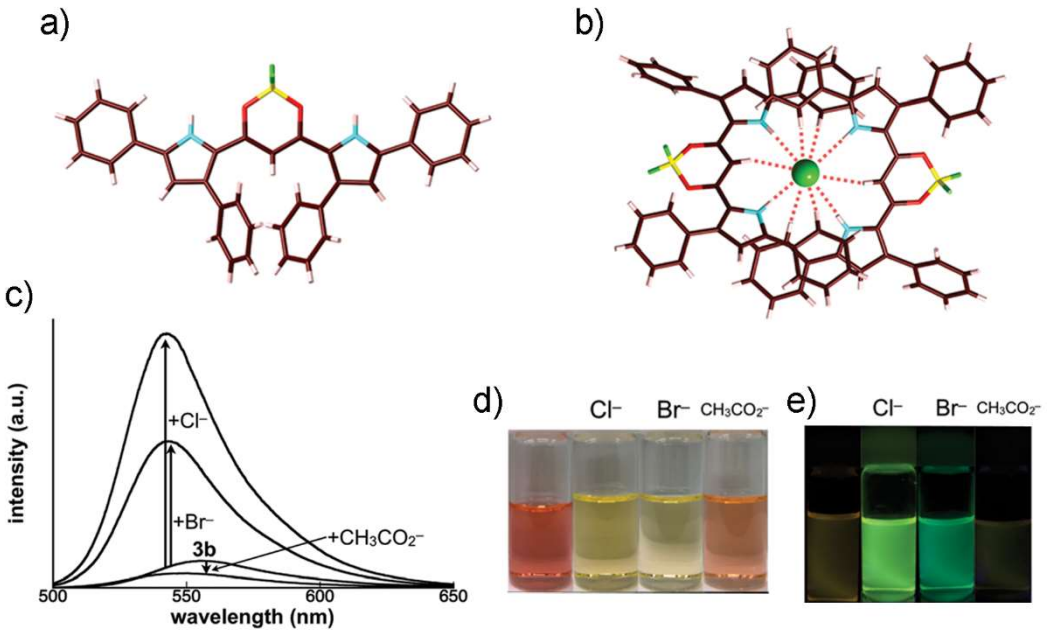

Fig. 24. Single-crystal X-ray structures of a) **31**; b) (**31**)$_2$.Cl^-; c) change in fluorescence emission intensity of **32** in CH_2Cl_2 upon the addition of Cl^-, Br^- and $CH_3CO_2^-$ as TBA salts; d) photographs of probe **32** in CH_2Cl_2 in the absence and presence of anions as TBA salts of Cl^-, Br^- and $CH_3CO_2^-$ under visible light and e) 365 nm UV light. Adapted with permission from Ref. [69].

Lewis, James and co-workers have developed boron-based azulene-based colorimetric probe **33** (Fig. 25a) for fluoride recognition [70]. Addition of different anions (F^-, Cl^-, Br^-, I^-) to the THF solution of probe **33** resulted in colour change in the case of fluoride only which could be observed by the naked eye (Fig. 25b). The authors rationalized this behaviour to the occupation of a vacant *p*-orbital on the boronic ester in **33** by fluoride with rehybridization from sp^2 to sp^3. This was confirmed using ^{11}B NMR experiments, and resulted in a change in the degree of conjugation experienced by the sensor [70]. Anion sensing of a series of anions (Fig. 26a) usually found in drinking water using probe **33** was investigated in EtOH/water (3:7 v/v) with a colour change only observed in the presence of fluoride and a limit of detection (LOD) = 5.75 mg/L [70]. Probe **33** was titrated in EtOH/water (3:7 v/v) with increasing concentrations of fluoride and a colour change occurred after 10-20 equivalents of NaF (Fig. 26b). The authors attributed the requirement for excess fluoride to reach the maximum spectroscopic response to the competition of hydroxide to bind boron and the extensive fluoride solvation shell in aqueous solution [70].

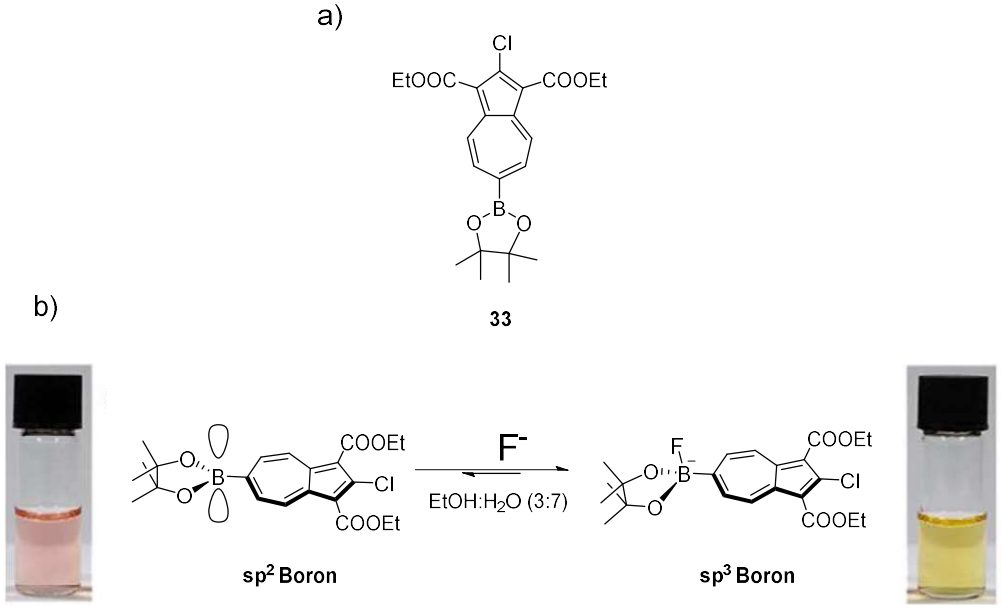

Fig. 25. a) Chemical structure of compound **33**; b) proposed mechanism of fluoride binding to the vacant *p*-orbital on the boronic ester in **33** which results in rehybridization from sp^2 to sp^3. Adapted with permission from Ref. [70].

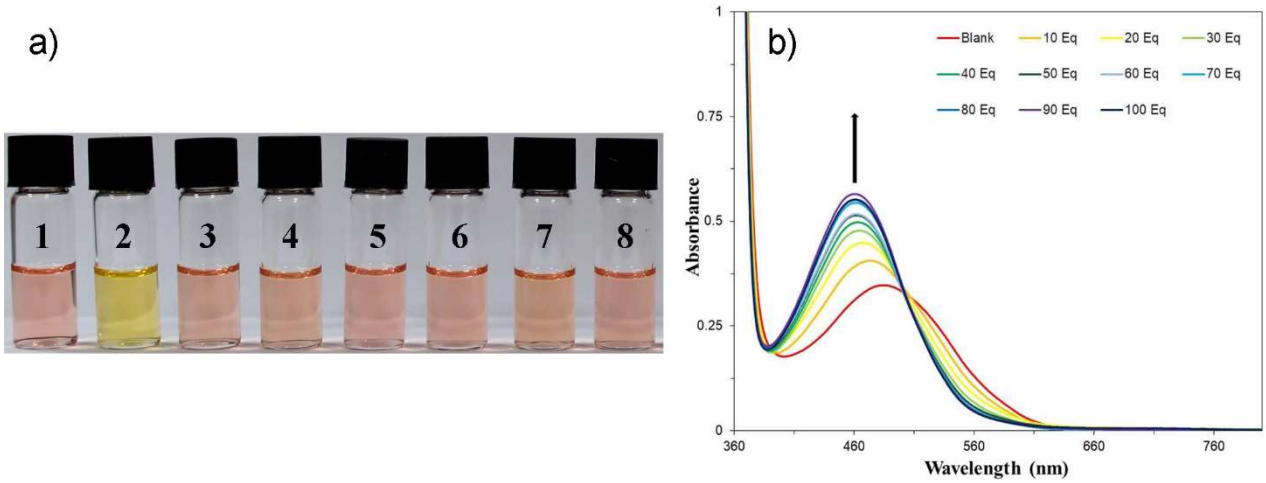

Fig. 26. a) Visual colour changes of probe **33** (0.5 mM) in EtOH/H_2O, (3:7 v/v) with 60 equivalents of analyte used. Each sample was incubated for 30 mins before spectra recording. (1) No analyte, (2) NaF, (3) NaCl, (4) NaBr, (5) NaI, (6) $NaNO_3$, (7) NH_4Cl, (8)Na_2SO_4; b) UV-vis titrations of compound **33** (0.5 mM) in EtOH/water (3:7 v/v) with NaF. Each sample was incubated for 30 min before spectra recording. Adapted with permission from Ref. [70].

5. Metal-based chemosensors

Transition-metal complexes are electron deficient, often photoactive, and exhibit well defined geometries with their organic ligands. They may be used for sensing when the addition of an anionic species results in a disruption of this geometry and/or induces a change in optical properties [71]. Recent examples have detected anions either *via* coordination and interaction directly with the metal centre [72-75], or by inducing changes in the coordination environment by binding to a ligated organic group [76-80].

Cao and co-workers have creatively repurposed platinum complex **34** as a halide-selective sensor (Fig. 27a) [81]. The square planar complex is non-emissive in aqueous solution, however in the presence of halide ions the system self-assembles to form higher-order stacked aggregates. Reduced intermolecular Pt-Pt distances result in the promotion of an intense, red-shifted phosphorescence band *via* metal-metal-to-ligand charge transfer (^{3}MMLCT) transitions [82]. An increase in chloride concentration (0-10 mM) lead to a significant increase in band intensity, as shown in Fig. 27b, and the probe was found to be robust both in the presence of competing ions and over a large pH range (3.0-9.0). These features prompted researchers to use the probe to monitor the concentration of chloride in living cells (Fig. 27c), which allowed changes in intracellular concentration to be successfully detected.

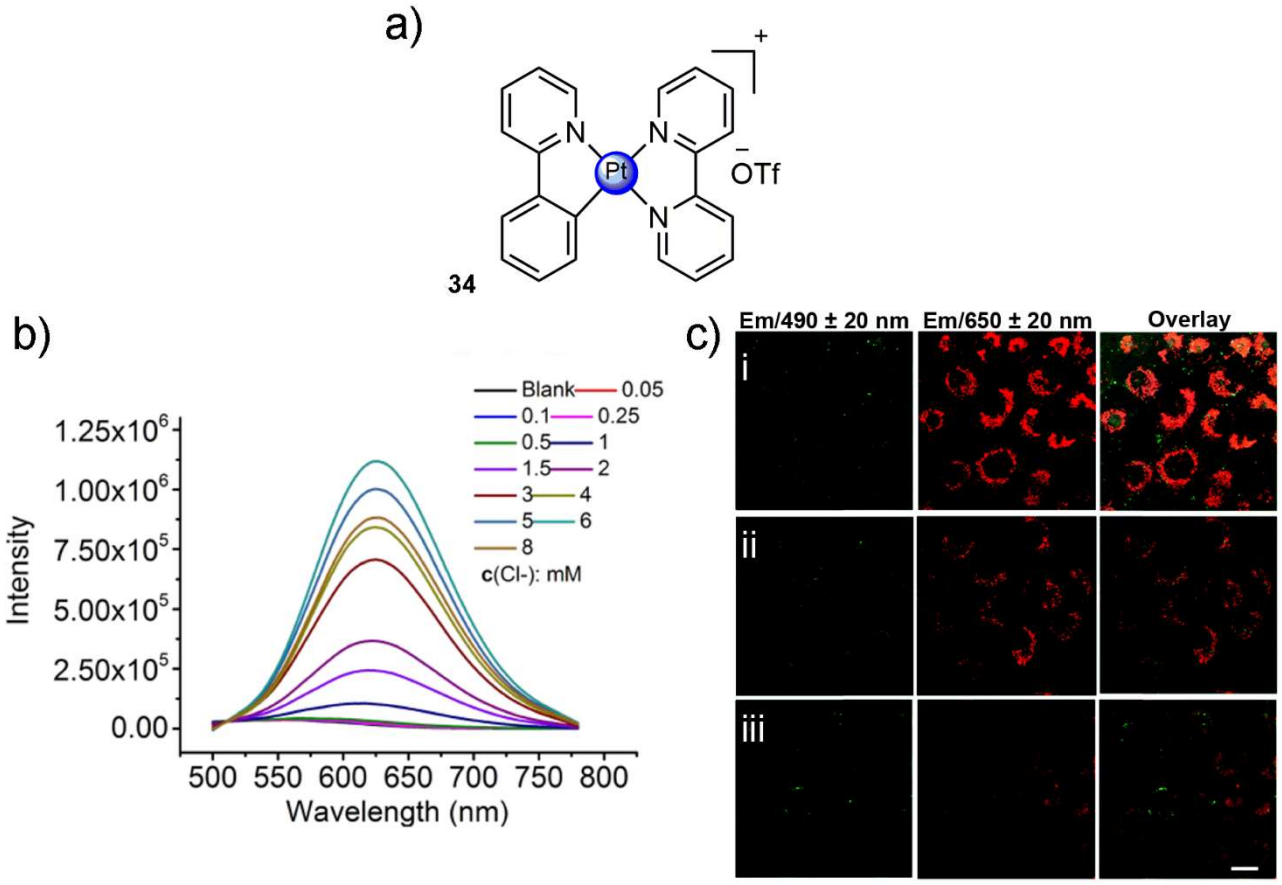

Fig. 27. a) The chemical structure of receptor **34**; b) emission spectra of **34** (20 µM) in H_2O when titrated against increasing concentrations of Cl^-; c) fluorescence imaging of MCF-7 cells treated with **34** (50 µM, 1h) in different solutions: i) Normal cell media (110mM of Cl^-); ii) Cl^- deficient media (4 mM); iii) Cl^- free buffer. The red channel emission is more intense at higher Cl^- concentrations. Adapted with permission from Ref. [81].

Sankar and co-workers reported the novel colorimetric detection of cyanide$^-$ using dodeca-substituted $Co^{(II)}$ porphyrins **35** and **36**, shown in Fig. 28a [83]. Interestingly, while many anions were able to axially coordinate to the metal centre, only cyanide triggered a colour change from yellow to red in a toluene solution (Fig. 28b). Upon addition of this anion to a solution of **35**, the absorbance bands at 447 and 561 nm decreased whilst new bands at 397 and 489 nm appeared, then increased ratiometrically (Fig. 28c). Electrochemical studies lead the researchers to attribute the change to an irreversible metal oxidation event ($Co^{(II)}$ to $Co^{(III)}$) by the cyanide anion followed by coordination to the oxidised centre. Interference experiments (Fig 28d) indicated that cyanide caused this oxidation-coordination pathway to occur even in the presence of other anions, confirming the high degree of selectivity exhibited by this probe.

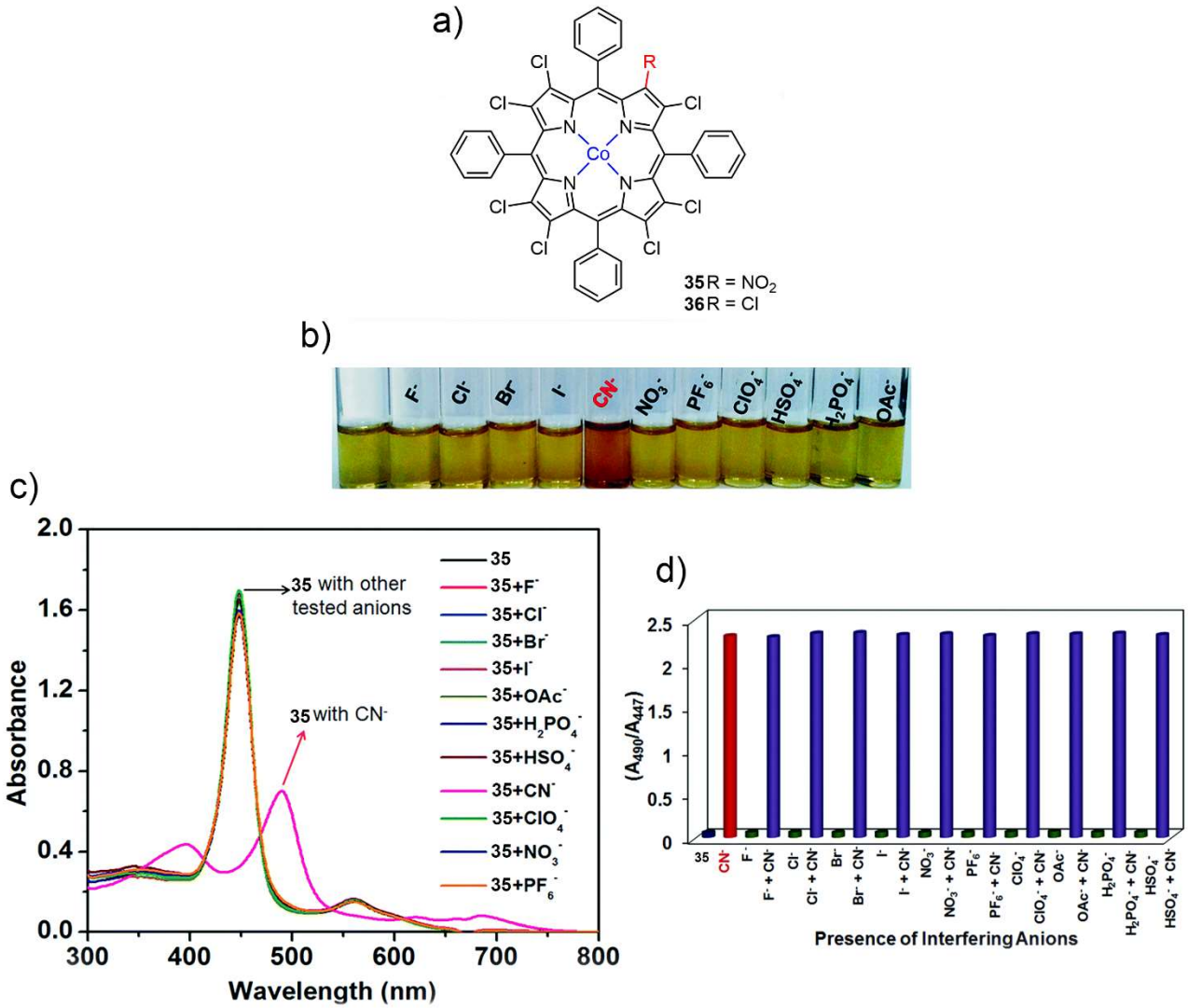

Fig. 28. a) Chemical structures of receptors **35 and 36;** b) colour change induced by TBACN addition to a solution of **35** in toluene at 298K, compared to the addition of other TBA salts; c) absorption spectra changes of **35** upon addition of excess TBA salts of anions in toluene at 298K; d) ratio of absorbance changes of **35** (10.4 μM) upon addition of an interfering anion (green, 10 equiv.) followed by the addition of CN^- (blue, 1-2 equiv.). Adapted with permission from Ref. [83].

Lanthanide complexes have unique properties that may be exploited in the field of anion sensing. Appealingly, luminescence from this class of complex gives rise to sharp emission peaks and has a relatively long lifetime, meaning that time-gated measurements can be implemented to remove background fluorescence in complex environments. Their affinity for various analytes can be modified though changes in ligand structure or by altering the coordination number of the central metal ion [84, 85]. An anion binding event can lead to detectable optical changes caused by alterations in the lanthanide-ligand coordination environment or by displacement of emission quenching water molecules, as demonstrated by a number of recent examples [85-89].

Europium-based probe **37,** developed by the Pierre group, recognises cyanide in pure water [90]. The complex (Fig. 29) includes a pendant lysine, to increase aqueous solubility, and an expanded coordination

sphere. The complex also contains three coordinated water molecules which act to quench the luminescence of the lanthanide centre. Direct coordination of cyanide causes displacement of water from the inner-sphere, leading to a 9-fold increase in luminescence and a naked-eye colour change under UV irradiation. Researchers discovered that all three water molecules were removed from the complex during binding, suggesting CN^- coordination in a 1:3 binding mode. The probe was also found to bind phosphate, carbonate, and fluoride, however their interference was removed in the presence of $CaCl_2$ which forms insoluble salts with these anions but not with CN^-.

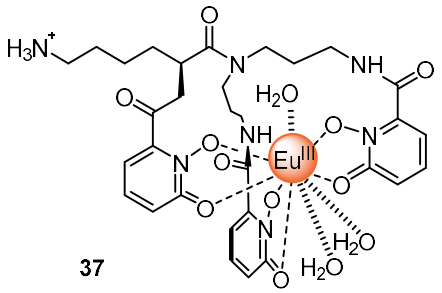

37

Fig. 29. Structure of europium-containing receptor **37**.

Parker and co-workers studied the sensing ability of their europium receptors, including **38** (Fig 30a)**,** towards the herbicide glyphosate in water [91]. Coordination of the phosphate group to the metal centre displaces a weakly bound pyridine, and the phosphate is stabilised further through a hydrogen bond with the tertiary amine (Fig. 30b). This interaction disrupts the lanthanide coordination sphere and causes a sharp increase in emission band intensity as well as a change in spectral form, as seen in Fig. 30c. Researchers plotted the ratio of intensities ($I_{604\text{-}614}/I_{614\text{-}620}$) for this receptor as a function of glyphosate concentration to return a linear relationship up to a saturation limit of 50 µM. Additionally, $ZnCl_2$ was added to each receptor solution to assess the effect of Zn^{2+} coordination by the picolyl groups on glyphosate affinity. However, no enhancement in sensing ability was recorded.

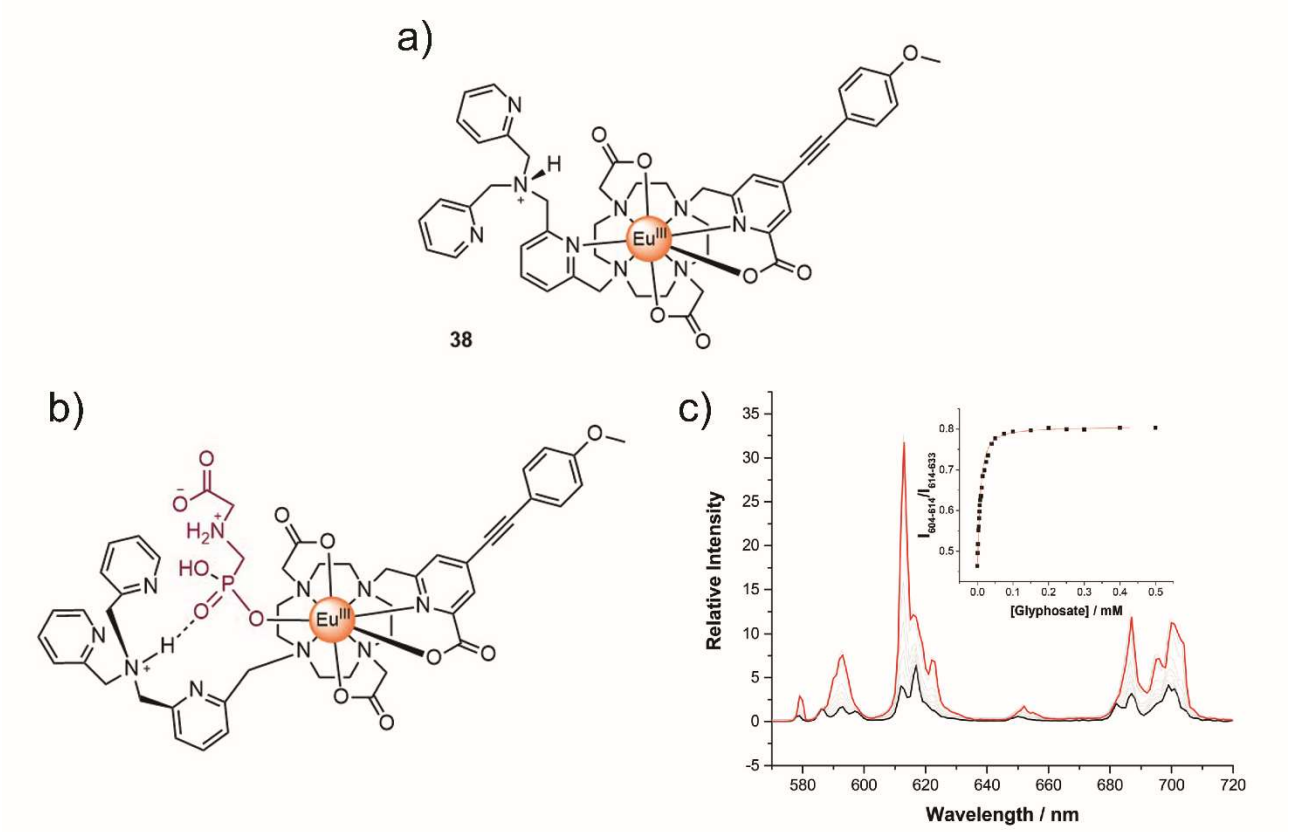

Fig. 30. Chemical structure of lanthanide receptor 38; b) schematic representation of the glyphosate binding mode of receptor **38**; c) change in emission intensity of **38** (6 μM, 0.1M NaCl, 0.1M MES, pH 5.9, 295 K, λ_{ex} 365 nm) before (black) and after (red) the addition of glyphosate, inset: ratio of emission intensities ($I_{604-614}/I_{614-633}$) against increasing glyphosate concentration. Adapted with permission from Ref. [91].

6. Anion Sensing Using Excimers

An excimer is formed following the association of an excited fluorophore with a molecule of the same species the ground state [92]. Fluorophores often interact due to π–π stacking, and excimer formation is commonplace amongst molecules with extended π systems such as derivatives of pyrene, anthracene and naphthalimide. Excitation energy is distributed across these extended structures, leading to fluorescence emission from the 'excited dimer' at a longer wavelength than that of the excited monomeric form. This photophysical property has been cleverly employed in anion sensing, including several recent examples discussed hereafter. A binding event may either assist in the formation of, or inhibit the assembly of an excimer, therefore inducing a detectable change in the fluorescence spectrum.

The Caballero group have developed a motif which displays selectively towards dihydrogen phosphate [93]. The researchers synthesised tripodal receptor **39** (Fig. 31a), containing a 2-Br-imidazolium on each arm capped with an anthracene fluorophore. In an acetonitrile solution, the addition of anions $H_2P_2O_7^{2-}$, SO_4^{2-} and F^- resulted in the conversion of the imidazolium group to 2-imidazolone and a decrease in monomer emission intensity in the fluorescence spectrum. Interestingly, addition of $H_2PO_4^-$ lead not only to a perturbation in the monomeric band, but the promotion of a broad, red-shifted excimer emission peak (Fig. 31b). A colorimetric response was also produced, as phosphate was the only anion added which resulted in the formation of a yellow solution (Fig 31c). Proton NMR titration studies (in 8:2 CD_3CN:CD_3OD) supported the hypothesis that

anion-induced supramolecular polymerisation was occurring. A proposed structure, containing overlapping anthracene groups capable of excimer formation, is shown in Fig. 31d.

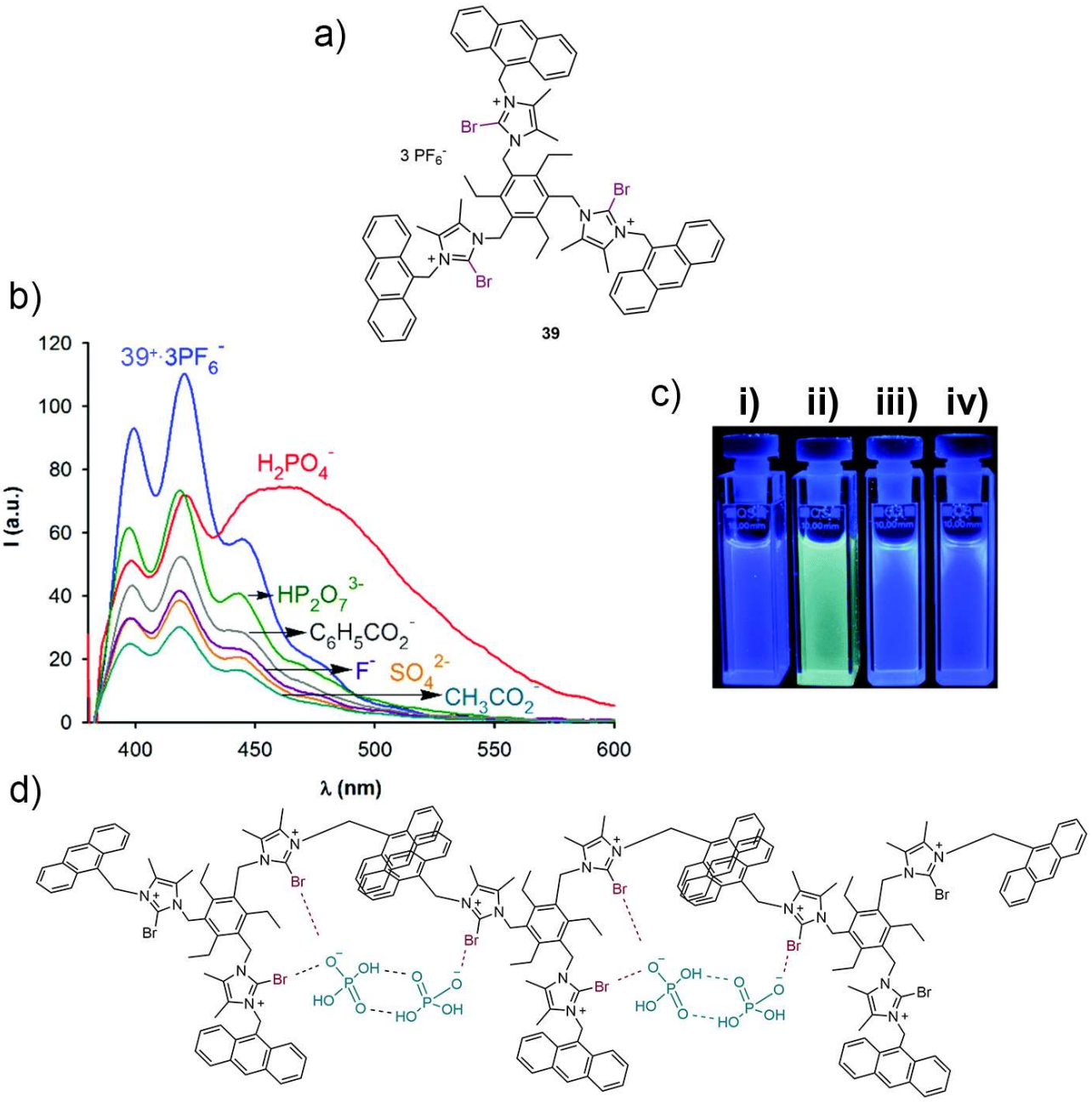

Fig. 31. a) Structure of receptor **39**; b) emission spectra of **39** (5 µM, , 298 K, λ_{ex} 370 nm) in acetonitrile upon addition of an excess of various anions; c) colorimetric response after irradiation of i) free receptor **39**, and after addition of ii) $H_2PO_4^-$, iii) SO_4^{2-} and iv) $HP_2O_7^{3-}$; d) schematic representation of the proposed polymeric structure formed between $H_2PO_4^-$ and **39**. Adapted with permission from Ref. [93].

Sessler, Gong and co-workers reported the first example of oxoanion sensing using excimer disaggregation induced emission (EDIE) [94]. Macrocycle **40**, comprised of two "halves" (one half consisting of three pyridine moieties and the other a bis-imidazolium system), was found to form excimer aggregates in acetonitrile

which had notably poor fluorescence. However, in the presence of hydrogen pyrophosphate $HP_2O_7^{3-}$, binding of the oxoanion within the macrocycle cleft resulted in disassociation of the aggregate and a greater than 200-fold enhancement in the emission intensity of the anion:monomer complex. The system was found to be highly selective and $HP_2O_7^{3-}$ could be detected in the presence of 100 equivalents of other anions. This fluorescence system also displayed a "turn-on" response for $H_2PO_4^-$ which prompted the formation of a 1:2 complex.

Saimoto and co-workers have previously reported the anion sensing properties of charged receptor **41** [95], and have since reimplemented the system as a novel polysaccharide sensor in aqueous solution [96]. The presence of sulfate-containing polysaccharides, such as **42**, induced a change in the wavelength of maximum emission from the monomer peak (395 nm) to a new excimer peak (495nm), as shown in Fig. 32b. This was discovered to be more pronounced as the number of sulfate groups present on the polymer increased. The switch was attributed to the aggregation of **41** in the presence of polymers *via* ionic bonding, which promotes excimer formation. Polysaccharides containing carboxylates induced a less significant degree of monomer-excimer switching, however they could be distinguished under UV irradiation due to a different decay process. A colour change from colourless to yellow occurred for solutions of **41** and a carboxylate-containing polysaccharide, most likely due to a photo-induced charge transfer reaction (Fig. 32c). This colour change faded over time but the absorbance peak maximum at 340 nm was not fully restored, indicating the photoreaction was irreversible. Elsewhere, researchers have developed a turn-off excimer emission receptor for chiral amino acids [97].

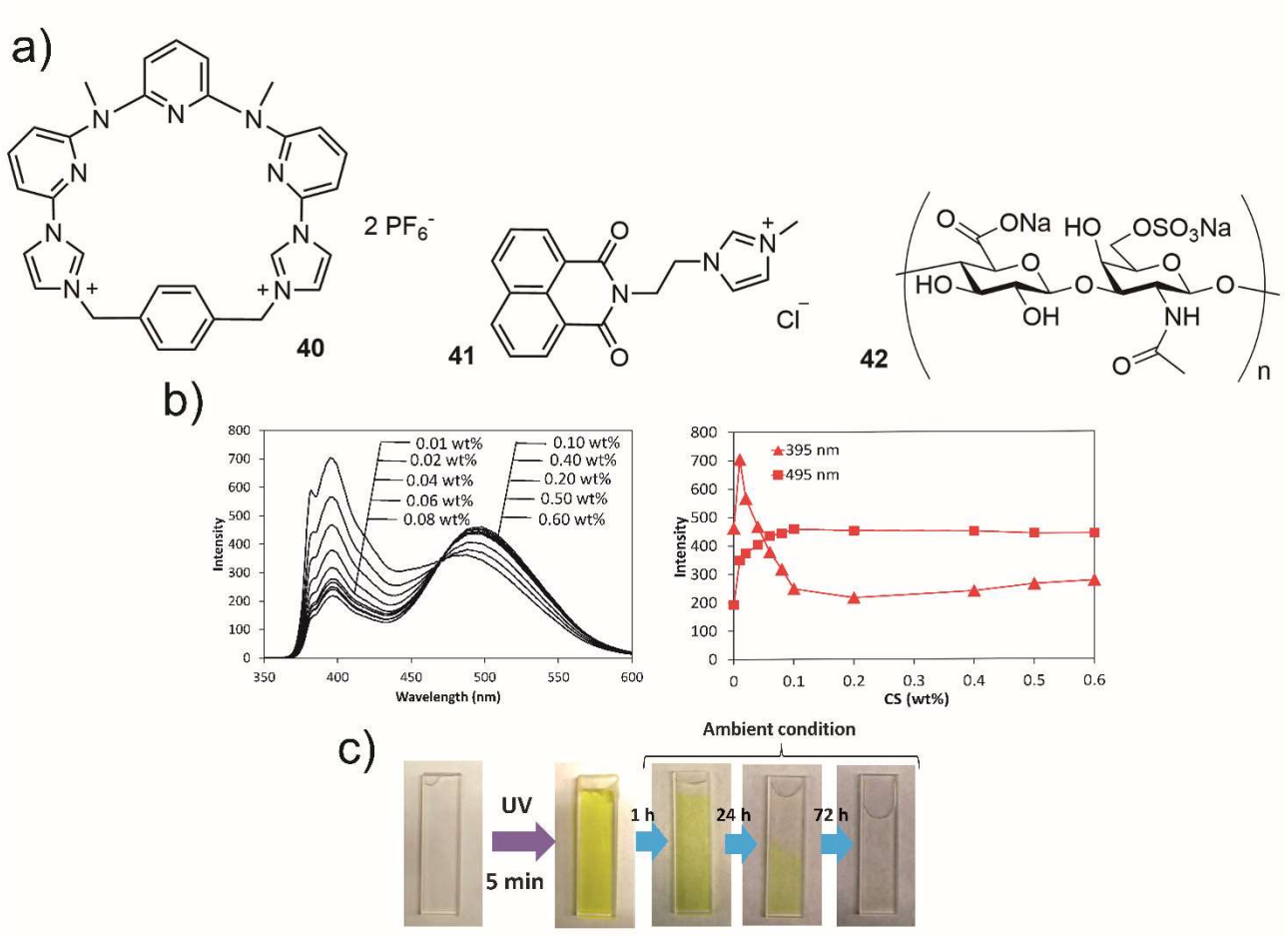

Fig. 32. a) Chemical structures of macrocycle **40**, sensor **41**, and polysaccharide **42**; b) emission spectra of **41** (1.5 mM, 298 K, λ_{ex} 365 nm) upon addition of increasing amounts of polysaccharide **42** (0.01-0.6 wt%) and the intensities of emission at 395 nm and 495 nm; c) colour change of solution containing **41** (1.5 mM, 298 K) after being treated with **42** (0.5 wt%). The colour disappears after 72 hours in ambient conditions. Adapted with permission from Ref. [96].

7. Charged chemosensors

Charged fluorescent chemosensors employ electrostatic interactions in combination with other non-covalent interactions to bind anions, resulting in fluorescence enhancement or quenching [98]. For example, Beer and co-workers have developed [3]-rotaxane molecular shuttle **43** containing a central C_{60} fullerene bis-triazolium axle and two ferrocenyl-functionalized isophthalamide anion binding sites (Fc). The axle also consists of a four-station bis-naphthalene diimide (NDI) (Fig. 33) [99]. The [3]-rotaxane shuttle showed an on/off switchable emission response mediated by anion binding (Fig. 33) in $CHCl_3$ [99]. A strong fluorescence band at 435 nm, with a high quantum yield, was observed for the [3]-rotaxane$(Cl)_2$ complex and the change was visible to the naked eye, a characteristic associated with NDI derivatives in $CHCl_3$ (Fig. 34) [100]. Interestingly, the same NDI emission band was quenched in [3]-rotaxane.$(PF_6)_2$ (Fig 33).

The authors ascribed this behaviour to the anion recognition-mediated shuttling leading to an anion switchable emission response [99]. In the presence of chloride, the [3]-rotaxane **43** binds to two chloride ions *via* hydrogen bonding (two with the adjacent amid NHs and one with CHs of the triazole rings) resulting in shuttling of the ferrocenyl functionalized macrocycles from the NDI stations to the triazolium groups at the centre of the axle (Fig. 33). Consequently, electron transfer to NDI from the ferrocene groups was precluded, leading to switching-on of the NDI fluorescence emission. In the absence of chloride as [3]-rotaxane.$(PF_6)_2$, the ferrocenyl appended macrocycles are bound to the NDI station resulting in photoinduced electron transfer (PET) from the ferrocenyl donor groups to the proximal NDI which in turn leads to fluorescence quenching (Fig 33).

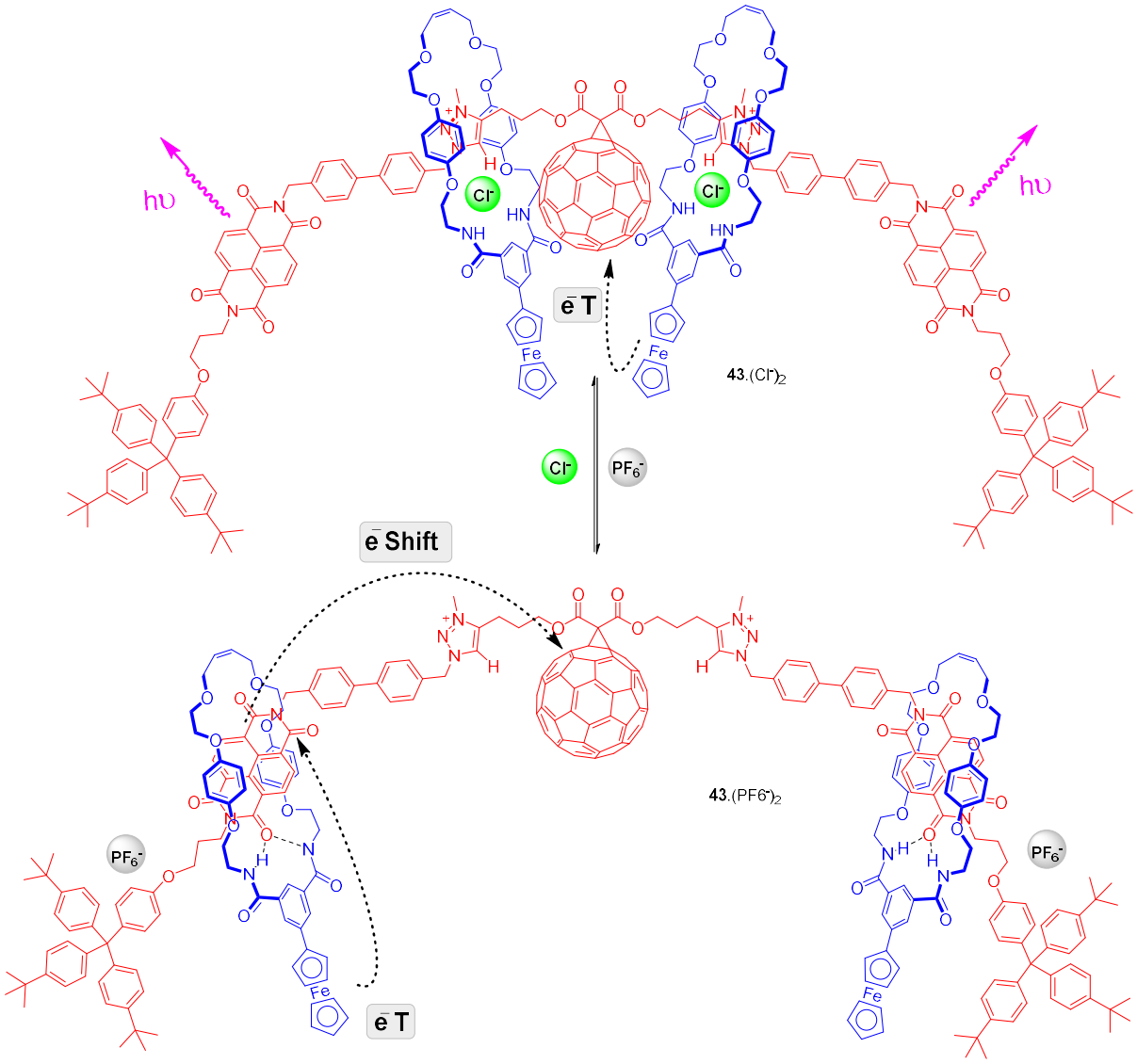

Fig. 33. Switchable [**43**]rotaxane.$(Cl)_2$ and [**43**]rotaxane.$(PF_6)_2$ *via* anion-induced molecular motion.

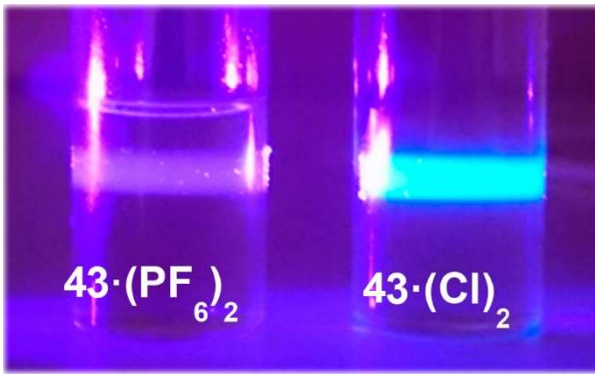

Fig. 34. Fluorescence switching-on of chloroform solution of [3]-rotaxane **43** (50 µM) in presence of chloride that is detectable by the naked eye, λ_{ex} = 400 nm. Adapted with permission from Ref. [99].

Khrustalev, Kataev and co-workers have recently reported the synthesis of naphthalimide-appended fluorescent tren-based macrocycle **44** (Fig. 35) [101]. As illustrated in Fig. 36c, macrocycle **44** shows high selectivity and affinity to fluoride in aqueous solutions at pH 6.2 with a binding constant of ~10^5 M^{-1} among tested anions, including Cl^-, Br^-, I^-, NO_3^-, SO_4^{2-}, $H_2PO_4^-$, and $C_2O_4^{2-}$. Fluorescence studies showed that the addition of more than one equivalent of fluoride to compound **44** induced a hypsochromic shift alongside an increase in fluorescence intensity (Fig. 36a) [101].

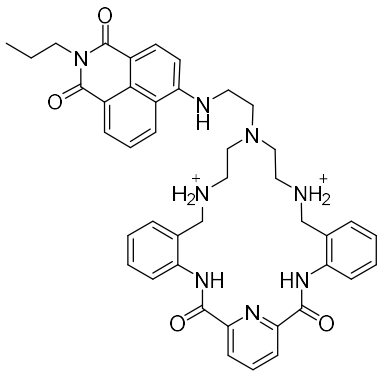

44

Fig. 35. Chemical structure of macrocycle **44** (at pH = 6.2).

Fluorescence measurements (in aqueous solutions at pH = 6.2), ^{1}H NMR and ^{19}F NMR titration studies (in DMSO/water (1:1 v/v) buffered at pH 6.2) along with computational studies using density functional theory (DFT) provided strong evidence that compound **44** can accommodate up to three fluorides (Fig. 36b) [101]. Two fluorides could fit inside the cavity of macrocycle **44** inducing the protonation of the tertiary amine, which resulted in fluorescence increase with only fluoride binding (Fig. 36a). The third anion is located outside the macrocycle cavity and could form a hydrogen bond with the ammonium ion (Fig. 36b). The acquired X-ray crystal structure of receptor **44** with chloride indicated that the cavity in receptor **44** could perfectly

accommodate one chloride anion. Interestingly, addition of more than one equivalent of chloride promoted aggregation-driven fluorescence quenching in aqueous media [101].

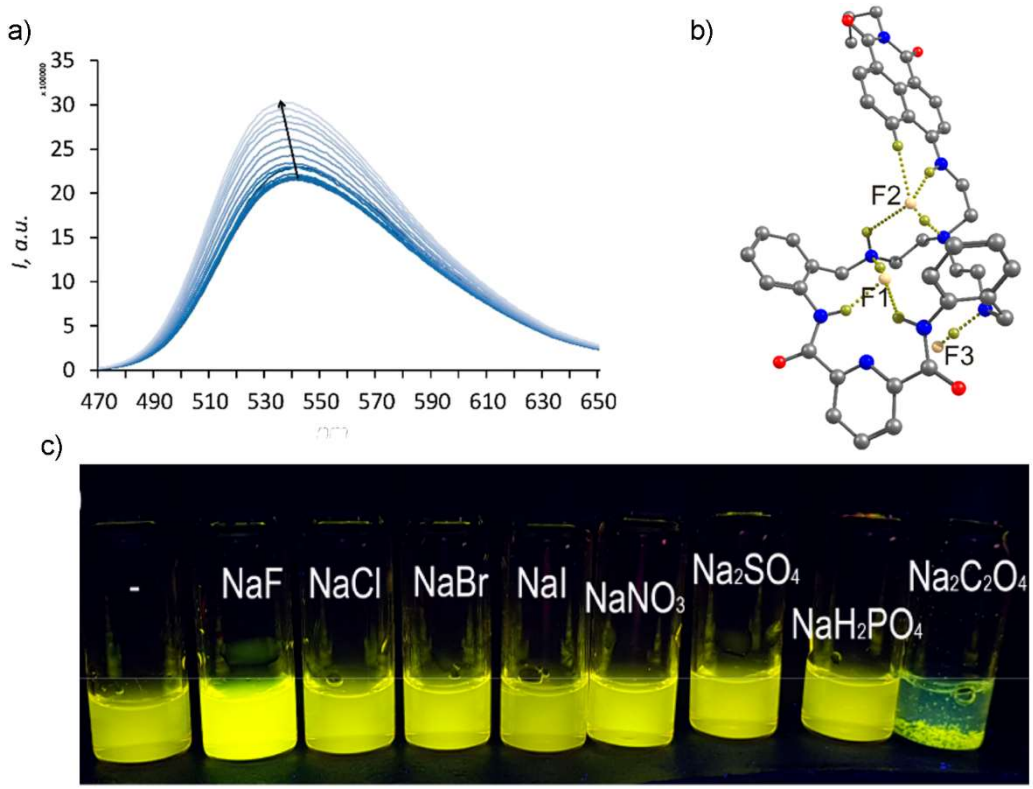

Fig. 36**.** a) Fluorescence changes upon titration of **44** with 50 equivalents of NaF in a 10 mM MES buffer (pH = 6.2, λ_{ex} = 440 nm); b) DFT optimized structures of **44**.3HF; c) changes in fluorescence of solutions of macrocycle **44** in a 10 mM MES buffer (pH = 6.2) in the absence and presence of 50 equivalents of various anions. Adapted with permission from Ref. [101].

Singh et al. have reported the use of thioflavin-T **45** (Fig. 37a) as a selective fluorescence turn-on chemosensor for perrhenate anion (ReO_4^-) recognition in water [102]. The authors ascribed the selectivity of the molecular rotor **45** towards perrhenate in aqueous solution to the contact ion pair interaction between the weakly hydrated perrhenate ion and compound **45**. This resulted in aggregation, assembly formation, and therefore an enhancement in fluorescence [102]. Upon addition of other anions such as sulfate, chloride and nitrate, to an aqueous solution of compound **45**, no fluorescence response was recorded even at high anion concentrations (10 equiv.) (Fig. 37c). Atomic Force Microscopy (AFM) measurements of the perrhenate-induced thioflavin T **45** aggregation suggested a dendritic growth of the formed aggregates (Fig. 37b). Temperature-dependent measurements of the aggregates showed that as temperature increased, from 25-70 °C, the emission fluorescence intensity reduced while UV-Vis measurements confirmed the recovery of the main monomeric absorption band at 410 nm (Fig. 37d).

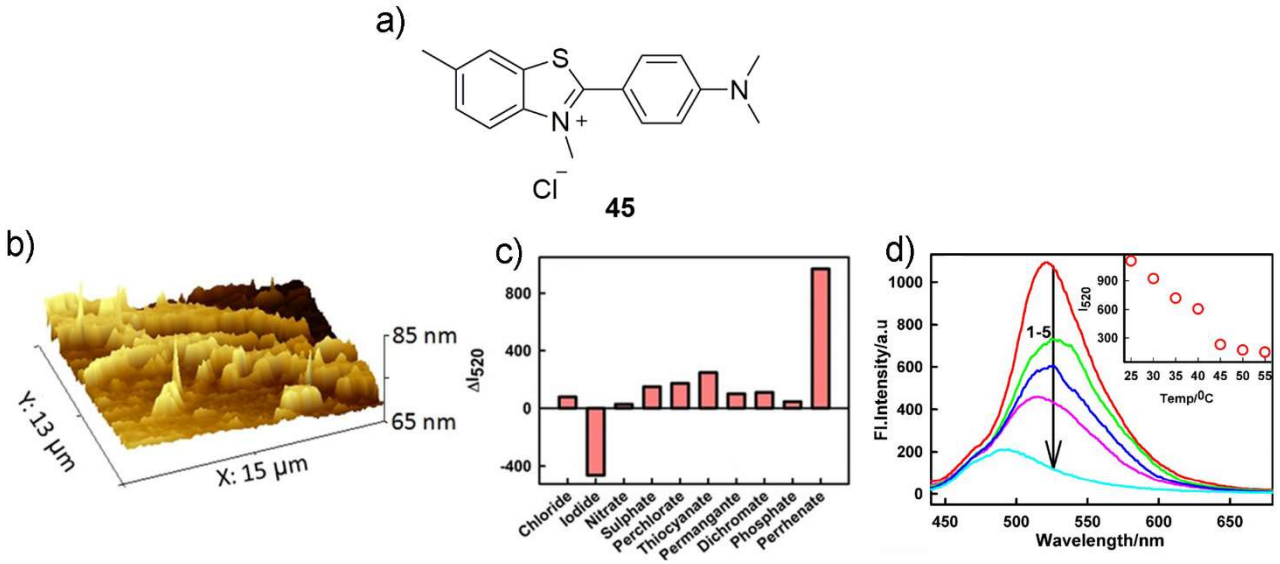

Fig. 37. a) Chemical structure of chemosensor **45**; b) AFM image of thioflavin T **45** aggregation in the presence of perrhenate; c) fluorescence intensity at 520 nm in aqueous solution of thioflavin T **45** in the presence of 50 mM perrhenate and 500 mM of chloride, iodide, nitrate, sulfate, perchlorate, thiocyanate, permanganate, dichromate, and phosphate; d) change in the steady-state emission spectrum at 520 nm of 40 mM Thioflavin T **45** (40 mm) in the presence of 32.4 mM perrhenate with increasing temperature: (1) 25, (2) 30, (3) 35, (4) 40, and (5) 50 °C. Adapted with permission from Ref. [102].

An example of a fluorescent probe based on the π-conjugated dicationic pyridinium derivative **46** (Fig. 38a) for tetrafluoroborate (BF_4^-) and hexafluorophosphate (PF_6^-) recognition in water and in living cells was reported [103]. This system demonstrated noticeable aggregation-initiated fluorescence changes only in the presence of BF_4^- and PF_6^-, among the other anions tested (Fig. 38b) in aqueous solution. Upon addition of BF_4^- and PF_6^- to **46**, transmission electron microscopy (TEM) and fluorescence assembly microscopy measurements revealed that compound **46** forms a ribbon-like self-assembly, which is presumably aided by π–π stacking, ionic binding and van der Waals forces. The authors further investigated this behavior in HeLa cells using fluorescence microscopy. As shown in Fig. 39, compound **46** demonstrated intense fluorescence emission in the blue channel and no noticeable fluorescence in the green and red channels. Strong fluorescence emission in the green and red channels was observed upon addition of BF_4^- and PF_6^- to compound **46** suggesting that these anions, although large and weakly coordinating, can permeate the plasma membrane and elicit a fluorescence response (Fig. 39).

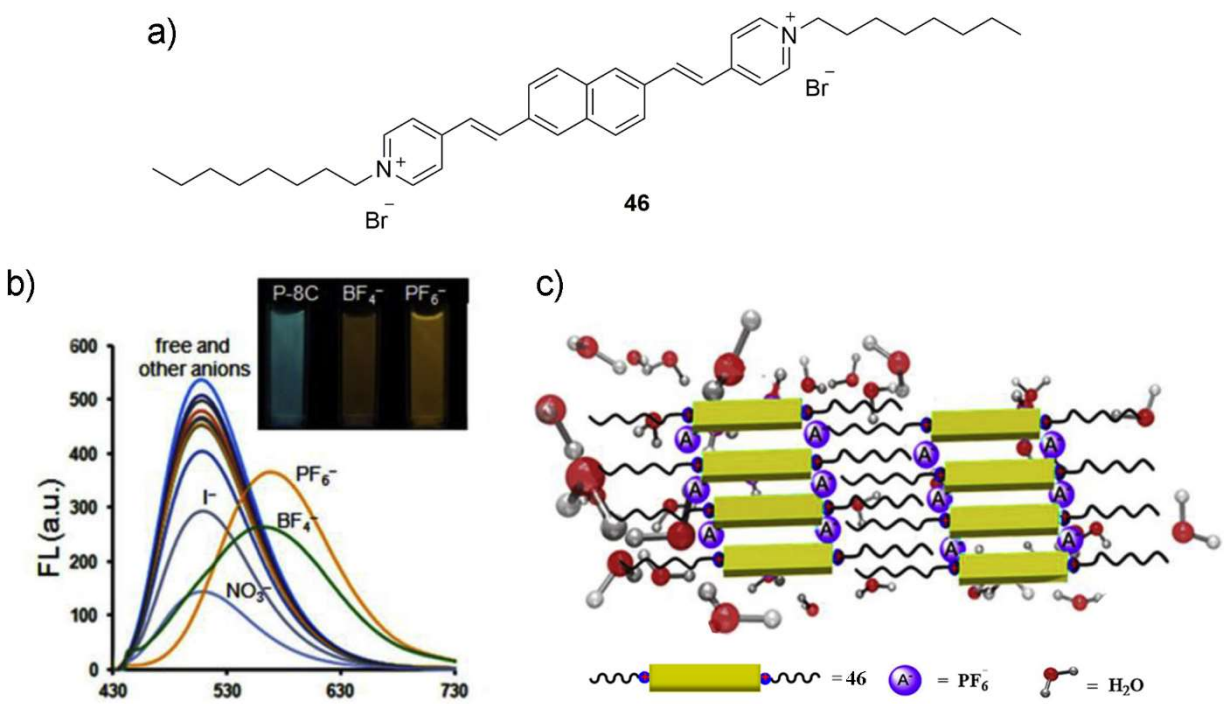

Fig. 38. a) Structure of fluorescent probe **46**; b) change in fluorescence intensities at λ_{ex} = 405 nm of **46** upon addition of 20 equiv. of various anions including, fluoride, bromide, iodide, sulfate, dihydrogen phosphate, nitrate, tetrafluoroborate, hexafluorophosphate, hydrogen sulfate, acetate, citrate, oxalate, perchlorate in 10 mM HEPES buffer (pH 7.4) at 298 K; c) schematic representation of the cationic fluorescent probe assembly initiated by the anion recognition in water. Adapted with permission from Ref. [103].

	HeLa cell lines		
	Blue Channel	Green Channel	Red Channel
Compound **46**	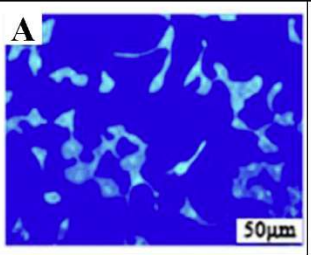	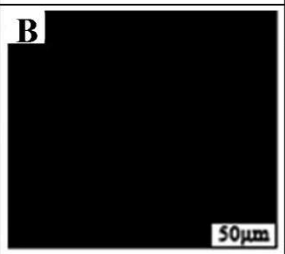	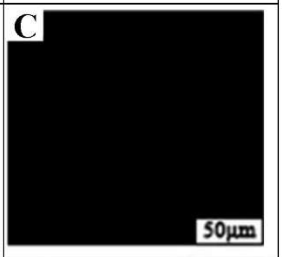
Compound **46** + PF_6^-		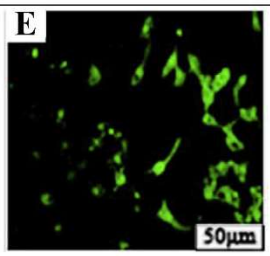	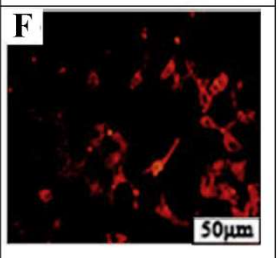

Fig. 39. (A–C) Fluorescence cell images of HeLa cell lines incubated with **46** (10.0 μM) for 20 min at 37 °C; and (D–F) fluorescence cell images of HeLa cell lines incubated with **46** (10.0 μM) in the presence of PF_6^- (0.2 mM) for 60 min at 37 °C. Reproduced with permission from Ref. [103].

8. Anion-π interactions in sensing

Anion-π interactions are non-covalent and attractive interactions between an anion and electron deficient arenes, that originates from electrostatic forces and anion induced polarization [104-106]. Wang and co-workers reported the synthesis of the tetrazines-based macrocycle **47**, over two steps by base catalysed coupling of 3,6-dichlorotetrazine and *p*-bis(hydroxymethyl)benzene fragments and have employed the macrocycle as an anion sensor (Fig. 40) [107]. Upon addition of different anions to macrocycle **47** in acetonitrile, it was found that only azide and thiocyanate anions caused a dynamic quenching in the fluorescence intensity (Fig. 41a-c) [107]. Macrocycle **47**, containing an electron deficient and tuneable box-like cavity, presumably formed complexes *via* anion–π interactions preferentially with the size-complementary azide and thiocyanate anions [107]. Furthermore, DFT computational studies provided a strong evidence of the anion–π or anion–lone pair interactions of macrocycle **47** with the azide and thiocyanate anions (Fig. 41d) [107].

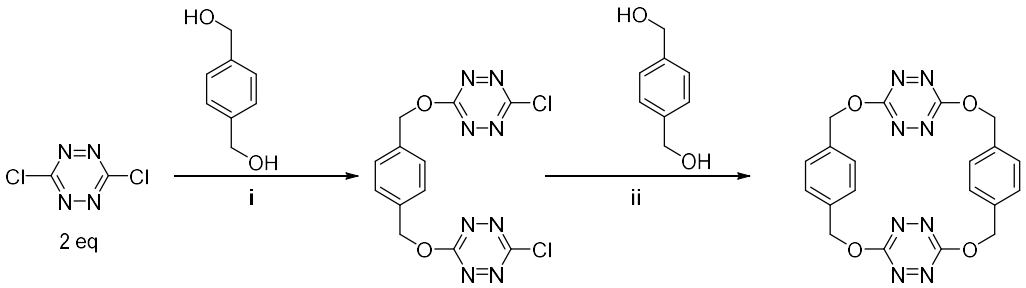

Fig. 40. i) Collidine (2.2 eq.) , $CHCl_3$, 2 h; ii) DMAP (2.2 eq.), $CHCl_3$, 4 h, 40 °C.

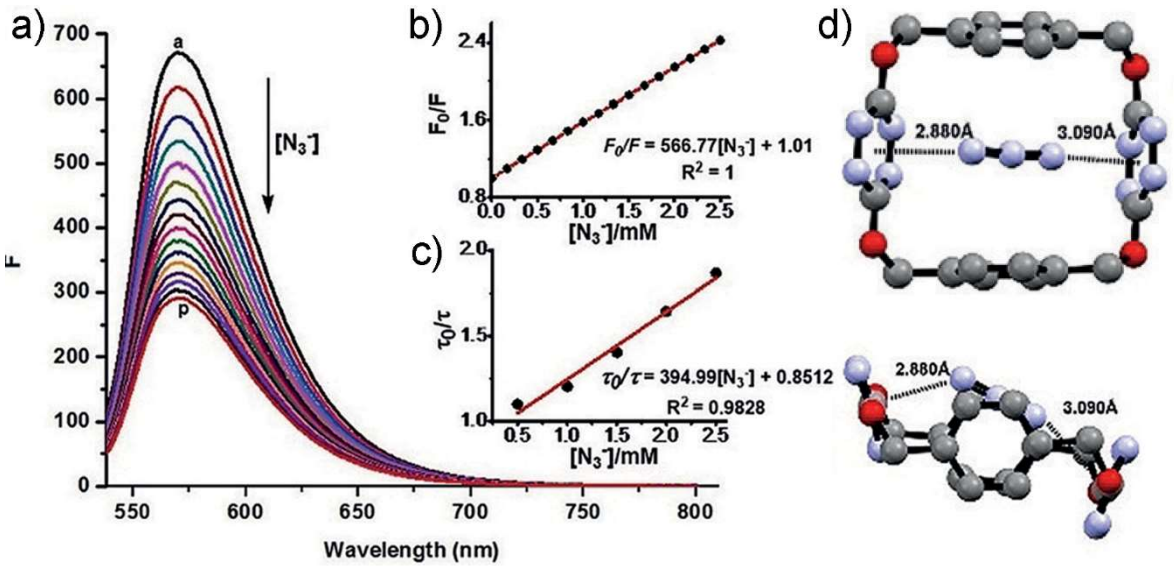

Fig. 41. a) Fluorescence titration of macrocycle **47** (5 x 10^{-5} mol L^{-1}) with gradual addition of azide in acetonitrile at 298 K (a = 0.000 mol L^{-1}, p = 2.500 x 10^{-5} mol L^{-1}); b) fluorescence intensity (F_0/F) changes of macrocycle **47** with increasing azide concentration; c) fluorescence lifetime changes of macrocycle **47** with increasing azide concentration; d) computed structures of anion- π complexes [**47**·N_3]$^-$ with top (top) and side (bottom) views. Reproduced with permission from Ref. [107].

An example of a cyanide-chemosensor based on anion-π interactions was reported by Jiang and co-workers [108]. Fluorescent chemosensor **48**, based on hexaazatriphenylene scaffold, exhibited a fluorescent and colorimetric ratiometric response to CN^- in CH_3CN and CH_3CN/H_2O (1:1) mixture (Fig. 42) [108]. Upon addition of cyanide ion (0-1 equiv.) to compound **48** in acetonitrile, anion-π interactions triggered the generation of a green non-fluorescent radical anion, which turned to a brown-yellow fluorescent dianion with subsequent addition of excess cyanide (1-10 equiv.) (Fig. 42). As shown in Fig. 43, the system was tested in the presence of aqueous solution of different anions (F^-, Cl^-, Br^-, I^-, AcO^-, BF_4^-, $H_2PO_4^-$, PF_6^- and CN^-) and a yellow colour was observed only in the presence of CN^-. Authors attributed the high selectivity of compound **48** for CN^-, even in the presence of other competitive anions, to the strong anion–π interaction of the electron deficient **48** with the Lewis basic CN^-, inducing electron transfer and triggering a turn-on fluorescence response [108].

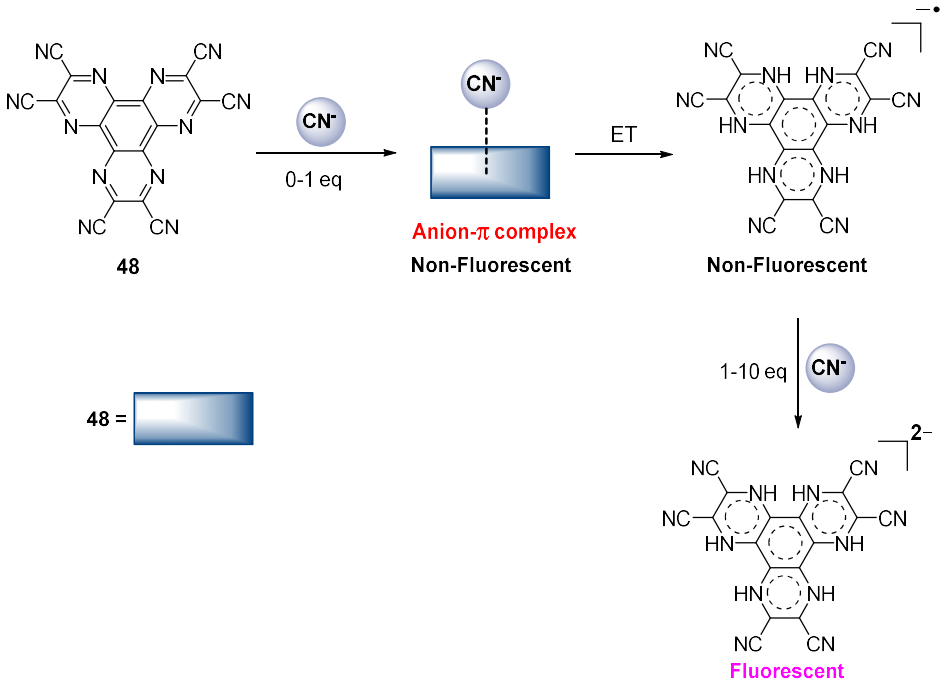

Fig. 42**.** Graphical representation of the fluorogenic response of compound **48** due to the formation of anion-π interaction which induced electron transfer between the cyanide anion and receptor **48**.

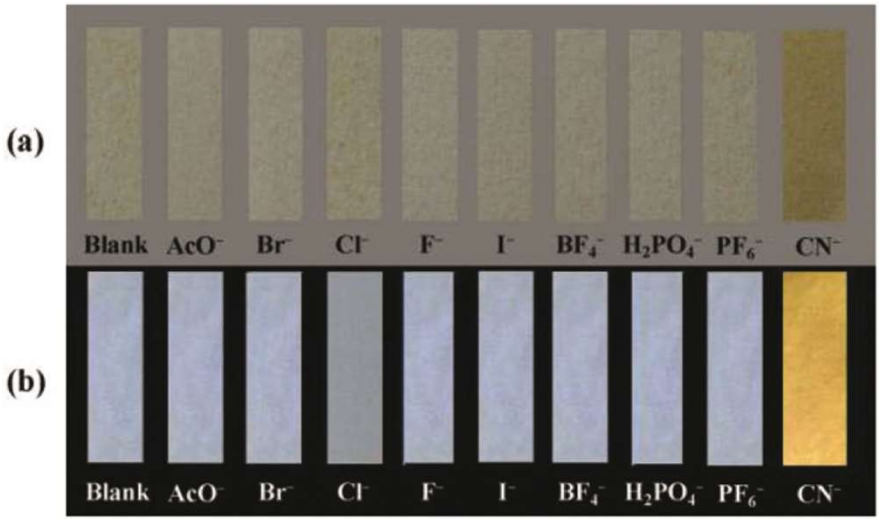

Fig. 43. Colour change of **48** (1 mM) test strips with and without addition of aqueous solutions of different anions (2 mM) under visible light (top) and at 365 nm UV light (bottom). Reproduced with permission from Ref. [108].

9. Photoswitchable Sensors

The design and development of photoswitchable receptors for selective recognition of anions have received considerable attention in recent years, not only in academic studies but also because of their application in diagnostics, imaging, and environmental science [109]. Several examples of photoswitchable chemosensors have been recently proposed enable to detect highly basic anions such as F^-, CN^- [110, 111]. In this context, Guo and co-workers reported the photoswitchable systems **49** and **50** consisting of dicyanovinyl-functionalized dithieenylethene, in which the dicyanovinyl group was able to respond to cyanide anion (Fig

44a) [112]. Surprisingly, **49** presented a triple sensing performance for CN^-. The receptors were able to undergo photoisomerization between ring open **49(o)** and **50(o)** and ring closed **49(c)** and **50(c)** isomers upon alternating irradiation at 365 nm and above 600 nm in acetonitrile, as shown in Fig. 44b and Fig. 44c. The UV-vis spectrum of the ring-open form displayed a maximum in absorption at 424 nm ($\varepsilon = 2.60 \times 10^4\ cm^{-1}\ M^{-1}$) which is ascribed to an intermolecular π–π* transition. Upon irradiation with UV light (365 nm), the yellow solution turned blue-green and a new absorption band appeared at 690 nm ($\varepsilon = 1.49 \times 104\ cm^{-1}\ M^{-1}$), due to the formation of the corresponding ring-closed isomers. The appearance of an isosbestic point at 474 nm further supports the presence of a two-component photochromic reaction between the open and the closed ring isomers. UV-Vis absorption spectra collected in a mixture of acetonitrile/H_2O (95:5 v/v) highlighted how the ring open isomer **49(o)** exhibited colorimetric sensing of CN^-. Upon the addition of an excess of cyanide (10 equiv.) the 424 nm band of **49(o)** diminished completely and a new absorption band at 284 nm appeared and the solution turned from yellow to colourless (Fig. 45a).

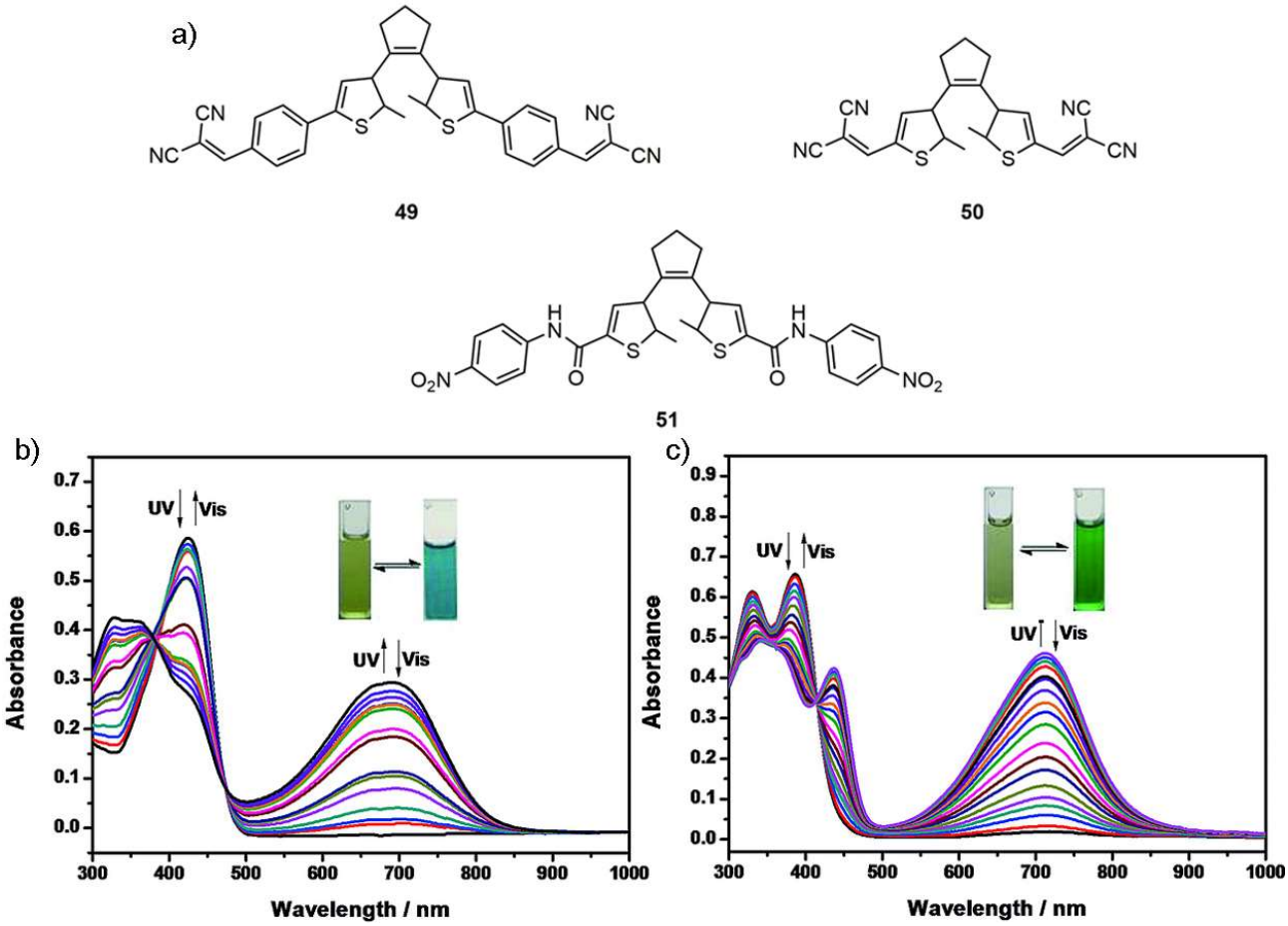

Fig. 44. a) Chemical structures of photoswitchable sensors **49**, **50** and **51**; b) UV/Vis absorption spectra changes of **49** and c) **50** with 365 nm UV and > 600 nm visible light irradiation in acetonitrile (2.0×10–5 mol L^{-1}) at 298 K, inset: corresponding colour changes of **49** and **50** upon photoirradiation. Reproduced with permission from Ref. [112].

The capability of the ring open isomer **49(o)** to detect CN^- was also investigated by means of fluorescence spectroscopy. The free **49(o)** in a mixture of acetonitrile/H_2O (95:5 v/v) presented an emission band at 533 nm (λ_{ex}= 424 nm) with moderate yellow fluorescence, which was turned off in the presence of CN^- (Fig. 45b). Finally, a third detection technique was determined by the ring –closed isomer **49(c)**, which displayed a near infra-red (NIR) colorimetric sensing of CN^- (green to purple). The NIR absorption band of **49(c)** at 690 nm gradually decreased while a new band at 552 nm emerged, which was responsible for the colour change (Fig. 45c). The mechanism of **49(o)** in sensing of CN^- was confirmed *via* ^1H NMR titration experiments in $CDCl_3$.

The same authors studied previously the photochromic behaviour of a dithienylethene **51** for the detection of F^- [113].

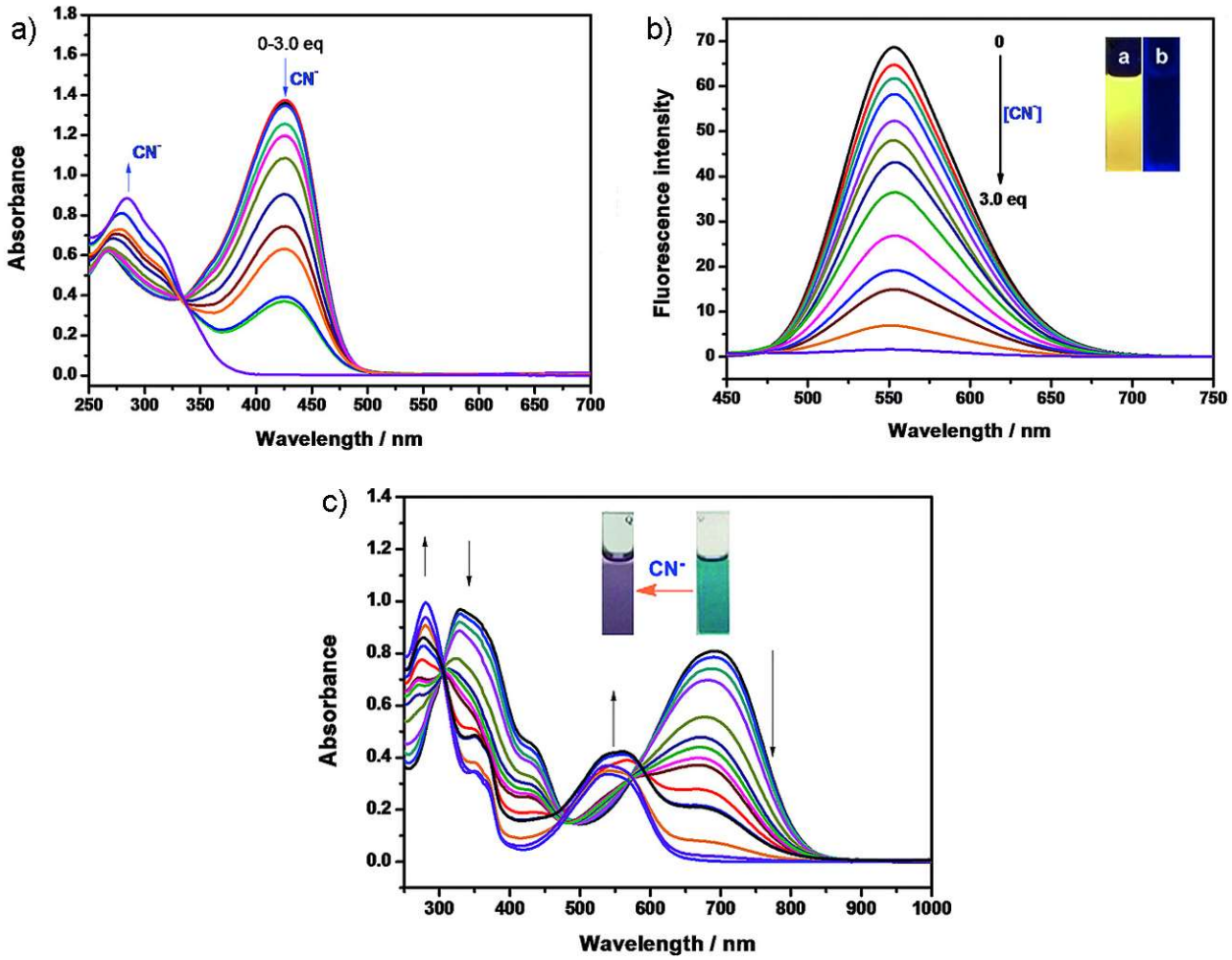

Fig. 45. a) UV/Vis absorption spectra changes of **49(o)** (20 µM) with gradual addition of CN^- (0–3.0 equiv.) in acetonitrile/H_2O (95:5 v/v); b) fluorescence spectra changes of **49(o)** (20 µM) in the presence of different amounts of CN^- (0–3.0 equiv.) in acetonitrile/H_2O (95:5 v/v), inset: photos of the solution of **49(o)** (20 µM) in the absence (a) and presence (b) of CN^- (3.0 equiv.) under 365 nm UV light; c) UV/Vis absorption spectra changes of **49(c)** (20 µM) at photostationary state (365 nm) with gradual addition of CN^- (0–3.0 equiv.) in acetonitrile/H_2O (95:5 v/v). Adapted with permission from Ref. [112].

Bandyopadhyay and co-workers reported the binding affinities towards various phosphorylated coenzymes under physiological condition of an azobenzene-based photoswitchable macrocyclic receptor **52** in its E and Z isomers, with particular selectivity for ATP in the E-form and towards GTP in the photoisomerized Z-form [114]. The photophysical switching behaviour of receptor **52** was investigated in acetonitrile. UV–Vis spectra were recorded upon irradiation at 366 nm and 466 nm (Fig. 46a). The thermally stable *trans* form (**52-E**) of the receptor showed a strong, distinctive absorption band at 319 nm ($\varepsilon = 8.96 \times 103\ M^{-1}\ cm^{-1}$) corresponding to the π–π* transition, and a weak absorbance band at 450 nm ($\varepsilon = 4.16 \times 102\ M^{-1}\ cm^{-1}$) attributed to the symmetry forbidden n–π* transition. Upon irradiation with UV light ($\lambda = 366$ nm, 2.3 mW cm^{-2}), the thermally stable **52-E** (30 µM) form progressively isomerized to **52-Z** and consequently the strong π–π* band gradually decreased, concordant with a spectral shift to the shorter wavelength (300 nm). Simultaneously the evolution of the n–π* band was also observed, indicating the Z-rich photostationary state (PSS). On the other hand,

conversion of the **52-Z** to the **52-E** isomer was accomplished by irradiating the **52-Z** solution with blue light (λ = 466 nm, 0.5 mW cm^{-2}). Photo-irradiation with 466 nm light, converted the Z-rich PSS to corresponding thermally stable **52-E** isomer.

The optical sensing of ATP, ADP, AMP, P_i and GTP anions was evaluated *via* the fluorescence response of **52-E** and **52-Z** forms in an aqueous solution of Tris (1mM at pH 6.8) at 25°C (Fig. 46b). The addition of ATP to **52-E** caused a dramatic enhancement of the characteristic emission band at 400 nm accompanied by a moderate red shift of 15 nm, while no appreciable changes were observed in the presence of an excess of GTP, ADP, or in the presence of a series of common anion species tested. This selectivity was attributed to the greater coulombic attraction between the highly charged guest and protonated receptor (at neutral pH), and a secondary H-bonding interaction between the amine group of the adenosine moiety and the lone pair of the azo -N=N- group. GTP is the wrong shape for this interaction to take effect and therefore exhibits a weaker interaction with **52-E**. Interestingly, upon exposure of the **52-E** -ATP system to 366 nm light, the system converted to the Z form ATP adduct, as suggested by a remarkable decrease of the emission intensity. The same behaviour was observed also for ADP, AMP, GTP, and Pi adducts.

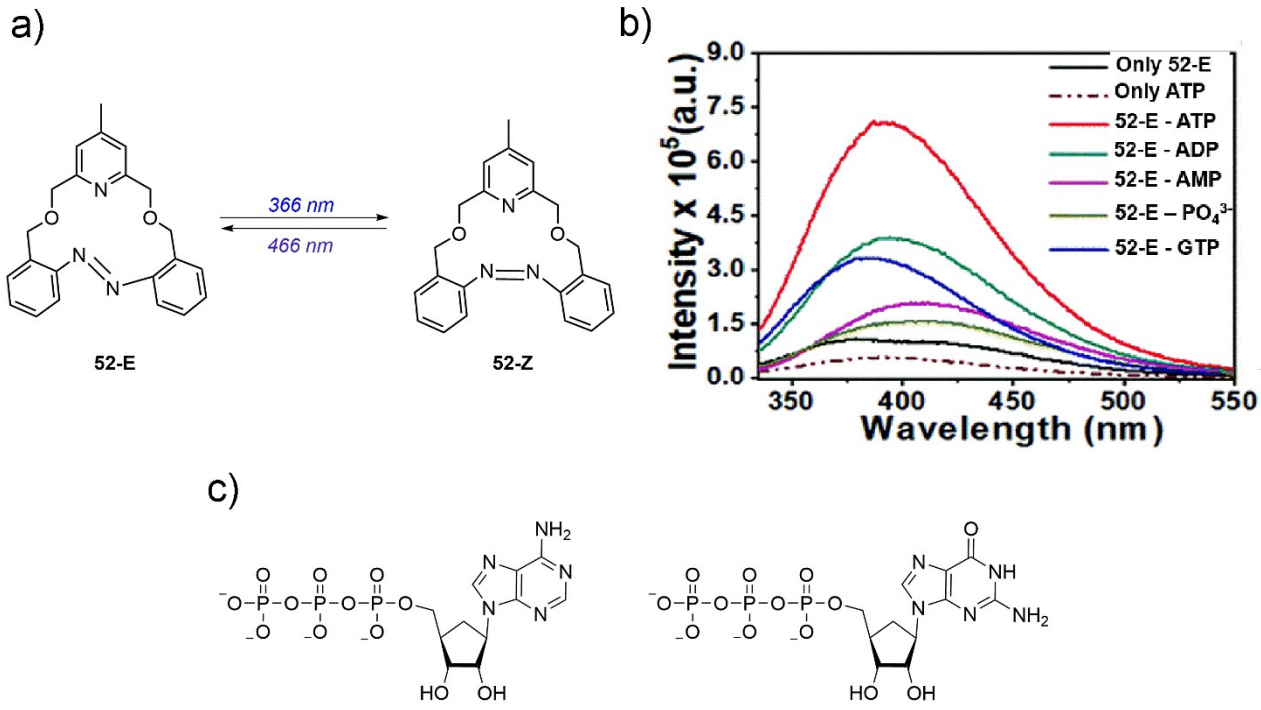

Fig. 46. a) Photomodulation of **52** from the E to the Z form; b) emission intensity of **52-E** (10 mM) with phosphate anions (10 equiv. each) in Tris buffer at pH 6.8; c) anions ATP^{4-} (left) and GTP Adapted with permission from Ref. [114].

The binding of **52-E** with ATP was evaluated also using ^1H NMR titrations which clearly demonstrated that the E isomer strongly binds to the ATP species (K_{11} = 5.36 x 10^{-3} M^{-1}). Moreover, **52-E** was used as a fluorescent probe for monitoring the progress of an enzymatic phosphate transfer reaction using a tyrosine kinase enzyme (c-Src kinase), which enabled real time monitoring of the *in vitro* kinase activity.

The following two examples are not strictly optical sensors; however they have still been included due to their interesting photoswitchable properties and binding modes. Flood and co-workers reported a

photoactive chiral aryl-triazole-based foldamer system **53** to study the allosteric regulation of anion binding [115]. Both small (Cl^-, Br^-, NO_2^-, I^-, NO_3^-) and large (SCN^-, BF_4^-, ClO_4^-, ReO_4^-, PF_6^-, SbF_6^-) anions interacted with the single and double helical structures, activating different functions in the photofoldamer (Fig. 47). In **53**, the light-driven *trans–cis* isomerization of azobenzenes alters the intrastrand π–π contacts, while the triazoles define the allosteric anion-binding site. Using a combination of ^{1}H-NMR investigations, circular dichroism (CD) and UV-Vis titrations, the behaviour and binding modes for the helix and photoswitchable states were evaluated in order to identify how the function of the photofoldamer changes with anion size. Contrary to expectations that single helices will expand to accommodate larger guests, this behaviour only occurred for smaller anions (Cl^- to NO_3^-; <45 Å^3) beyond which the larger anions formed double helices (SCN^- to SbF_6^-; >45 Å^3). With smaller anions, the single helix regulates anion concentrations when the azobenzenes are photoswitched. The binding of large anions favours a chiral double helix and activates light-driven switching into racemic single helices thereby modulating the quaternary structure and chiroptical activity.

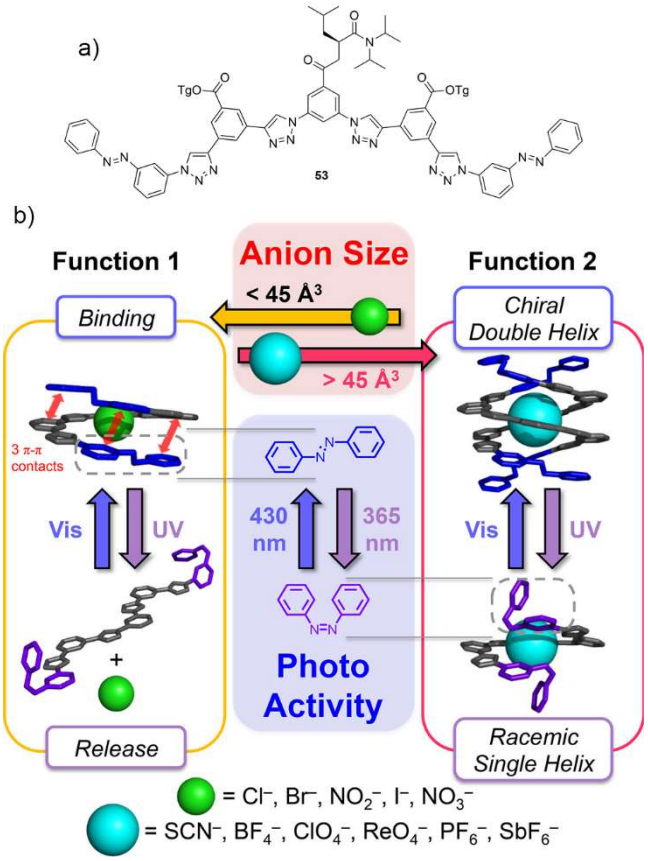

Fig. 47. a) The structure of foldamer **53** and b) cartoon illustrating the photoswitching behaviour of the foldamer in the presence of different anionic guests. Reproduced with permission from Ref. [115].

Finally, elegant work was reported by Sessler and co-worker on the expanded "Texas-sized" molecular box **54** (Fig. 48), incorporating photoresponsive azobenzene bridging subunits and anion recognition motifs, which is capable of recognising various aryl dicarboxylates and releasing them upon photoirradiation [116]. The cavity shape of **54** can be controlled through photoirradiation. Indeed, a solution of **54** in DMSO shows an intense absorption band at 330 nm and a relatively weak absorption feature at 438 nm. These characteristics are in agreement with the strong π–π*and weak n–π*absorption features expected for an azobenzene system. Upon UV light irradiation (365 nm), the intensity of the band corresponding to the π–π*transition decreases sharply and is accompanied by an increase in the intensity of the n–π* absorption

band, consistent with E→Z photoisomerization of the azobenzene subunits. This isomerization can be reversed by exposure to visible light (420 nm). In the absence of UV light, **54** acts as an effective receptor for aryl dianions in DMSO-d_6 as demonstrated by ^{1}H NMR spectroscopy. Exposure to UV light causing the photoisomerization of the macrocyclic host promotes guest release.

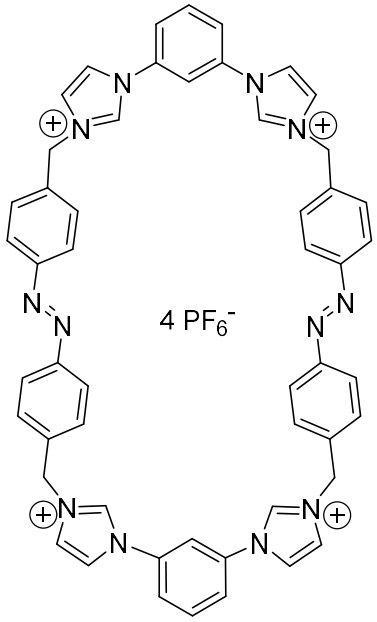

54

Fig. 48. Chemical structure of macrocycle **54**.

10. Chemodosimeters

Chemodosimeters are compounds that react with a substrate selectively giving a colorimetric or fluorescence response allowing them to be used as a sensor. Among the most interesting systems recently proposed, Yi and co-workers described the chemodosimeter **55** (Fig. 49a) [117]. In the presence of fluoride, a desilylation reaction occurred with the release of the free methylene blue and a fluorescence response in the Near Infrared Region at 690 nm in DMSO/HEPES (3:2 v/v) at pH = 7.2 with a very high selectivity (Fig. 49b). This probe was also able to distinguish between different sources of fluoride (organic and inorganic) and was able to sense fluoride in real samples such as toothpastes. Moreover, chemodosimeter **55** was used to visualize fluoride in a dental plaque biofilm using confocal laser scanning microscopy. The results demonstrated that **55** was able to distinguish between non-fluoride and fluoride toothpastes by visualizing fluoride uptake into naturally grown human plaque biofilms (Fig 49c). In addition, **55** could be used as a fluoride regulated prodrug for antimicrobial photodynamic therapy (Fig. 49d).

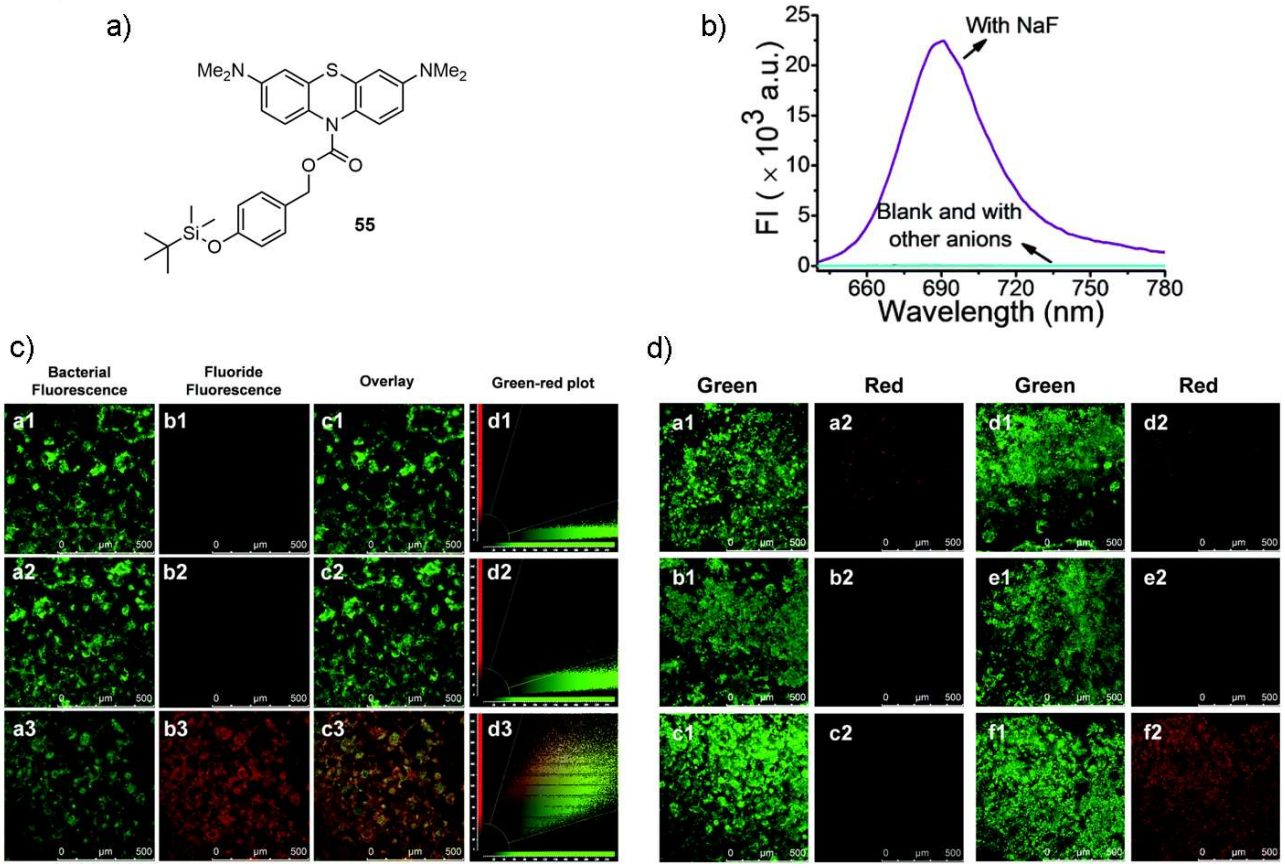

Fig. 49. a) Chemical structure of chemodosimeter **55**; b) fluorescence spectra of **55** in the presence of NaF and other anion guests (CO_3^{2-}, PO_4^{3-}, C: $H_2PO_4^-$, NO_3^-, NO_2^-, SO_4^{2-}, SO_3^{2-}, $S_2O_3^{2-}$, AcO^-, Cl^-, Br^-,I^-, N_3^-, SCN^-, $C_2O_4^{2-}$ in DMSO/HEPES (3:2 v/v, pH = 7.2); c) confocal laser scanning microscopy images of fluoride in human *in situ* plaque biofilms. (a1–d1), (a2–d2) and (a3–d3) show plaque biofilms treated with PBS, fluoride free toothpaste and fluoride containing toothpaste for 2 min, respectively. (a1, a2, and a3) are green channels for SYTO® 9 probe staining (λ_{ex} = 488 nm, λ_{em} = 500–550 nm); (b1, b2, and b3) are near-infrared channels for **55** probe staining (λ_{ex} = 633 nm, λ_{em} = 670–720 nm); (c1, c2, and c3) are overlay images; (d1, d2, and d3) are green-red scattered plots of all non-black pixels of (c1, c2, and c3), respectively; d) confocal laser scanning microscopy images of human *in situ* plaque biofilms upon PDT treatment. (a1 and a2) Without any treatment as control; (b1 and b2) treated only with free **55** (50 mg mL^{-1}) for 30 min; (c1 and c2) with NaF (50 mg mL^{-1}) for 60 min; (d1 and d2) with **55** (50 mg mL^{-1}) for 30 min and then NaF (50 mg mL^{-1}) for 60 min; (e1 and e2) only with light (100 mW cm^2) for 5 min; (f1 and f2) with **55** (50 mg mL^{-1}) for 30 min then NaF (50 mg mL^{-1}) for 60 min and then light (100 mW cm^2) for 5 min. (a1, b1, c1, d1, e1, and f1) are green channels for ® 9 probe staining (λ_{ex} = 488 nm, λ_{em} = 500–550 nm); (a2, b2, c2, d2, e2, and f2) are red channels for propidium iodide probe staining (lex = 488 nm, lem = 600–650 nm). Adapted with permission form Ref. [117].

Chemodosimeter **56** was proposed by Shabat and Gnaim for fluoride sensing using an auto-inductive mode of action and a distinct chemiluminescent response [118]. As shown in Fig. 50b the amplification cycle is initiated by removal of the tertbutyldimethylsilyl triggering group of **56** by fluoride, generating a phenolate intermediate which undergoes 1,6-elimination to release additional fluoride and quinonemethide. Fluoride then activates an additional probe molecule, and the quinonemethide reacts with an available nucleophile to regenerate a phenolate that undergoes chemiexcitation to release benzoate in its excited state. The benzoate is stabilized through an emission of a blue photon. This reaction sequence leads to a progressive increase in signal as shown in Fig. 50c. Subsequently, the fluorescence response of **56** incubated with different concentrations of TBAF in DMSO was monitored by light emission analysis at 499 nm. The time to reach maximum signal intensity increased with decreasing amount of fluoride. In the presence of 1.0 equiv.

(200 mM) of fluoride, the chemiluminescence signal reached a maximum intensity within 3 minutes. Maximum intensity was reached in about 12 minutes at 0.1 equiv, 22 minutes at 0.01 equiv, 32 minutes at 0.001 equiv, and 38 minutes in the absence of fluoride. The chemiluminescence molecular probe **56** showed a limit of detection of fluoride of 0.2 mM and has high selectivity over other anions such as NO_3^-, NO_2^-, Cl^-, Br^-, I^-, and N_3^-.

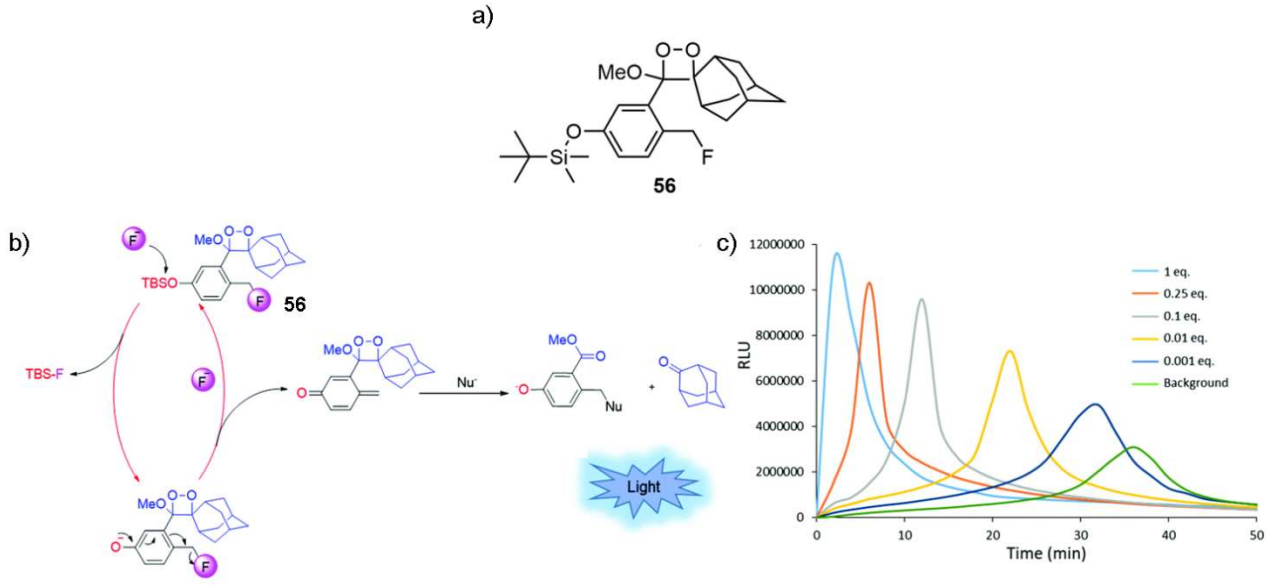

Fig. 50. a) Structure of fluoride sensor **56**; b) auto-inductive disassembly and chemiluminescence emission of chemodosimeter **56** triggered by fluoride; c) chemiluminescence kinetic profiles of **56** (200 mM) with 0, 0.2, 2, 20, 50, and 200 mM TBAF in the presence of 0.1% (v/v) TEA in DMSO. Adapted with permission from ref. [118].

Another example of a chemodosimeter (an "off-on" hydrophilic luminescent polymer composed of amino-functionalized polyhedral oligomeric silsesquioxane and perylene diimides) was proposed by Su, Lv, and co-workers [119]. The reaction responsible for the optical response was induced *via* desylilation promoted by the anion.

Sensing of cyanide by means of nucleophilic addition reactions is quite common and examples based on polymers or helicenoids has been recently reported [120, 121]. A classic reaction that can be exploited for anion sensing is the addition of cyanide to dicyanovinyl moieties. An example of an OFF-ON chemodosimeter (**57**) for cyanide detection in food samples and living systems has been reported by Wu, Li, Fan and co-workers [122]. The system consists in a triphenylamine moiety as an electron-donating group, a dicyanovinyl group as an electron-accepting group, and an electron-deficient benzothiadiazole group. Nucleophilic addition of cyanide (Fig. 51a) caused an increase in the fluorescent emission of **57** at 600 nm upon excitation at 466 nm. The other anions tested did not cause any changes in the fluorescent properties of **57**. When BEAS-2B human lung epithelial cells were incubated with **57**, weak fluorescence was observed (Fig. 51b. a&b). However, the addition of 5 mM of CN^- and 30 min incubation (Fig. 51b. c&d) caused the fluorescence signal to be significantly enhanced, demonstrating that **57** has good cell-membrane permeability and strong binding ability with CN^- in living cells. The application of **57** for *in vivo* detection of cyanide was further investigated in BALB/C mice. When the mice were injected with only **57** (0.5 mmol) weak fluorescence was observed (Fig. 51b. e). However, when the mice were injected with 0.25 mmol of CN^- and 0.5 mmol of **57** a strong fluorescence was clearly observed after 10 minutes (Fig. 51b. f). The fluorescence from the mice injected with **57** and CN^- was 11.5-fold larger than that from the mice with **57** only, suggesting that chemodosimeter **57** could be used as a sensitive fluorescence probe to monitor the changes in cyanide levels within biological systems.

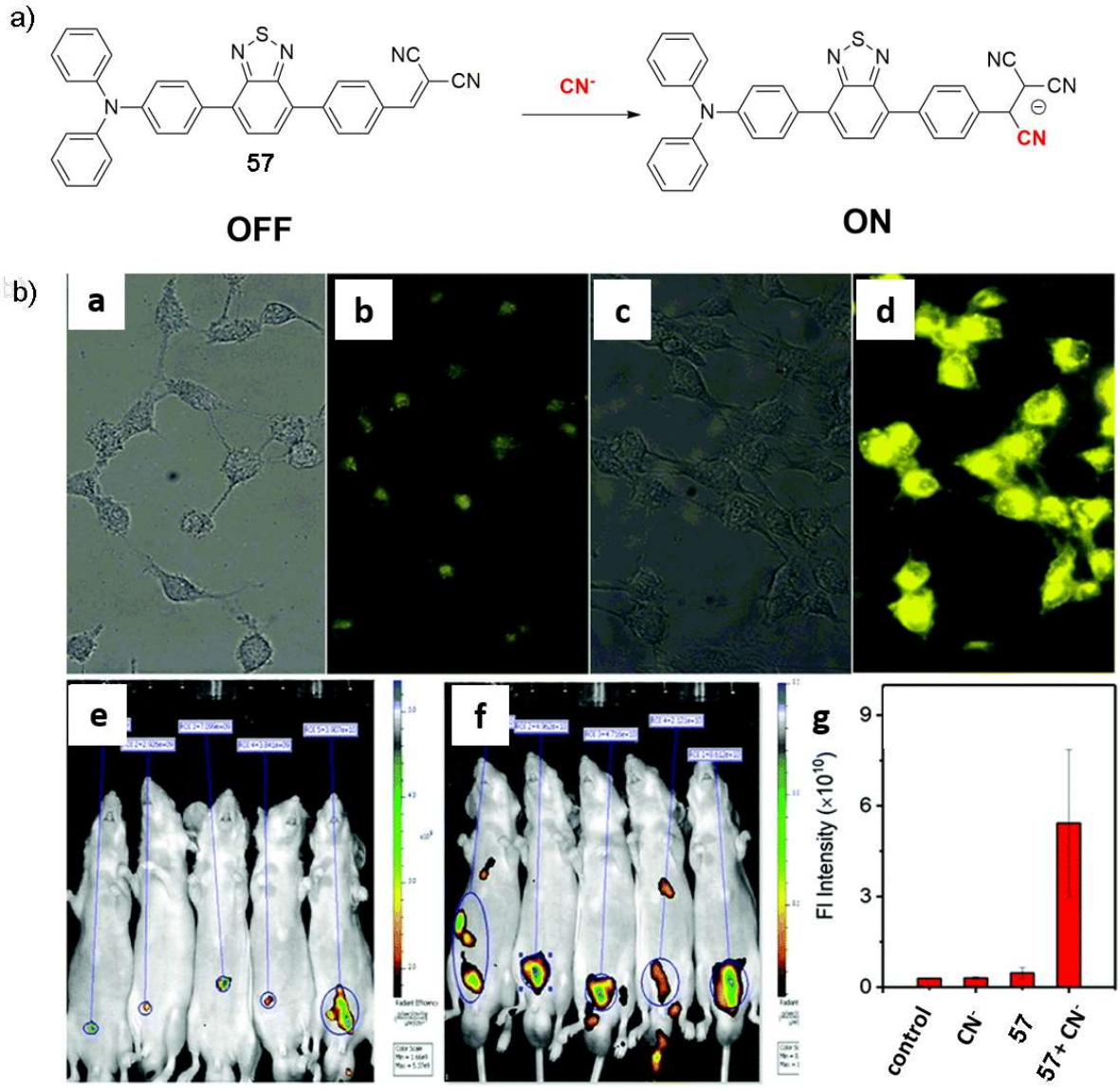

Fig. 51. a) Proposed mechanism for the sensing of cyanide with chemodosimeter **57**; b) bright field and fluorescence images of BEAS-2B cells incubated with **57** (a and b), and **57** for 30 min and then incubated with CN^- for a further 30 min (c and d), respectively (λ_{ex} = 485 nm). In vivo fluorescence imaging of BALB/C living mice with 0.5 mmol **57** (e), 0.5 mmol **57** and 0.25 mmol CN^- (f), (g) average fluorescence intensity calculated from the images. Adapted with permission from Ref. [122].

Gosh and Panja reported the chemodosimeter **58** in which a pyridyl-azo derivative with a dicyanovnyl-appended group undergoes addition of cyanide in acetonitrile accompanied by a unique gel-sol transition and an increase in the fluorescence emission of the free receptor (Fig. 52) [123].

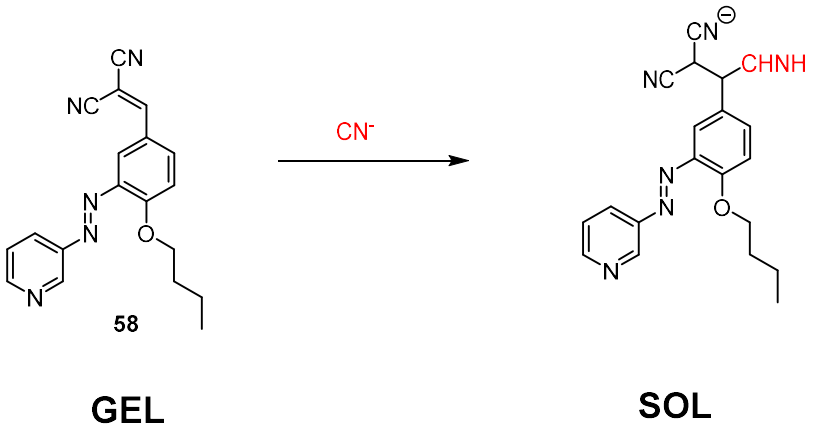

Fig 52. Addition of CN^- to **58** results in a gel-sol transition.

A chemodosimeter for nitrite colorimetric and fluorometric sensing based on anthracene carboxyimide **59** was reported by Zeng, Niu, Kim and collaborators [124]. The recognition is based on the reaction between vicinal aryl diamines and NO_2^- to form triazoles (Fig. 53a), which confirmed by ^1H NMR spectroscopy. Vicinal aryl diamines with strong electron donating abilities can quench the emission of adjacent fluorophores due to an efficient photoinduced electron transfer (PET) process. Upon triazole formation, the PET mechanism can be inhibited, and thus the fluorophores recover their strong emission properties. Upon addition of nitrate to a solution of **59** in EtOH/HCl (1:4 v/v) at pH = 1, a dramatic increase of the fluorescence at 522 nm was observed (Fig. 53b). At the same time, the maximum absorption wavelength of **59** gradually blue-shifted from 500 to 440 nm (Fig. 53c) and the colour of the solution turned from brown to yellow, which could easily be observed by the naked eye, resulting from the reduced ICT effect after the reaction with NO_2^-. A fast response (< 4 min), very high selectivity and low detection limit (84 nM) makes **59** an excellent candidate for real life application. The authors applied their sensor to paper strips by immobilising **59** on filter paper and used them for determining NO_2^- content in food samples.

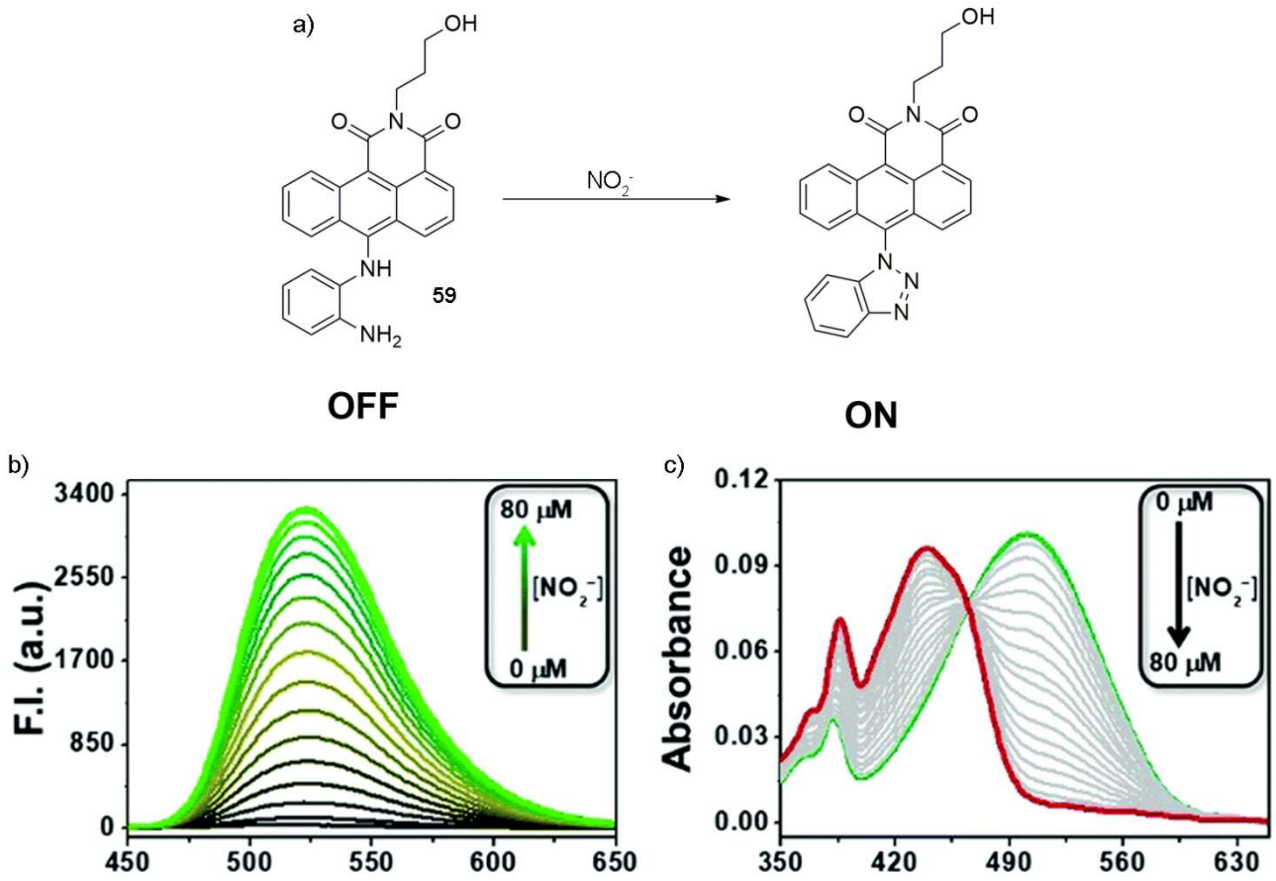

Fig. 53. a) Proposed mechanism for nitrite sensing; b) changes in the fluorescence spectra of **59** upon addition of increasing amount of nitrite in EtOH/HCl (1:4 v/v) at pH = 1; c) changes in the UV-Vis spectra of **59** in the same conditions. Adapted with permission form Ref. [124].

A highly selective chemodosimeter (**60**) for detecting peroxynitrite in live cells was reported by Han, Lin and co-workers [125]. Receptor **60** consists in 2-(2'-hydroxyphenyl)benzothiazole-based probe and, as shown in Fig. 54a, two highly specific reactions trigger the analyte sensing process. **60** is a weakly emissive species, because the N-phenyl group incorporated to replace the 2'-hydroxyl group of the fluorophore blocks the excited-state intramolecular proton transfer (ESIPT) process and quenches the fluorescence. In the presence of $ONOO^-$, the N-dearylation reaction exerted by $ONOO^-$ transforms this reaction trigger to a simple N–H group so as to restore the ESIPT process and therefore restore the fluorescence. Secondly, a merocyanine group was appended opposite the N-phenyl group. Peroxynitrite causes an oxidative cleavage of the merocyanine group, blueshifting the emission from red to green. Notably, other oxidants can induce the N-dearylation reaction but not the nucleophilic attack to the merocyanine group, meaning the response towards peroxynitrite is highly selective. The capability of **60** to image endogenous $ONOO^-$ in EA.hy926 endothelial cells was tested. As shown in Fig. 54b, **60** responded to exogenous $ONOO^-$ sensitively, with the emission of the green channel (420–500 nm, λ_{ex} = 405 nm) intensified in a $ONOO^-$ dose-dependent way while the emission of the red channel (560–630 nm, λ_{ex} = 543 nm) first intensified and then attenuated as more $ONOO^-$ was added.

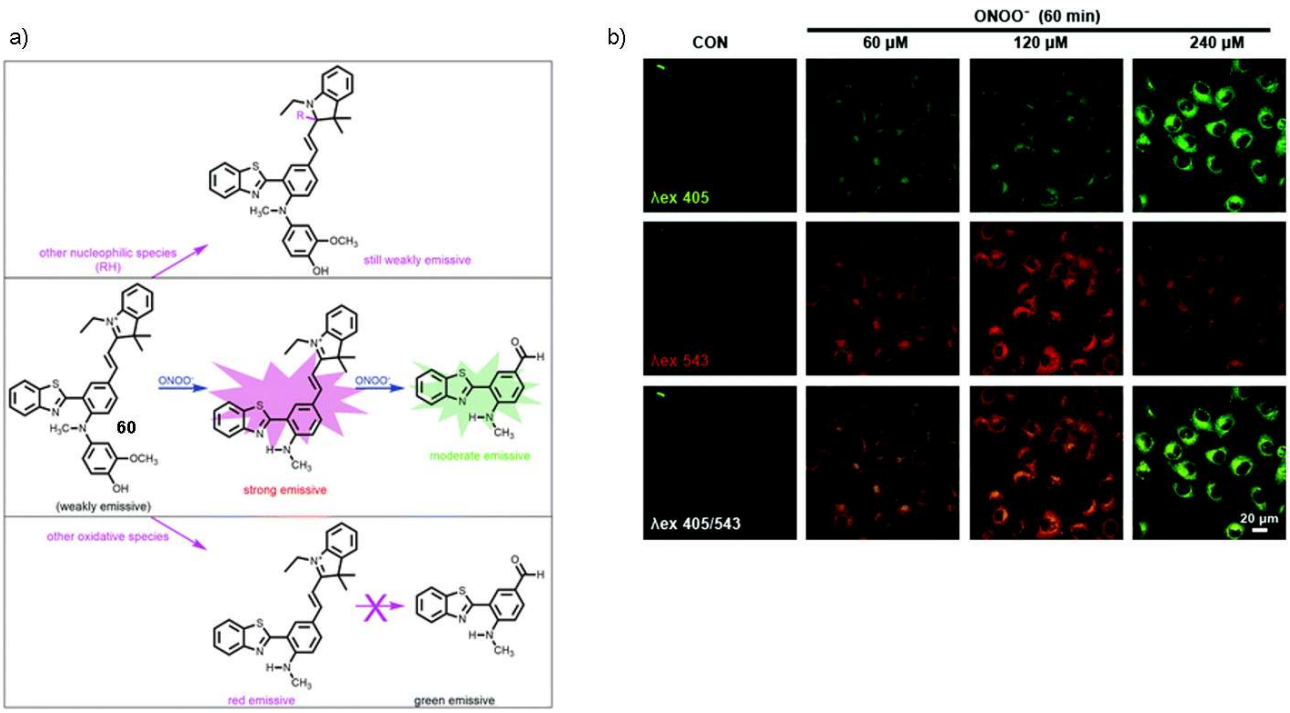

Fig. 54. a) Proposed mechanism for peroxynitrite sensing by **60**; b) imaging exogenous $ONOO^-$ in EA.hy926 live endothelial cells using **60**. Cells were incubated with $ONOO^-$ at various concentrations for 1 h, followed by staining with **60** (5 mM) for 0.5 h. Cells were then fixed in 4% PFA for 10min and imaged using a confocal microscope. The intracellular **60** fluorescence was recorded with excitation at 405 nm and emission at 420–500 nm for the green channel colour, and excitation at 543 nm and emission at 560–630 nm for the red channel colour. Adapted with permission from Ref. [125].

Three highly selective probes for sulfide sensing have been developed (**61**-**63**) [126], implementing two novel strategies. The first deals with a sulfide-mediated reduction of an azide and a subsequent annulation, forming a new fused ring system (probes **61**-**62**) (Fig. 55). The second strategy exploits a non-fluorescent tetrazole ring system that can be formally considered as a latent (or camouflaged) azide. Reduction of the latent azide destroys the fused ring, ensuing a push-pull mechanism (probe **63**). The two mechanisms proposed for **61**-**63** were confirmed by X-ray diffraction analysis (Fig. 56a). Upon addition of Na_2S in aqueous solution (pure water for **61** and a mixture of H_2O/acetonitrile for **62** and **63**) a significant enhancement of the fluorescence emission of 70-fold for **61**, 10-fold for **62**, and 70-fold for **63**, at λ_{em} 445, 440, and 432 nm, for **61**, **62**, and **63**, respectively, was observed (Fig. 56b). An LOD of 2.07, 0.67, and 1.73 μM was determined for **61**, **62**, and **63**, respectively. Probe **61** was finally used to determine the blind concentration of sulphide with RGB analysis using a smartphone and bioimaging in the ovary of fruit flies.

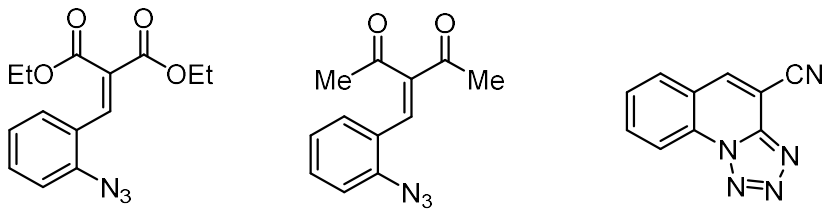

61 **62** **63**

Fig. 55. Chemical structures of sulfide detectors **61**-**63**.

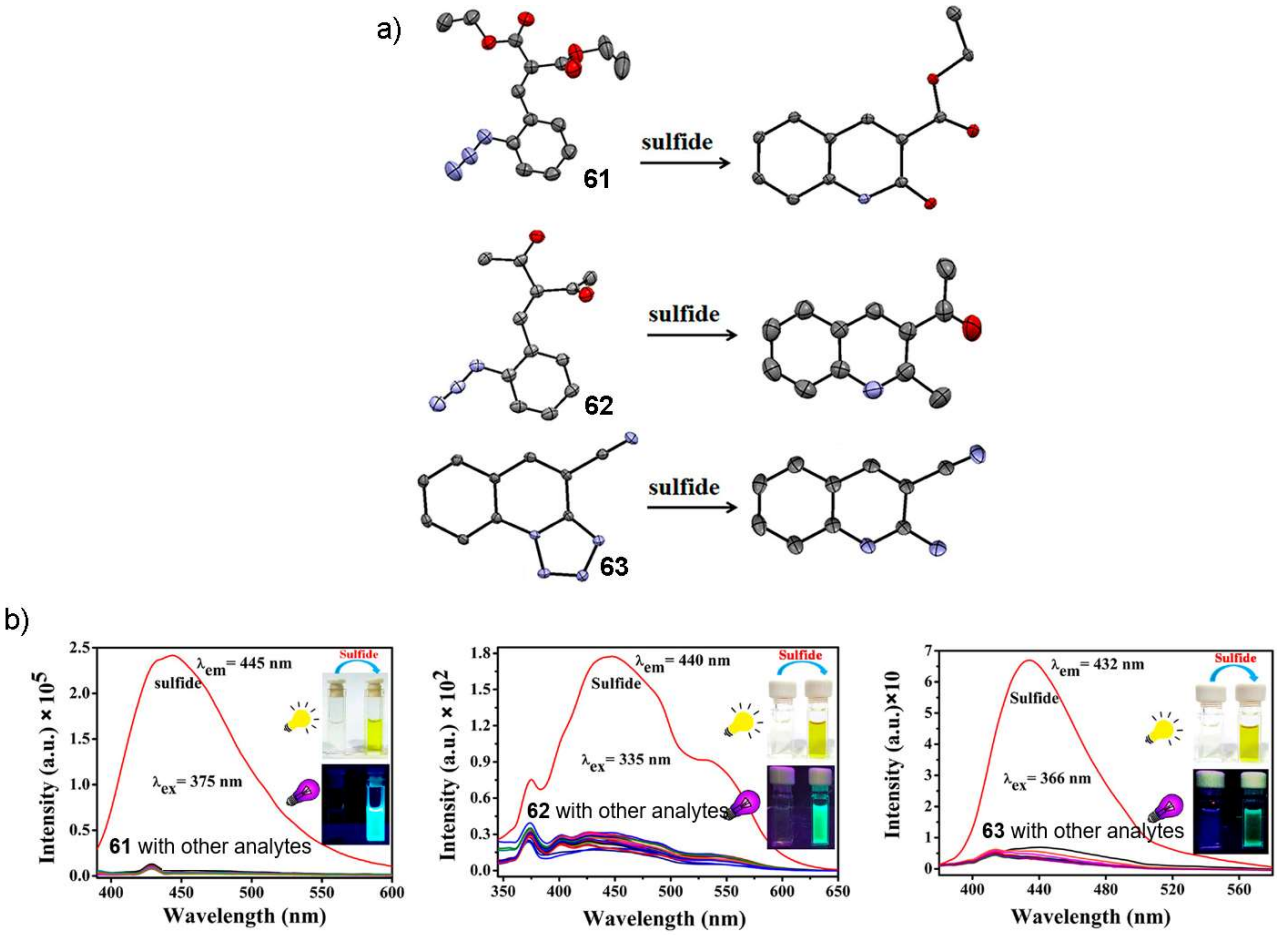

Fig. 56 a) Crystal structures of probes **61**-**63** and their corresponding products obtained upon addition of sulfide; b) fluorescence spectral changes of (from left to right) probe **61**, probe **62**, and probe **63** (100 µM each) upon addition of various analytes (H_2O_2, perborate, aerial oxygen, ascorbate, $S_2O_3^{2-}$, $S_2O_4^{2-}$, $S_2O_5^{2-}$, HSO_3^-, CN^-, SCN^-), inset: visual changes of the respective probes before and after addition of sulfide under ambient light (above) and UV light (below). Adapted with permission from Ref. [126].

Two chemodosimeters with a ratiometric response to mitochondrial superoxide were reported (**64** and **65**) [127, 128]. Salt **64** contains 1,8-naphthalimide as a fluorophore, a triphenylphosphonium cation as the mitochondria-targeting group, and a diphenylphosphinate moiety as the $O_2^{\bullet-}$ recognition group. Probe **64** showed rapid response, high sensitivity and selectivity to $O_2^{\bullet-}$ and accumulated in mitochondria allowing for the visualization of superoxide fluctuations in live cells and inflammatory *Daphnia magna*. In the case of **65,** the diphenylphosphinate moiety was used as the $O_2^{\bullet-}$ recognition group, while diketopyrrolopyrrole functionalised with a pyridinium group was used as the fluorogenic fragment. This probe was used for the endogenous superoxide anion detection and imaging in living cells and in mice.

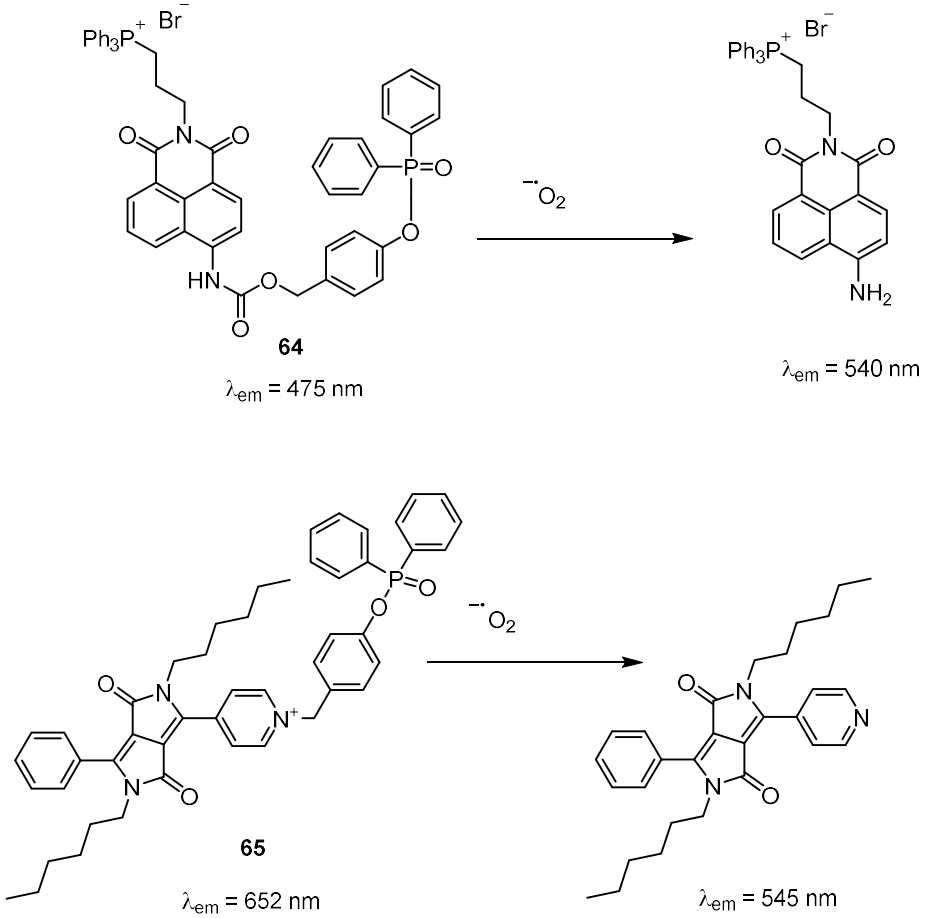

Fig. 57. Chemical structures and reaction with superoxide of chemodosimeters **64** and **65**.

11. Anion Sensing Using Arrays

Multi-component arrays have been employed to great effect to the task of sensing anionic species. Receptors, which are perhaps unselective individually, are employed together to produce a unique fingerprint response for a given analyte [129]. These responses may be collected discretely, or the receptors are applied onto a gel or polymeric surface to afford a sophisticated structure capable of distinguishing anionic species with a high degree of accuracy.

Anzenbacher and co-workers have expanded on their previous research by synthesising a series of dye-appended calixpyrroles (**66-70**) for sensing dicarboxylates (Fig 58) [130]. Probes **68** and **69** contain expanded calixpyrrole cores to promote the inclusion of larger carboxylate ions. However, fluorescence titration data, measured in acetonitrile, indicated that these probes demonstrated no significant selectivity and the binding affinities were lower than those of the parent macrocycles. This cross-reactivity prompted the incorporation of the sensors into a collaborative array which produced a distinct response pattern for each species. Specifically, the receptors were incorporated into a urethane hydrogel matrix and applied to a multi-well glass surface; the colorimetric response to an excess of various anions in shown in Fig. 59a. Linear discriminant analysis (LDA) was performed and the model enabled the correct identification of 18 distinct anions (Fig. 59b). The system was also discovered to be sensitive to oxalate and malonate concentration, and calibration curves were constructed to quantitively determine the concentration of these anions in an unknown solution with a root mean square error of less than 1%.

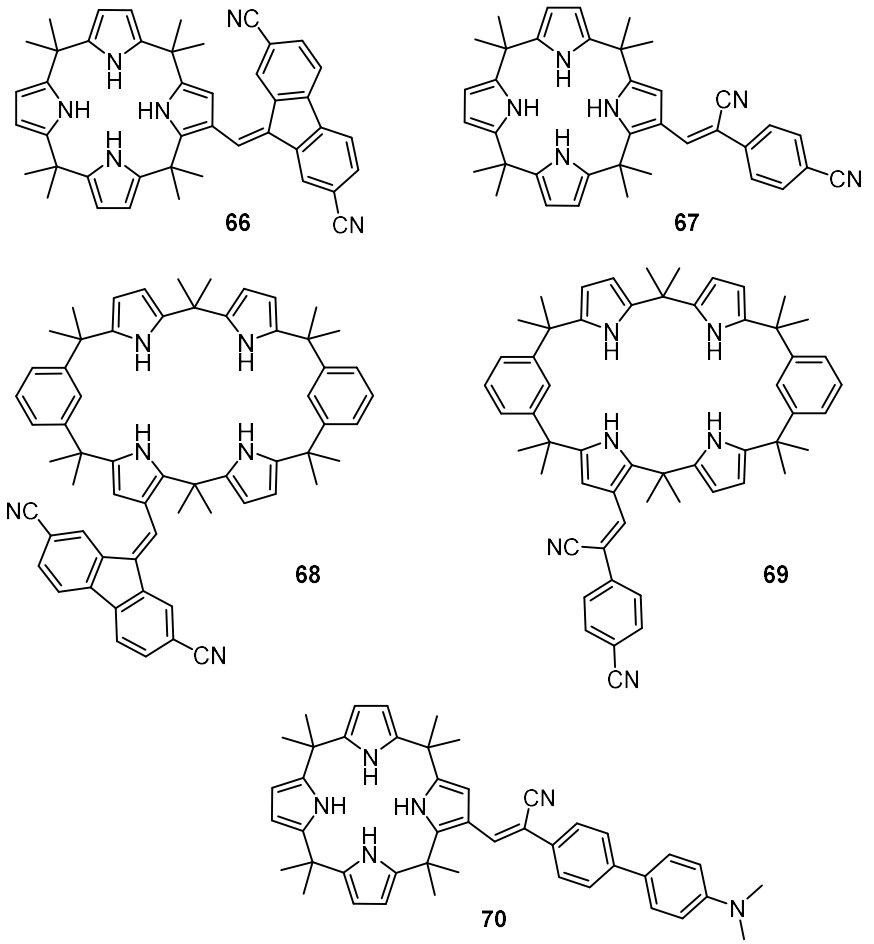

Fig. 58. Chemical structures of dicarboxylate sensors **66**-**70**.

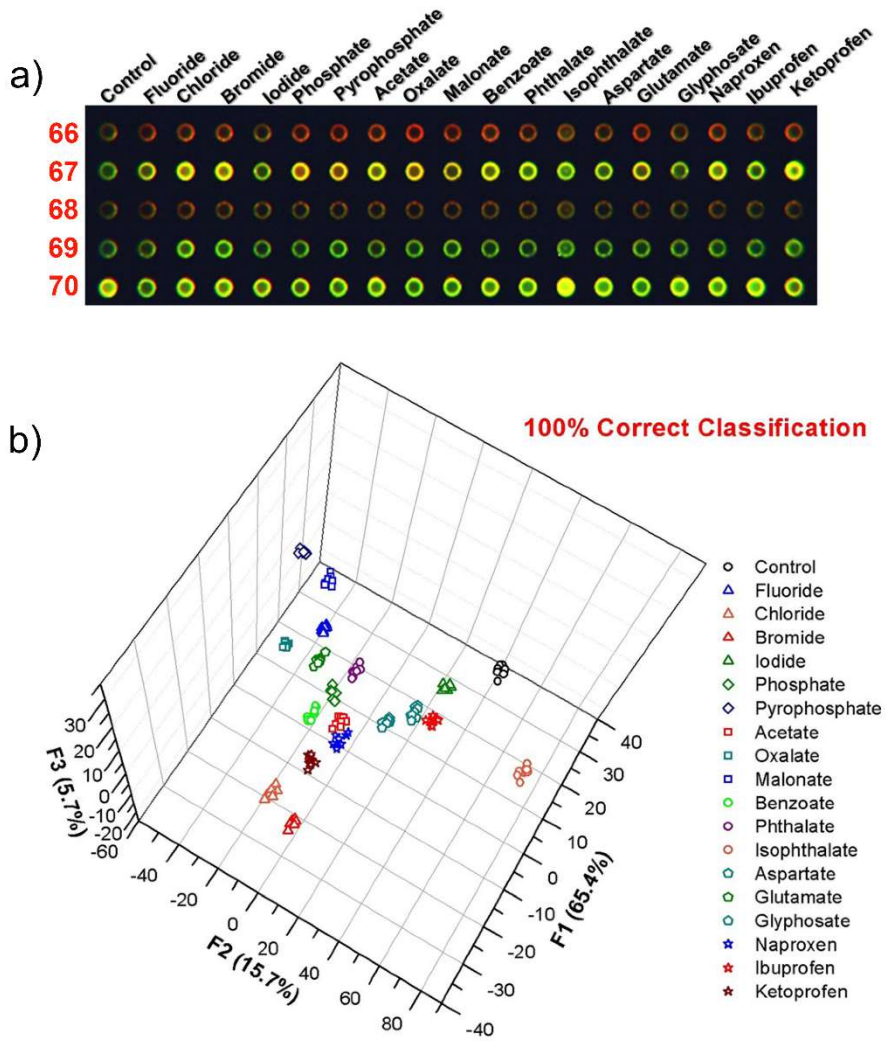

Fig. 59. a) Image of the response of sensors **66-70** to various anions under UV excitation after being embedded into a polyurethane matrix (H_2O/THF); B) output of the LDA, profiling the response of 18 anionic species to an array of sensors **66-70**. Reproduced with permission from Ref. [130].

Butler and co-workers have developed a time-gated, array network comprised of europium- and terbium-based receptors **71-74.** These complexes (Fig. 60) were capable of detecting large, biologically important polyphosphates, such as ATP, in aqueous solution [131]. The modulation in intensity of multiple emission bands upon anion binding (Fig. 61a) and changes in luminescence lifetimes (which were determined using time-resolved measurements) provided several variables for each binding event. Initially, the response pattern for a single receptor was interrogated using principal component analysis (PCA) and the components were plotted, showing clustering for four adenosine-derived anions. The application of PCA to a combination of luminescence data from all four receptors demonstrated the system's ability to discriminate eight nucleotides in buffered aqueous solution (Fig. 61b).

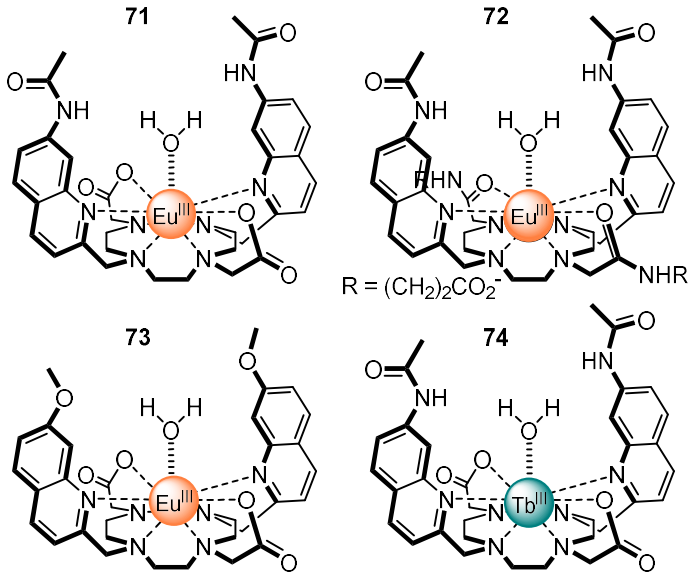

Fig. 60. Chemical structures of lanthanide-complexed receptors **71**-**74.**

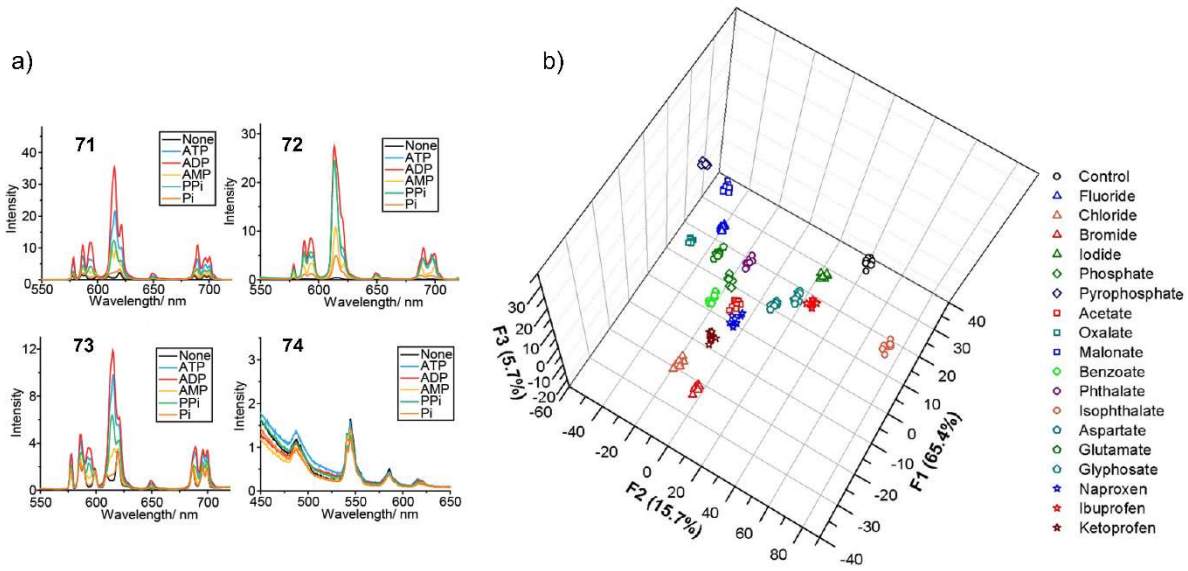

Fig. 61. a) Emission spectra of **71** (8 µM), **72** (13 µM), **73** (10 µM) and **74** (15 µM) upon the addition of various anions (1 mM, 10mM HEPES, pH 7.0); b) PCA outputs for an array of **71-74** (at same relevant concentrations) with a series of adenosine- and guanosine-derived phosphate anions (1 mM, 10mM HEPES, pH 7, 298 K). Reproduced with permission from Ref. [131].

Research by Minami and co-workers has focused on the use of a coordination binding-based colorimetric sensor array (CBSA) to identify oxoanions [132]. The chemosensors were prepared by complexing an

indicator dye molecule to a Zn^{2+} centre to create a series of four coordinated dyes **75-78** (Fig. 62). Introduction of an anion causes competitive coordination to occur, and displacement of the indicators resulting in detectable changes in the system's optical properties. Interestingly, the dyes displayed unique changes in absorbance intensity when displaced by structurally similar phosphates and carboxylates (Fig. 63a). LDA was used to elucidate patterns in the responses, and the model was applied to classify 10 carboxylate and phosphate species in HEPES buffered aqueous media with 100% success. Glyphosate, which contains both a carboxylate and phosphate group, produced a concentration-dependent response pattern, as seen in Fig. 63b. This allowed researchers to use an artificial neural network regression model to construct a calibration curve (Fig. 63c) and correctly predict its concentration in samples of a commercial herbicide and tap water.

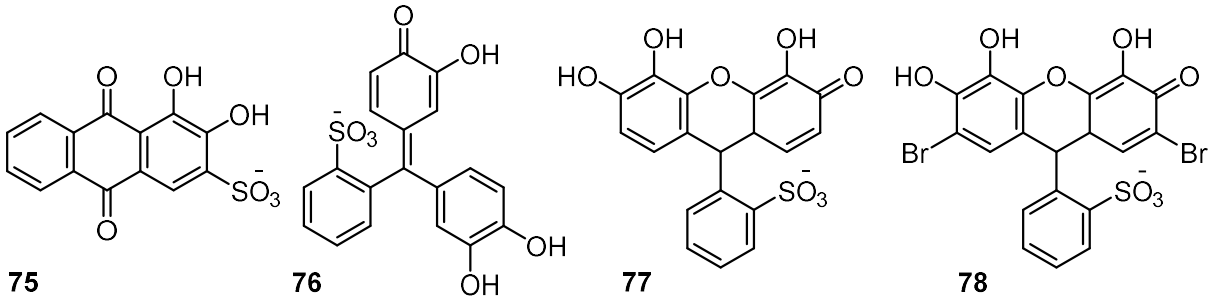

Fig. 62. Structures of coordinated dyes **75-78**.

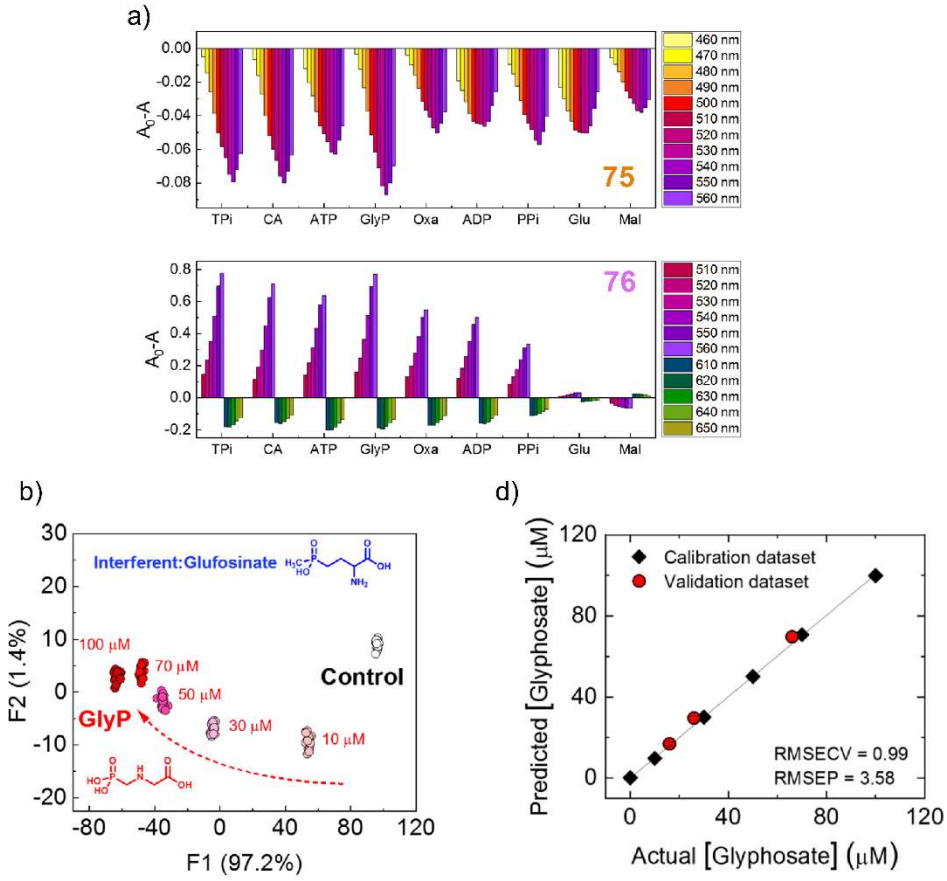

Fig. 63. a) Examples of the colorimetric response of dye-Zn^{2+} complexes (40 µM) after the addition of different phosphate species; b) LDA plot for the assay of **75-78** for increasing concentrations of glyphosate (GlyP, 0-100 µM) in the presence of glufosinate (1 mM). Each concentration was repeated 24 times; c) results of the

ANN regression for glyphosate (black), and results from unknown samples (red). Reproduced with permission from Ref. [132].

12. Molecular Logic Gates

The field of molecular logic gates has been pioneered by A.P. de Silva.[133] Molecular logic gates can accept a number of inputs and give an output based on Boolean logic. Several examples of molecular logic gates have been recently proposed in which the deprotonation of the chemosensors upon the addition of highly basic anions such as F^-, CN^-, AcO^- or $H_2PO_4^-$ caused a colour change, a quenching of the fluorescence properties, or an enhancement/shift of the photochemical properties of the free probes. By incorporating these responses as 'inputs', molecular logic gates have been developed, for example by introducing a protic source into the system (i.e. TFA) in order to restore the original properties of the free chemosensors. [134, 135]

In this context, Banarjee and co-workers have reported a combination of NAND, NOT and NOR logic function for the simple urea-based chemosensor **79** (Fig. 64a) [136]. As shown in the Fig. 64b, **79** exhibited a characteristic absorption band at 290 nm in a mixture of DMSO/CH_3CN (9:1 v/v) which diminished upon the addition of increasing amount of F^-, with a concomitant formation of a new band at 590 nm and a distinct colour change from colourless to dark blue in the presence of fluoride (Fig. 64b).

Analytical experiments, such as ^1H NMR measurements, along with theoretical calculations suggested a strong host-guest interaction corroborated by the high binding constant value calculated from the Benesi-Hildebrand equation ($>10^4\ M^{-1}$). The appearance of the signal attributed to the HF species in the ^1H NMR and ^{19}F NMR spectra suggested that the recognition event is followed by the partial deprotonation of the NHs adjacent to the phenyl group of **79**. From the UV-Vis spectra, it was clearly observed that the addition of H^+ into the **79**-F^- system was able to quench the absorption band at 590 nm restoring the initial peak at 290 nm of the free receptor (Fig 64c). The truth table successfully evidenced the mimic the logic functions AND-NOT-NOR for **79** in the presence of F^- and H^+. The output is 1 when both inputs 1 (sensor) and 2 (F^-) are present, while when the input 3 (H^+) is added the process is inhibited, and the output signal is 0 (Fig 64d).

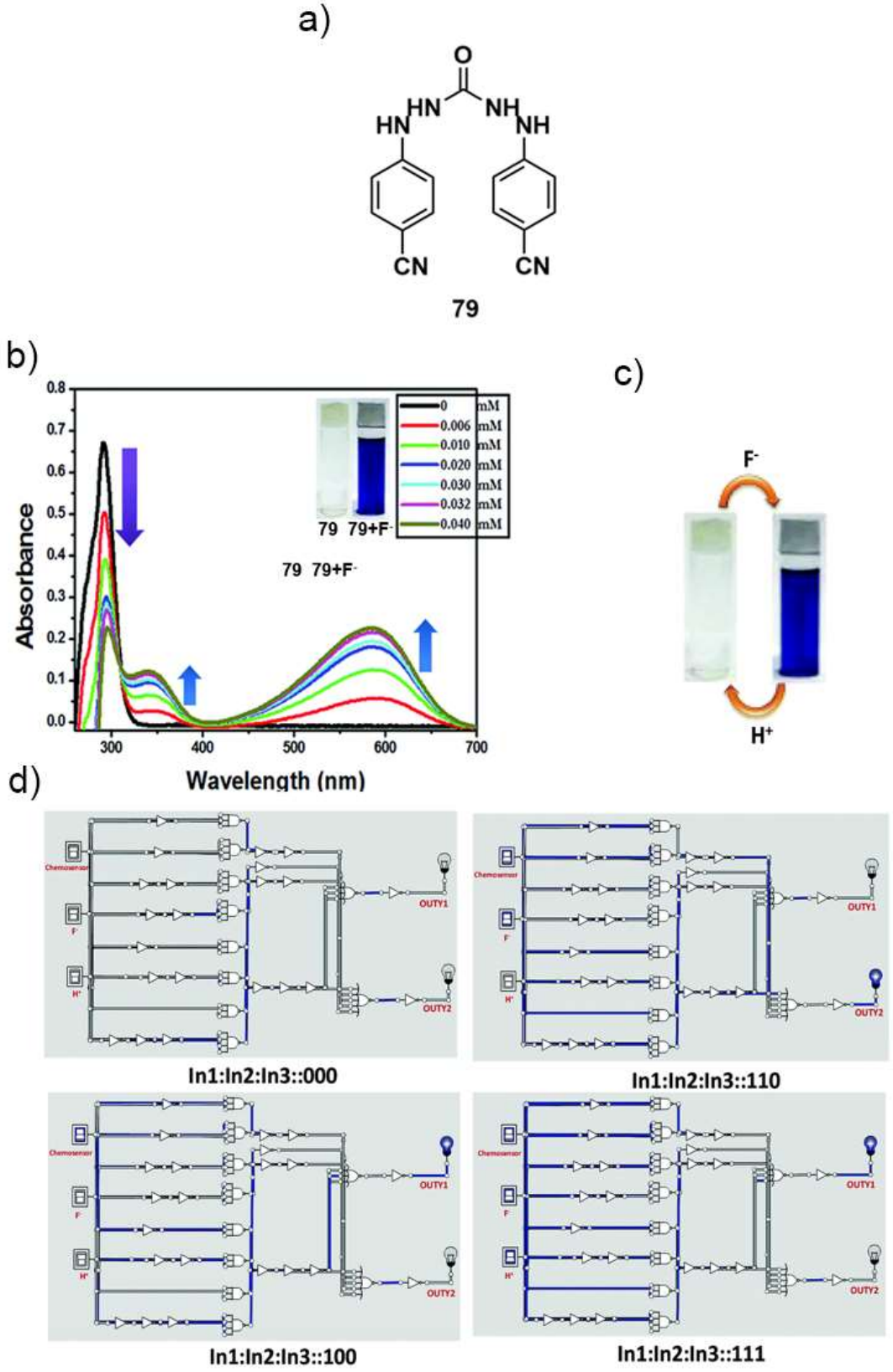

Fig. 64. a) Chemical structure of urea-based receptor **79**; b) absorption spectra of **79** upon gradual addition of F^- in a mixture of DMSO/acetonitrile (9:1 v/v); c) colorimetric responses of **79** with the alternative addition of F^- and H^+; d) fabrication of the logic gate with outputs (Y1 and Y2) upon alternative inputs of NAND-NOT-NOR logic functions for **79** with F^- and H^+. Reproduced with permission from Ref. [136].

Another approach frequently employed in the design of new molecular logic devices exploits the multianalyte detection capability of some chemosensors. Particularly, several examples have been developed in which the chemosensor was able to bind a metal ion, such as Cu^{2+}, Zn^{2+} or Hg^{2+} causing a modification of the colorimetric of photochemical properties of the chemosensor that are then restored by the secondary detection of an anionic species. Indeed, the complex served as a secondary chemosensor probe responding specifically to an anionic species [137-141].

Ghosh and co-workers reported the INHIBIT logic gate for a dual response OFF-ON-OFF system displayed by the chemosensor **80** designed for the recognition of zinc ions over other transition metal ions *via* fluorescence ON response (Fig. 65a) [138]. The chemosensor was non-fluorescent in a mixture of DMSO/ water (1:9 v/v). Upon the addition of increasing amount of Zn^{2+} the formation of a new fluorescence band at λ_{max} = 521 nm was observed (Fig. 65b), which was negligible in the presence of the other transition metal ions tested (Fig 65c).

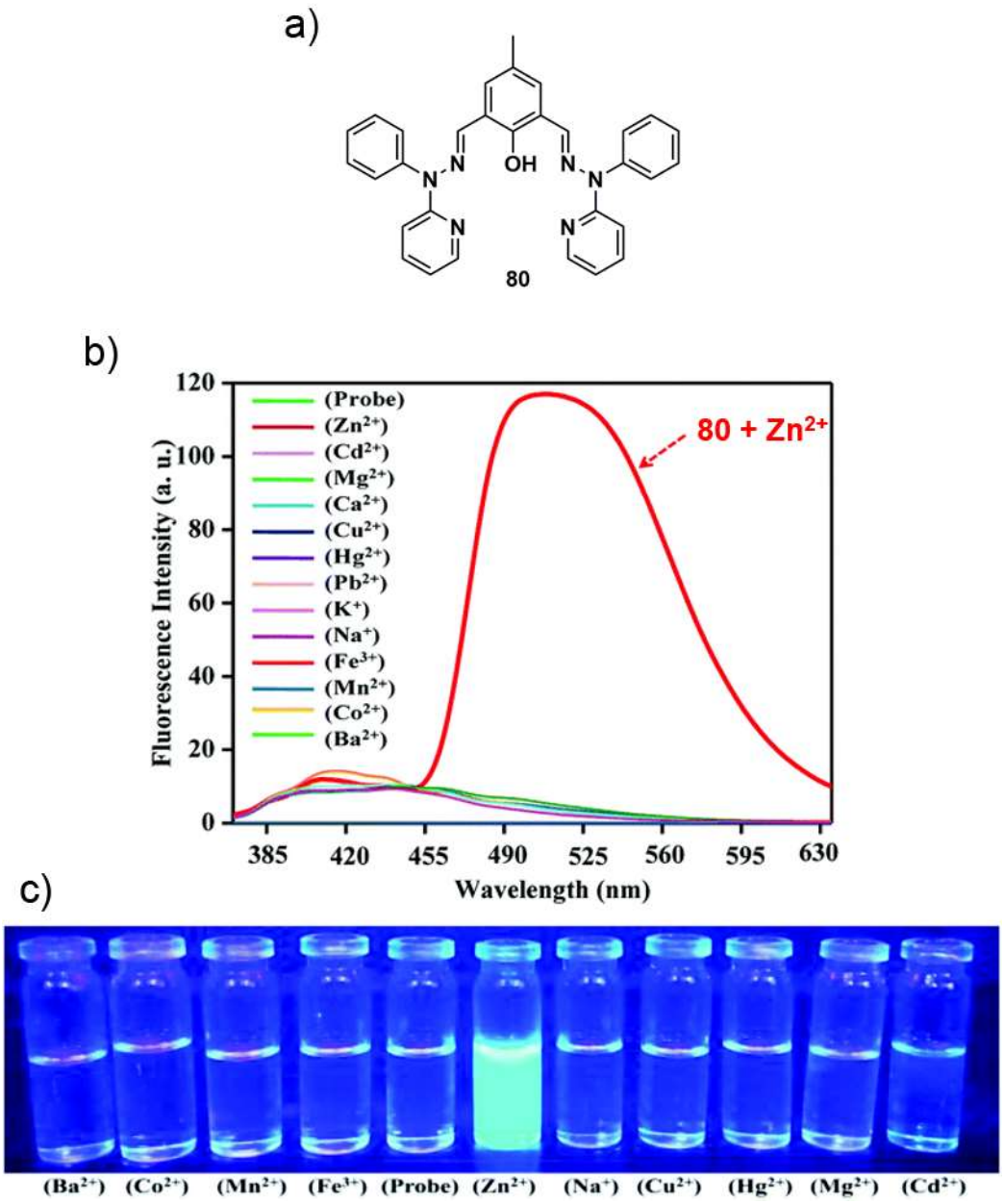

Fig. 65. a) Chemical structure of chemosensor **80**; b) emission spectral changes of **80** (40 µM) upon addition of metal ions (40 µM) in DMSO/H_2O (1:9 v/v) (λ_{ex} = 400nm); c) bright blue fluorescence exhibited by the zinc complex of **80** under UV light. Reproduced with permission from Ref. [138].

Surprisingly, fluorescence spectral studies of the zinc complex in the presence of a series of anionic species indicated that remarkable quenching of the emission properties was caused by the addition of PPi. In addition, a bathochromic shift (from 521 nm to 526 nm) of the emission band was observed. The fluorescent properties displayed by **80** have been applied to an INHIBIT logic gate with two binary inputs represented by Zn^{2+} and PPi^{3-} and adopting as output signal the fluorescent band at 523 nm. As shown in the truth table in Fig. 66, if **80** is treated with Zn^{2+} the fluorescence is switched on and the output signal is 1, while if both the inputs are present at the same time the fluorescence is quenched as response to the detection of the PPi and the output signal is 0.

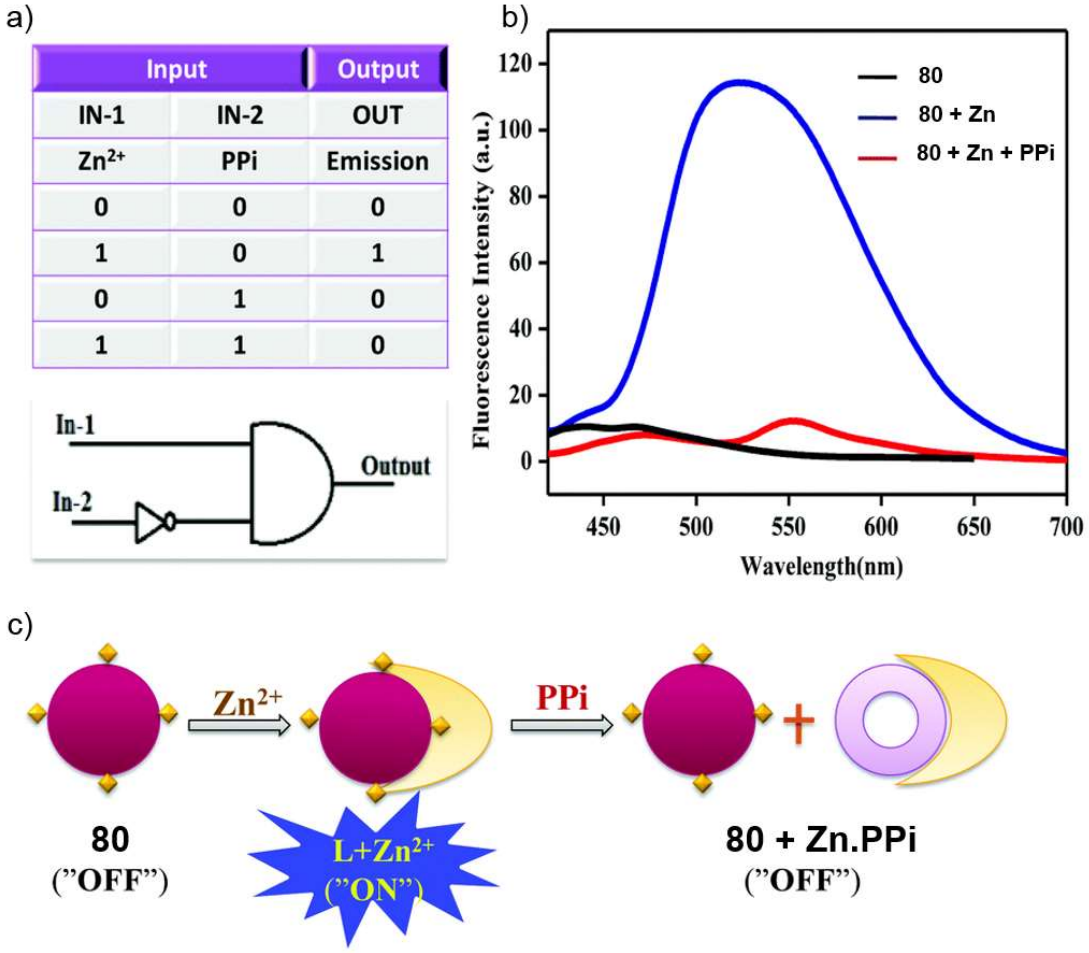

Fig. 66. a) Truth table and the respective symbolic representation of the INHIBIT logic gate; b) emission spectra depicting the conditions mentioned in table; c) schematic representation showing fluorescence "OFF-ON-OFF" mechanism. Adapted with permission from Ref. [138].

Das, Escudero and co-workers reported the first example of INHIBIT logic gate response for F^-/H^+ and AcO^-/H^+ in aqueous methanolic solution for the tetranuclear Zn^{2+} complex of macrocycle **81** (Fig 67a) [142]. Upon the addition of an aqueous solution of F^- and AcO^- (as tetrabutylammonium salts) to a methanol solution of **81** the band at 411 nm decreased while the band at 361 nm increased with a blue shift up to 355 nm (Fig. 67b), which was not observed in the case of other anions. Furthermore, the addition of F^- and AcO^- ions caused a change in the fluorescence emission of the complex, which showed a maximum at 472 nm when excited at 375nm, with a considerable blue shift along with an incremental increase in fluorescence intensity (Fig. 67c).

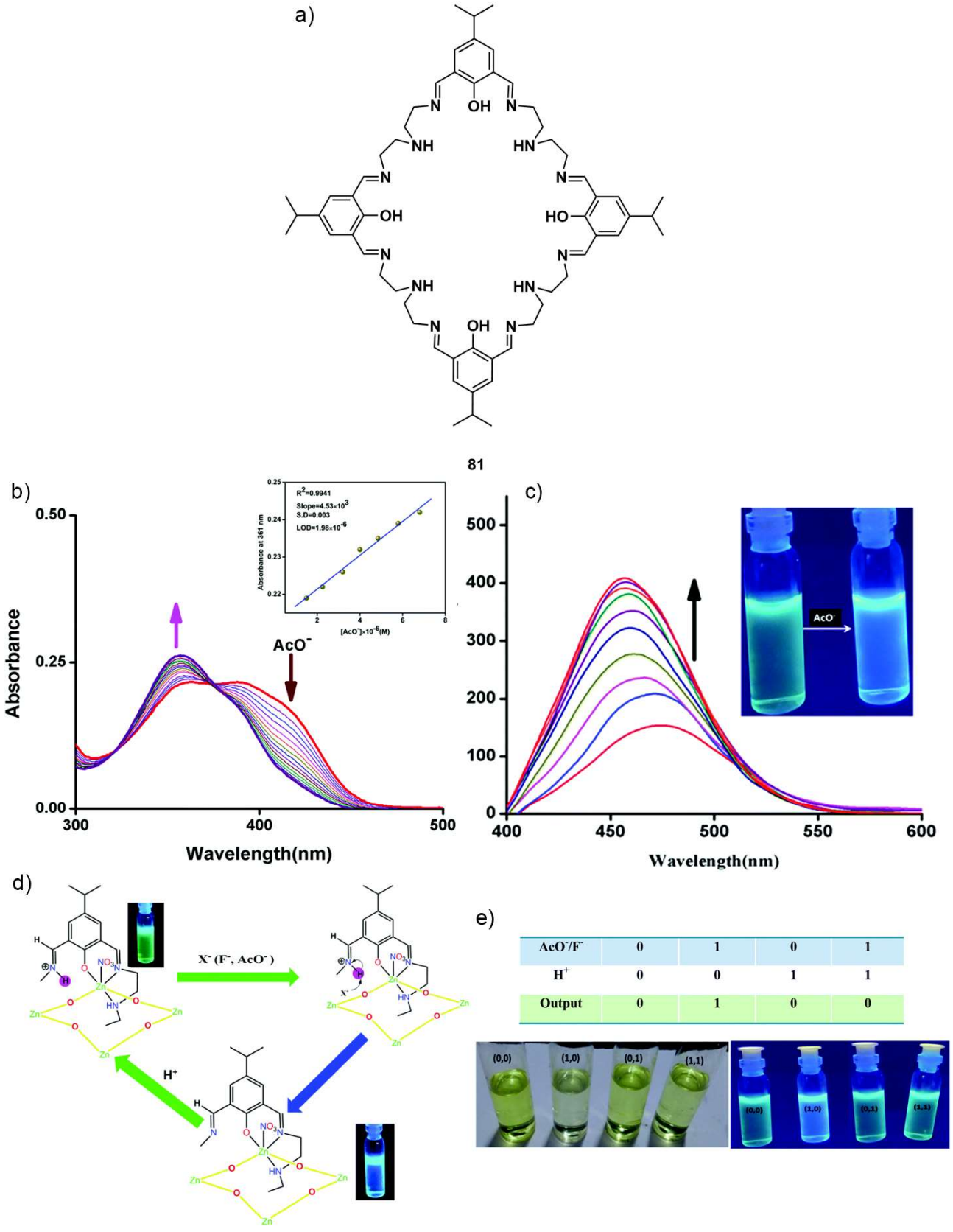

Fig. 67. a) Structure of macrocycle **81**; b) Uv-vis titration of the tetranuclear Zn^{2+} complex of **81** (25 µM) with AcO^-, inset: calibration curve for the determination of the LOD; c) fluorescence spectral changes of the tetranuclear Zn^{2+} complex of **81** (25µM) upon the addition of AcO^- (5 equivalents) in MeOH; d) proposed mechanistic pathway of the tetranuclear Zn^{2+} complex of **81** binding the anion species F^- and AcO^-; e) truth

table for the proposed INHIBIT logic gate response with colour change in the solution phase under the naked-eye as well as under a UV lamp. Reproduced with permission from Ref. [142].

^{1}H NMR titrations of the tetranuclear Zn^{2+} complex of **81** in the presence of F^- and AcO^- suggested how the optical response of the system towards these anions is solely guided by deprotonation of the iminium proton from the complex. Since the deprotonation of tetranuclear Zn^{2+} complex of **81** was induced by the presence of anions, it was checked whether the deprotonation can be reversed by introducing a proton source to the **81**-anion ensemble. The reversibility of the mechanism by addition of a protic acid (trifluoroacetic acid, TFA) was checked in order to provide a chemical INHIBIT logic gate where AcO^- and H^+ act as the inputs. The truth table, along with the naked eye change reported in Fig. 67e, highlights how the behaviour of the system rightly mimicked the logic gate circuit proposed. Interestingly, the system was also used for the detection of fluoride in commercially available toothpaste as well as solid state detection of F^- and AcO^- by paper strips.

Piramuthu and co-workers described the first example of a naked eye cyanide sensing *via* the bound fluoride displacement assay [143]. The tripodal receptor **82** (Fig. 68a) showed appreciable sensing ability towards F^- and CN^-, as suggested by naked-eye colorimetric experiments and UV-Vis spectroscopy. Fascinatingly, by studying the selectivity of the receptor for F^-, the researchers observed that the colour of the adduct formed upon the addition of CN^- to the fluoride adduct was dark orange, almost similar to the colour of the adduct of the **82** in the presence of the CN^- species. This evidence was confirmed by UV-Vis measurements, which clearly indicated the CN^- species was able to replace the F^- from the **82**-F^- adduct. Upon the addition of both F^- and CN^- (as tetrabutylammonium salts) to the solution of **82** in acetonitrile, the band of the free receptor centred at 342 nm was red shifted to 350 and 352 nm for F^- and CN^-, respectively, as a response to the π-π^* transition to a lower energy. In addition, the presence of CN^- caused the appearance of a new band at 453 nm that increased gradually upon the addition CN^- into the system (Fig. 68b). The same response was observed when cyanide was added to the 1:1 adduct of **82** with fluoride (Fig. 68c).

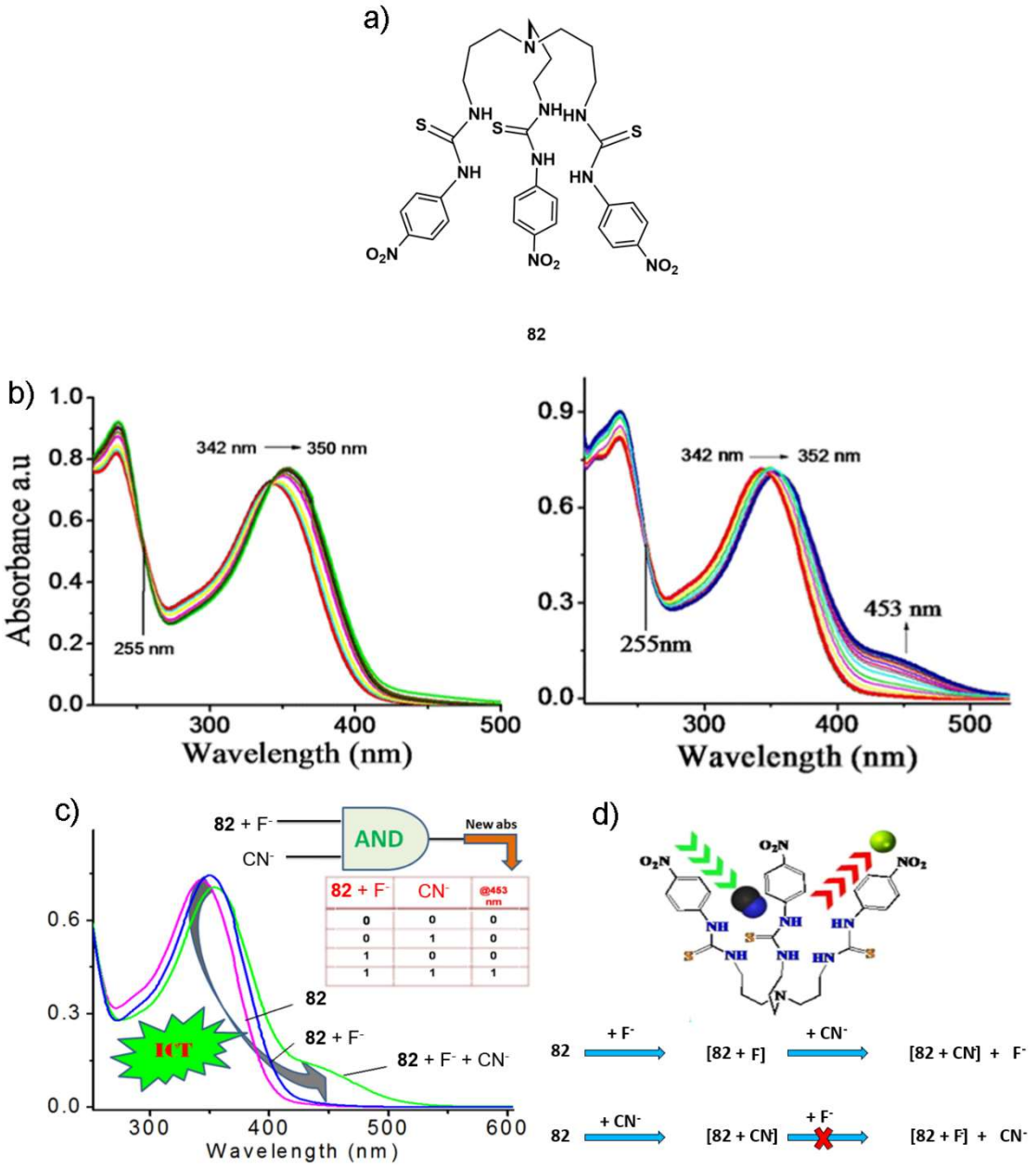

Fig. 68. a) Chemical structure of **82**; b) change in the UV-Vis spectra of **82**-F^- in the presence of various concentrations of CN^- in acetonitrile, yielded **82**-CN^-; c) the changes of absorbance at 453 nm in the presence of chemical inputs with **82**-F^- and CN^-, inset: the logic circuit and corresponding truth table for the AND logic gate; c) the proposed mechanism for the selective binding of CN^- over F^- by **82**. Adapted with permission from Ref. [143].

Furthermore, calculated binding constant by means UV-Vis titrations evidenced how the constant for the 1:1 adduct **82**-CN^- (K_{11} = 2.51 x 10^5 M^{-1}) was three order of magnitudes higher than that calculated for **82**-F^-(K_{11} = 1.92 x 10^2 M^{-1}). Motivated by this behaviour, the authors decided to employ the sensory system as an AND gate. Thus, by considering the absorbance of the adduct **82**-F^-at 453 nm as the output signal using **82**-F^-, the truth table presented in Fig. 68c (inset) confirmed how the output signal appeared only in the presence of CN^- while remained zero in the presence of the other combinations of inputs.

Gao and co-workers reported the bipyridinium Zr (IV) metal organic framework UiO-67-DQ for multipurpose use as anion sensor and chemical logic gate operations [144]. The authors investigated the MOF properties as a chemical sensor for the detection of I^- in solution. UiO-67-DQ in water or ethanol consisted of a stable milky suspension with a characteristic fluorescence emission at 423 nm. The addition of I^-, Br^- and SCN^- caused an anion dependent colour change and fluorescence quenching of the system, as shown in Fig. 69a and 69b, specifically for I^-. Fluorescence titrations conducted in water and ethanol highlighted how the addition of increasing amount of KI lead to quenching of the emission band at 423 nm, with a quenching efficiency of 83% and 94%, in water and ethanol, respectively. The switching properties of the present MOFs were used in the construction of new chemical logic gate circuit in which I^- operating on UiO-67-DQ mimics a NOT gate when the output is the fluorescence emission at 423 nm.

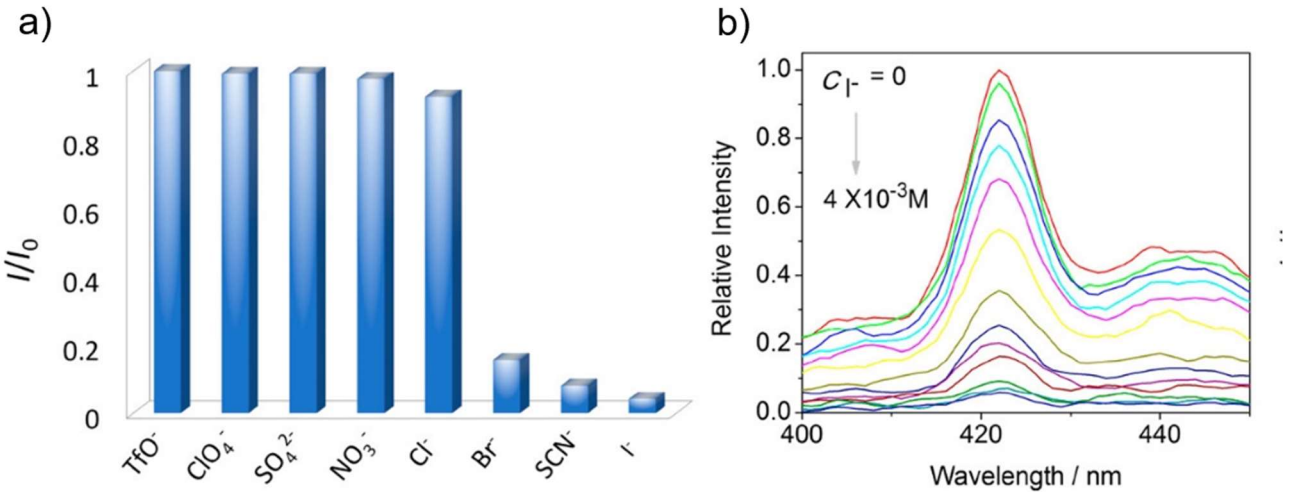

Fig. 69. a) Relative fluorescence intensity (at 423 nm) of UiO-67-DQ-TfO/EtOH dispersions in response to various anions (4 mM); b) variation of fluorescence spectra upon incremental addition of KI. Adapted with permission from Ref. [144].

Sun, Lu, and co-workers reported the ternary NOR logic gate for PPi, ATP and ADP [145]. While investigating the brilliant peroxidase-mimic activity of histidine-protected gold nanoclusters (His-AuNCs), the authors discovered the intriguing ability of some phosphate-containing metabolites including PPi, ATP and ADP, to hamper the nanocluster peroxidase-mimic activity. By using His-AuNCs-catalyzed chromogenic reaction of TMB-H_2O_2 as signal generator and amplifier, a colorimetric switch for phosphate-containing metabolites was produced.

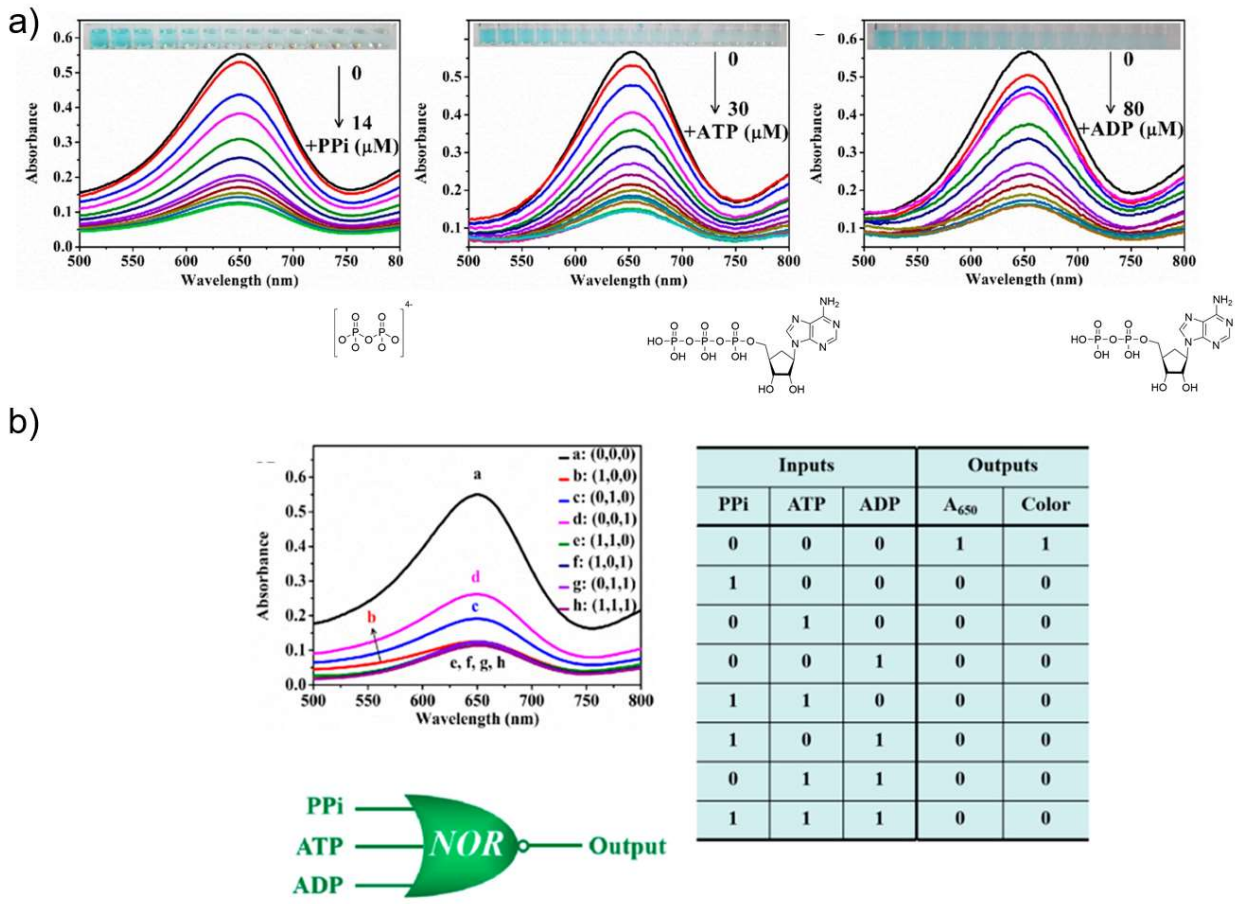

Inputs			Outputs	
PPi	ATP	ADP	A_{650}	Color
0	0	0	1	1
1	0	0	0	0
0	1	0	0	0
0	0	1	0	0
1	1	0	0	0
1	0	1	0	0
0	1	1	0	0
1	1	1	0	0

Fig. 70. a) UV-vis absorption spectra and colour changes of His-AuNCs-H_2O_2 systems in the presence of different concentration of PPi, ATP and ADP; b) UV-vis absorption spectra, truth table and schematic diagram of the ternary NOR logic gate. Reproduced with permission from reference [145].

As shown in Fig. 70a, in the presence of H_2O_2 and TMB at pH 5.2, the absorbance characteristic of the system at 652 nm declines progressively with an increase in the concentrations of PPi, ATP and ADP and a colorimetric detection of the three phosphate-based anions was enabled. On the basis of the colorimetric response for the phosphate-containing metabolites, the authors rightly fabricated a NOR logic gate circuit, constructed by using PPi, ATP and ADP as inputs and the absorbance at 652 nm as the output signal. The logic circuit and the truth table shown in Fig. 70b evidenced how with no inputs (0,0,0 state) the His-AuNCs can catalyse the oxidation of TMB to oxTMB with a blue signal and intense absorbance (output 1), whereas the addition of PPi, ATP or ADP greatly inhibits the catalytic activity of the system (output 0).

13 Conclusions

This review highlights the growing number of sensors for anionic species that have excellent selectivity. We have also seen the development of sensors that can function in biological systems including in bacteria and in mammalian cells. Recently in seminal contributions to anion sensing, Dodani & co-workers identified both naturally occurring[146] and engineered proteins[147] which are capable of acting as turn-on fluorescent sensors for chloride. The former was found in the jellyfish *Phialidium sp.* (phi YFP), and a chloride binding event at pH 5.5. resulted in the protonation of a chromophore phenolate close to the binding cleft. Resultant excitation with λ_{ex} = 400 nm lead to a detectable ESPT fluorescence response. The group touched on the potential to further improve the selectivity of these proteins through mutagenesis, and their inherent biocompatibility should provide much inspiration for receptors in the future. As the selectivity and robustness

of receptor systems continues to improve, we can look forward to the development of sensors for anions that work effectively in a number of real-world applications.

Acknowledgements

PAG would like to thank the Australian Research Council (DP180100612 and DP200100453) and the University of Sydney for funding. CC would like to thank MIUR (PRIN 2017 project 2017EKCS35) Università degli Studi di Cagliari (FIR 2016-2019) and Fondazione di Sardegna (FdS Progetti Biennali di Ateneo, annualità 2018) for financial support.

References

[1] P.A. Gale, C. Caltagirone, Coord. Chem. Rev., 354 (2018) 2-27.
[2] B. Babür, N. Seferoğlu, Z. Seferoğlu, J. Mol. Struct., 1161 (2018) 218-225.
[3] C. Chatterjee, S. Sethi, V. Mukherjee, P.K. Sahu, N. Behera, Spectrochim. Acta - Part A: Mol. Biomol. Spect., 226 (2020).
[4] T. Gao, W.F. Zhou, Y. Zhao, L. Shen, W.Y. Chang, R.K. Musendo, E.Q. Chen, Y.L. Song, X.K. Ren, Chem. Commun., 55 (2019) 3012-3014.
[5] W. Gao, H. Li, Y. Zhang, S. Pu, Tetrahedron, 75 (2019) 2538-2546.
[6] P.S. Kumar, P.R. Lakshmi, K.P. Elango, New J. Chem., 43 (2019) 675-680.
[7] Z. Li, C. Rao, L. Chen, C. Fu, T. Zhu, X. Chen, C. Liu, J. Org. Chem., 84 (2019) 7518-7522.
[8] A. Panja, K. Ghosh, Supramol. Chem., 31 (2019) 239-250.
[9] C. Pati, K. Ghosh, Supramol. Chem., 31 (2019) 732-744.
[10] C. Pati, R. Raza, K. Ghosh, Spectrochim. Acta - Part A: Mol. Biomol. Spect., 229 (2020).
[11] P.R. Sahoo, A. Kumar, S. Choudhary, Hitaish, R. Chhikara, K. Malik, S. Nirwan, C. Seth, G. Duggal, S. Kumar, J. Incl. Phenom. Macrocyclic Chem., 96 (2020) 181-195.
[12] J. Tummachote, W. Punyain, S. Thanomsak, A. Sirikulkajorn, B. Tomapatanaget, Spectrochim. Acta - Part A: Mol. Biomol.Spect., 214 (2019) 384-392.
[13] I. Yahaya, E. Keleş, A.U. Putra, M. Yahya, N. Seferoğlu, Z. Seferoğlu, J. Mol. Struct., 1204 (2020).
[14] Y. Yin, T. Sarma, F. Wang, N. Yuan, Z. Duan, J.L. Sessler, Z. Zhang, Organic Lett., 21 (2019) 1849-1852.
[15] N. Wu, L.X. Zhao, C.Y. Jiang, P. Li, Y. Liu, Y. Fu, F. Ye, J. Mol. Liquids, 302 (2020).
[16] Q.X. Liu, Z.L. Hu, Z.X. Zhao, Tetrahedron, 74 (2018) 6710-6716.
[17] S.K. Dwivedi, S.S. Razi, A. Misra, New J. Chem., 43 (2019) 5126-5132.
[18] A. Sheykhi-Estalkhjani, N.O. Mahmoodi, A. Yahyazadeh, M.P. Nadamani, Tetrahedron, 74 (2018) 4868-4874.
[19] M. Chemchem, I. Yahaya, B. Aydıner, N. Seferoğlu, O. Doluca, N. Merabet, Z. Seferoğlu, Tetrahedron, 74 (2018) 6897-6906.
[20] A.J. Blok, M.R. Johnston, C.E. Lenehan, Sci. Rep., 7 (2017).
[21] H.D.P. Ali, P.E. Kruger, T. Gunnlaugsson, New J. Chem., 32 (2008) 1153-1161.
[22] R.M. Duke, T. Gunnlaugsson, Tetrahedron Lett., 48 (2007) 8043-8047.
[23] R.M. Duke, T. Gunnlaugsson, Tetrahedron Lett., 52 (2011) 1503-1505.
[24] R.M. Duke, E.B. Veale, F.M. Pfeffer, P.E. Kruger, T. Gunnlaugsson, Chem. Soc. Rev., 39 (2010) 3936-3953.
[25] T. Gunnlaugsson, P.E. Kruger, P. Jensen, J. Tierney, H.D.P. Ali, G.M. Hussey, Journal of Organic Chemistry, 70 (2005) 10875-10878.
[26] F.M. Pfeffer, A.M. Buschgens, N.W. Barnett, T. Gunnlaugsson, P.E. Kruger, Tetrahedron Lett., 46 (2005) 6579-6584.
[27] E.B. Veale, G.M. Tocci, F.M. Pfeffer, P.E. Kruger, T. Gunnlaugsson, Org. Biomol. Chem., 7 (2009) 3447-3454.
[28] H. Huang, Z. Xin, L. Yuan, B.Y. Wang, Q.Y. Cao, Inorg. Chim. Acta, 483 (2018) 425-430.
[29] K. Osawa, H. Tagaya, S.I. Kondo, Chemistry Lett., 49 (2020) 290-294.
[30] L.M. Lopéz-Martínez, J. García-Elías, A. Ochoa-Terán, H.S. Ortega, K. Ochoa-Lara, C.U. Montaño-Medina, A.K. Yatsimirsky, J.Z. Ramírez, V. Labastida-Galván, M. Ordoñez, Tetrahedron, 76 (2020).

[31] P. Kumar, V. Kumar, S. Pandey, R. Gupta, Dalton Trans., 47 (2018) 9536-9545.
[32] T.A. Shumilova, T. Rüffer, H. Lang, E.A. Kataev, Chem. Eur. J., 24 (2018) 1500-1504.
[33] Q. Lin, G.F. Gong, Y.Q. Fan, Y.Y. Chen, J. Wang, X.W. Guan, J. Liu, Y.M. Zhang, H. Yao, T.B. Wei, Chem. Commun., 55 (2019) 3247-3250.
[34] K.M. Bąk, K. Chabuda, H. Montes, R. Quesada, M.J. Chmielewski, Org. Biomol. Chem., 16 (2018) 5188-5196.
[35] O.A. Adegoke, Spectrochim. Acta Part A: Mol. Biomol. Spect., 83 (2011) 504-510.
[36] S. Pangannaya, V. Thimaradka, D.R. Trivedi, Supramol. Chem., 30 (2018) 103-114.
[37] D. Li, S. Zheng, H. Lin, Z. Yang, W. Huang, Supramol. Chem., 30 (2018) 681-686.
[38] L.-M. Pu, X.-Y. Li, J. Hao, Y.-X. Sun, Y. Zhang, H.-T. Long, W.-K. Dong, Sci. Rep., 8 (2018) 14058.
[39] E. García-España, P. Díaz, J.M. Llinares, A. Bianchi, Coord. Chem. Rev., 250 (2006) 2952-2986.
[40] A.S. Oshchepkov, R.R. Mittapalli, O.A. Fedorova, E.A. Kataev, Chem. Eur. J., 23 (2017) 9657-9665.
[41] J. Cai, J.L. Sessler, Chem. Soc. Rev., 43 (2014) 6198-6213.
[42] N. Kwon, G. Baek, K.M.K. Swamy, M. Lee, Q. Xu, Y. Kim, S.J. Kim, J. Yoon, Dyes and Pigments, 171 (2019).
[43] X. Zhang, G. Ko, J.F. Joung, M. Li, Y. Jeong, K.M.K. Swamy, D. Lee, Y. Liu, S. Lee, S. Park, T.D. James, J. Yoon, Chem. Commun., 54 (2018) 13264-13267.
[44] H. Zhang, K. Yang, C. Chen, Y. Wang, Z. Zhang, L. Tang, Q. Sun, S. Xue, W. Yang, Polymer, 149 (2018) 266-272.
[45] Y. Zhang, X. Yang, G. Sun, H. Zhang, X. Liu, F. Zhu, S. Qin, Z. Zhao, Y. Cui, Spectrochim. Acta - Part A: Mol. Biomol. Spect., 199 (2018) 161-169.
[46] Y. Zhou, X. Bao, Spectrochim. Acta - Part A: Mol. Biomol. Spect., 210 (2019) 1-8.
[47] C. Guo, S. Sun, Q. He, V.M. Lynch, J.L. Sessler, Org. Lett., 20 (2018) 5414-5417.
[48] R. Azadbakht, N. Chehri, New J. Chem., 42 (2018) 17690-17699.
[49] Y. Liu, Z. Zhao, R. Huo, Q. Liu, Sci. Rep., 9 (2019).
[50] M.M. Rhaman, M.H. Hasan, A. Alamgir, L. Xu, D.R. Powell, B.M. Wong, R. Tandon, M.A. Hossain, Sci. Rep., 8 (2018).
[51] P.R. Sharma, S. Pandey, V.K. Soni, G. Choudhary, R.K. Sharma, Supramol. Chem., 31 (2019) 634-644.
[52] P.G. Sutariya, H. Soni, S.A. Gandhi, A. Pandya, New J. Chem., 43 (2019) 737-747.
[53] W. Zhu, H. Fang, J.X. He, W.H. Jia, H. Yao, T.B. Wei, Q. Lin, Y.M. Zhang, New J. Chem., 42 (2018) 11548-11554.
[54] M. Singh, N. Singh, J.R. Ascenso, P.M. Marcos, Supramol. Chem., 31 (2019) 313-321.
[55] H.F. Xie, C. Wu, J. Zou, Y.X. Yang, H. Xu, Q.L. Zhang, C. Redshaw, T. Yamato, Dyes and Pigments, 178 (2020).
[56] K. Norvaiša, K.J. Flanagan, D. Gibbons, M.O. Senge, Angew. Chem. Int. Ed., 58 (2019) 16553-16557.
[57] S.S.R. Namashivaya, A.S. Oshchepkov, H. Ding, S. Förster, V.N. Khrustalev, E.A. Kataev, Organic Lett., 21 (2019) 8746-8750.
[58] A.S. Oshchepkov, T.A. Shumilova, M. Zerson, R. Magerle, V.N. Khrustalev, E.A. Kataev, J. Org. Chem., 84 (2019) 9034-9043.
[59] B. Uttam, R. Kandi, M.A. Hussain, C.P. Rao, J. Org. Chem., 83 (2018) 11850-11859.
[60] W. Chen, C. Guo, Q. He, X. Chi, V.M. Lynch, Z. Zhang, J. Su, H. Tian, J.L. Sessler, J. Am. Chem. Soc., 141 (2019) 14798-14806.
[61] W. Huang, L. Sun, Z. Zheng, J. Su, H. Tian, Chem. Commun., 51 (2015) 4462-4464.
[62] R. Hein, P.D. Beer, J.J. Davis, Chem. Rev., 120 (2020) 1888-1935.
[63] R. Tepper, U.S. Schubert, Angew. Chem. Int. Ed., 57 (2018) 6004-6016.
[64] P. Sabater, F. Zapata, B. López, I. Fernández, A. Caballero, P. Molina, Dalton Trans., 47 (2018) 15941-15947.
[65] J.Y.C. Lim, I. Marques, V. Félix, P.D. Beer, Chem. Commun., 54 (2018) 10851-10854.
[66] J.Y.C. Lim, I. Marques, V. Félix, P.D. Beer, Angew. Chem. Int. Ed., 57 (2018) 584-588.
[67] H.A. Klein, H. Kuhn, P.D. Beer, Chem. Commun., 55 (2019) 9975-9978.
[68] J. Zheng, Q. Zeng, R. Zhang, D. Xing, T. Zhang, J. Am. Chem. Soc., 141 (2019) 19226-19230.
[69] S. Sugiura, Y. Kobayashi, N. Yasuda, H. Maeda, Chem. Commun., 55 (2019) 8242-8245.
[70] L.C. Murfin, K. Chiang, G.T. Williams, C.L. Lyall, A.T. Jenkins, J. Wenk, T.D. James, S.E. Lewis, Frontiers in Chemistry, 8 (2020) 10-10.

[71] K.-C. Chang, S.-S. Sun, M.O. Odago, A.J. Lees, Coord. Chem. Rev., 284 (2015) 111-123.
[72] Y. Chen, X. Shang, W. Pan, C. Li, T. Wang, J. Coord. Chem., 71 (2018) 3487-3499.
[73] H.-H. Meng, C.-Y. Wang, W. Xi, X.-Q. Song, L. Wang, Dalton Trans., 48 (2019) 12326-12335.
[74] D. Bansal, R. Gupta, Dalton Trans., 48 (2019) 14737-14747.
[75] A.K. Purohit, S.K. Padhan, J.R. Mohanty, P.K. Kar, Photochem. Photobiol. Sci., 17 (2018) 815-821.
[76] R.C. Knighton, S. Dapin, P.D. Beer, Chem. Eur. J., 26 (2020) 5288-5296.
[77] T. Kim, H.J. Kim, I.-S. Shin, J.-I. Hong, Anal. Chem., (2020).
[78] T.K. Ghosh, S. Mondal, S. Bej, M. Nandi, P. Ghosh, Dalton Trans., 48 (2019) 4538-4546.
[79] S. Mondal, T.K. Ghosh, B. Chowdhury, P. Ghosh, Inorg. Chem., 58 (2019) 15993-16003.
[80] M. Ramachandran, S. Anandan, New J. Chem., (2020).
[81] J. Yang, L. Sun, L. Hao, G.-G. Yang, Z.-C. Zou, Q. Cao, L.-N. Ji, Z.-W. Mao, Chem. Commun., 55 (2019) 11191-11194.
[82] K. Li, G.S. Ming Tong, Q. Wan, G. Cheng, W.-Y. Tong, W.-H. Ang, W.-L. Kwong, C.-M. Che, Chem. Sci., 7 (2016) 1653-1673.
[83] N. Chaudhri, R.J. Butcher, M. Sankar, New J. Chem., 42 (2018) 8190-8199.
[84] S.J. Butler, D. Parker, Chem. Soc. Rev., 42 (2013) 1652-1666.
[85] S.-Y. Huang, M. Qian, V.C. Pierre, Inorg. Chem., 58 (2019) 16087-16099.
[86] J. Hai, T. Li, J. Su, W. Liu, Y. Ju, B. Wang, Y. Hou, Angew. Chem. Int. Ed., 57 (2018) 6786-6790.
[87] A. Nonat, T. Liu, O. Jeannin, F. Camerel, L.J. Charbonnière, Chem. Eur. J., 24 (2018) 3784-3792.
[88] R. Mailhot, T. Traviss-Pollard, R. Pal, S.J. Butler, Chem. Eur. J., 24 (2018) 10745-10755.
[89] K. Gupta, A.K. Patra, Eur. J. Inorg. Chem, 2018 (2018) 1882-1890.
[90] S.-Y. Huang, V.C. Pierre, Chem. Commun., 54 (2018) 9210-9213.
[91] L.B. Jennings, S. Shuvaev, M.A. Fox, R. Pal, D. Parker, Dalton Trans., 47 (2018) 16145-16154.
[92] J.C. Lindon, G.E. Tranter, D. Koppenaal, Encyclopedia of spectroscopy and spectrometry, Academic Press, 2016.
[93] P. Sabater, F. Zapata, A. Bastida, A. Caballero, Org. Biomol. Chem., 18 (2020) 3858-3866.
[94] J. Yang, C.-C. Dong, X.-L. Chen, X. Sun, J.-Y. Wei, J.-F. Xiang, J.L. Sessler, H.-Y. Gong, J. Am. Chem. Soc., 141 (2019) 4597-4612.
[95] H. Izawa, S. Nishino, M. Sumita, M. Akamatsu, K. Morihashi, S. Ifuku, M. Morimoto, H. Saimoto, Chemical Communications, 51 (2015) 8596-8599.
[96] H. Izawa, M. Wada, S. Nishino, M. Sumita, T. Fujita, K. Morihashi, S. Ifuku, M. Morimoto, H. Saimoto, Bull. Chem. Soc. Japan, 91 (2018) 1220-1225.
[97] S.-i. Kondo, K. Sato, Y. Matsuta, K. Osawa, Bull. Chem. Soc. Japan, 91 (2018) 875-881.
[98] P.A. Gale, C. Caltagirone, Coord. Chem. Rev., 354 (2018) 2-27.
[99] T.A. Barendt, I. Rašović, M.A. Lebedeva, G.A. Farrow, A. Auty, D. Chekulaev, I.V. Sazanovich, J.A. Weinstein, K. Porfyrakis, P.D. Beer, J. Am. Chem. Soc., 140 (2018) 1924-1936.
[100] S.V. Bhosale, C.H. Jani, S.J. Langford, Chem. Soc. Rev., 37 (2008) 331-342.
[101] A.S. Oshchepkov, T.A. Shumilova, S.R. Namashivaya, O.A. Fedorova, P.V. Dorovatovskii, V.N. Khrustalev, E.A. Kataev, The Journal of Organic Chemistry, 83 (2018) 2145-2153.
[102] A.M. Desai, P.K. Singh, Chemistry - A European Journal, 25 (2019) 2035-2042.
[103] X. Gong, Q.-L. Zhang, S. Zhang, Y. Xia, Q. Bai, S. Chen, X.-L. Ni, Dyes and Pigments, 163 (2019) 502-508.
[104] B.L. Schottel, H.T. Chifotides, K.R. Dunbar, Chem. Soc. Rev., 37 (2008) 68-83.
[105] I. Alkorta, I. Rozas, J. Elguero, J. Am. Chem. Soc., 124 (2002) 8593-8598.
[106] M. Giese, M. Albrecht, K. Rissanen, Chem. Rev., 115 (2015) 8867-8895.
[107] H.-B. Liu, Q. Zhang, M.-X. Wang, Angew. Chem. Int. Ed., 57 (2018) 6536-6540.
[108] G. Men, W. Han, C. Chen, C. Liang, S. Jiang, Analyst, 144 (2019) 2226-2230.
[109] B.S. Khakh, R. Alan North, Nature, 442 (2006) 527-532.
[110] Z. Shi, Y. Tu, R. Wang, G. Liu, S. Pu, Dyes and Pigments, 149 (2018) 764-773.
[111] H.M. Tran, T.H. Nguyen, V.Q. Nguyen, P.H. Tran, L.D. Thai, T.T. Truong, L.T.T. Nguyen, H.T. Nguyen, Macromol. Res., 27 (2019) 25-32.
[112] Z. Li, Y. Dai, Z. Lu, Y. Pei, Y. Song, L. Zhang, H. Guo, Eur. J. Org. Chem., 2019 (2019) 3614-3621.
[113] Z. Li, H. Zhang, H. Zhang, Y. Xie, H. Chen, C. He, Y. Wang, H. Ya, H. Guo, J. Chem. Res., 42 (2018) 305-308.

[114] M.S. Hossain, S.A. Rahaman, J. Hatai, M. Saha, S. Bandyopadhyay, Chem. Commun., 56 (2020) 4172-4175.
[115] F.C. Parks, Y. Liu, S. Debnath, S.R. Stutsman, K. Raghavachari, A.H. Flood, J. Am. Chem. Soc., 140 (2018) 17711-17723.
[116] X. Chi, W. Cen, J.A. Queenan, L. Long, V.M. Lynch, N.M. Khashab, J.L. Sessler, J. Am. Chem. Soc., 141 (2019) 6468-6472.
[117] P. Wei, F. Xue, Y. Shi, R. Strand, H. Chen, T. Yi, Chem. Commun., 54 (2018) 13115-13118.
[118] S. Gnaim, D. Shabat, Chem. Commun., 54 (2018) 2655-2658.
[119] M. Sun, H. Liu, Y. Su, W. Yang, Y. Lv, Anal. Chem., 92 (2020) 5294-5301.
[120] V.N. Khose, M. Hasan, S.C. Khot, S.M. Mobin, V. Borovkov, A.V. Karnik, J. Org. Chem., 85 (2020) 1847-1860.
[121] R.I. Stock, J.P. Dreyer, G.E. Nunes, I.H. Bechtold, V.G. Machado, ACS Appl. Poly. Mat., 1 (2019) 1757-1768.
[122] H. Wu, M. Chen, Q. Xu, Y. Zhang, P. Liu, W. Li, S. Fan, Chem. Commun., 55 (2019) 15137-15140.
[123] A. Panja, K. Ghosh, ChemistrySelect, 3 (2018) 1809-1814.
[124] J. Wu, L. Jiang, P. Verwilst, J. An, H. Zeng, L. Zeng, G. Niu, J.S. Kim, Chem. Commun., 55 (2019) 9947-9950.
[125] D. Li, J. Cheng, C.K. Wang, H. Ying, Y. Hu, F. Han, X. Li, Chem. Commun., 54 (2018) 8170-8173.
[126] S. Ghosh, B. Roy, S. Bandyopadhyay, J. Org. Chem., 84 (2019) 12031-12039.
[127] J. Wang, L. Liu, W. Xu, Z. Yang, Y. Yan, X. Xie, Y. Wang, T. Yi, C. Wang, J. Hua, Anal. Chem., 91 (2019) 5786-5793.
[128] Z. Zhang, J. Fan, Y. Zhao, Y. Kang, J. Du, X. Peng, ACS Sensors, 3 (2018) 735-741.
[129] S.L. Wiskur, P.N. Floriano, E.V. Anslyn, J.T. McDevitt, Angew. Chem. Int. Ed., 42 (2003) 2070-2072.
[130] M. Pushina, P. Koutnik, R. Nishiyabu, T. Minami, P. Savechenkov, Anzenbacher P, Jr., Chem. Eur. J., 24 (2018) 4879-4884.
[131] S.H. Hewitt, G. Macey, R. Mailhot, M.R.J. Elsegood, F. Duarte, A.M. Kenwright, S.J. Butler, Chem. Sci., 11 (2020) 3619-3628.
[132] V. Hamedpour, Y. Sasaki, Z. Zhang, R. Kubota, T. Minami, Anal. Chem., 91 (2019) 13627-13632.
[133] A.P. de Silva, S. Uchiyama, Nature Nanotechnology, 2 (2007) 399-410.
[134] N. Borah, B. Nayak, A. Gogoi, G. Das, New J. Chem., 43 (2019) 16497-16505.
[135] A. Kushwaha, S.K. Patil, D. Das, New J. Chem., 42 (2018) 9200-9208.
[136] A. Mondal, A. Roy Chowdhury, S. Bhuyan, S.K. Mukhopadhyay, P. Banerjee, Dalton Trans., 48 (2019) 4375-4386.
[137] P. Alreja, N. Kaur, Inorg. Chim. Acta, 480 (2018) 127-131.
[138] K. Mawai, S. Nathani, P. Roy, U.P. Singh, K. Ghosh, Dalton Trans., 47 (2018) 6421-6434.
[139] S.P. Parua, D. Sinha, K.K. Rajak, ChemistrySelect, 3 (2018) 1120-1128.
[140] R. Purkait, A.D. Mahapatra, D. Chattopadhyay, C. Sinha, Spectrochim. Acta - Part A: Mol. Biomol. Spect., 207 (2019) 164-172.
[141] K. Rezaeian, H. Khanmohammadi, S. Gholizadeh Dogaheh, New J. Chem., 42 (2018) 2158-2166.
[142] T. Chakraborty, S. Dasgupta, A. Bhattacharyya, E. Zangrando, D. Escudero, D. Das, New J. Chem., 43 (2019) 13152-13161.
[143] K. Murugesan, V. Jeyasingh, S. Lakshminarayanan, S. Narayanan, L. Piramuthu, Spectrochim. Acta - Part A: Mol. Biomol. Spect., 223 (2019).
[144] N.N. Yang, J.J. Fang, Q. Sui, E.Q. Gao, ACS Appl. Mater. Interfaces, 10 (2018) 2735-2744.
[145] C. Chen, D. Zhao, Y. Jiang, P. Ni, C. Zhang, B. Wang, F. Yang, Y. Lu, J. Sun, Anal. Chem., 91 (2019) 15017-15024.
[146] J.N. Tutol, W. Peng, S.C. Dodani, Biochem., 58 (2019) 31-35.
[147] J.N. Tutol, H.C. Kam, S.C. Dodani, ChemBioChem, 20 (2019) 1759-1765.